Impedance analysis of electrical resonance and harmonics in HVDC connected Wind Power Plants

Igor Sowa

30.05.2016

Abstract

During the last years the development of first HVDC connected offshore wind power plants increased. As the first wind farms of this type were commissioned, an unexpected phenomenon occurred. The phenomenon of electrical resonance in the offshore AC grid led to outages of the HVDC transmission system. The thesis presents the phenomenon and methods of its investigation.

The study focuses on harmonic frequencies identification excited through the resonance phenomena between the elements within WPP's inner AC network. The analysis includes observations from three tested topology cases by different methods: frequency sweep and harmonic resonance modal analysis. The comparison is performed for diverse converter models: voltage source based, current source based and nonlinear impedance model obtained by harmonic linearization method. The results of the analysis are verified by the outcome attained in DIgSilent Power Factory software. The study also includes the stability analysis performed Nyquist criterion based.

Furthermore, the result of investigation exposes the clues for possible subsequent implementation of harmonic filters as well as for beneficial control of converters. Feasible measures for resonance mitigation by these two approaches are briefly described.

Acknowledgement

BLALBALBALBLBA

Contents

Chapter 1

Introduction

1.1 Background and introduction to the study

Motivation to the study presented in this thesis is determined by recent experiences in operation of first high-power HVDC connected off-shore wind power plant connected to island AC grid. In that plant phenomenon of harmonic resonance occurs in normal working conditions. In such a power electronics dominated grid power converters go into resonance between each other causing oscillations and instabilities in AC network. These problems were not considered during planning period of the wind power plant. Due to future plans of common development of off-shore wind farms, to avoid such problems, new methods of investigation and analysis for resonance should be developed or current ones should be extended.

In contrast to the continental European grid, in the off-shore one there is not enough resistive loads. Thus in such a network dominated by converters the resonance damping of harmonic frequencies is not sufficient. Moreover, in the offshore WPP the collection grid from turbines consist of long cables which have much higher capacitance than regular overhead line. In such a way, high capacitance of the grid switches the resonance frequencies to the lower levels where the other harmonics are present and could be amplified i.e. harmonic resonance phenomenon occurs.

The purpose of the thesis is to analyse, understand and compare the resonance applying some available methods in order to detect possible occurrence of phenomena in off-shore wind farm grids. Furthermore, the study is coupled with stability analysis based on Nyquist stability criterion illustrated on the Bode diagram. The accuracy of this study is significantly determined by the quality of utilized model and its elements therefore we use more different approaches of power converters impedance modelling.

1.2 Theoretical introduction

1.2.1 Basic information about harmonics

Generation of electricity in power system is usually at the frequency constant level of either 50Hz or 60Hz. Waveforms produced by rotating generator is practically sinusoidal

and in this shape they should be delivered to every customer. However, when sinusoidal waveform is applied to nonlinear load the resulting current is not purely sinusoidal. This current, which is not perfectly sinusoidal, leads to not perfectly sinusoidal voltage drop due to system impedance. Hence, the voltage distortion at load terminals is produced. The problem of presence of these distortions is not new in the power system. However the devices responsible for producing distorted waveforms and devices suffering from presence of the distortion have changed down the years.

A distorted, non-sinusoidal waveform can be expressed in a very simple way as a sum of so-called harmonic components. Harmonic component in power system is a perfectly sinusoidal waveform that has frequency equal to integer multiple of the fundamental frequency:

$$f_h = h \cdot f_1 \tag{1.1}$$

where h is an integer (harmonic order) and f_1 is fundamental frequency (usually 50 Hz or 60 Hz). If h is not an integer, such a waveform is called *interharmonic* component. As aforementioned, any sinusoidal waveform can be expressed as sum of its harmonic components. Exemplary distorted current waveform for fundamental frequency and 3^{rd}, 5^{rd} and 7^{rd} harmonics could be expressed as follows:

$$I = I_1 sin(\omega t) + I_3 sin(3\omega t + \delta_3) + I_5 sin(5\omega t + \delta_5) + I_7 sin(7\omega t + \delta_7) \tag{1.2}$$

where I_1, I_3, I_5, I_7 are peak RMS values of fundamental component and harmonic components and $\delta_3, \delta_5, \delta_7$ are possible phase shifts of each harmonic.

Concerns for harmonics rises from power quality requirements. Power quality requirements are introduced to prevent from negative effects on electrical equipment which are sensitive to poor power quality. The most popular regulations for power quality with regard to harmonic content are described in Section 1.7. Poor power quality leads to damages of equipment, in other words, causes great money losses for industry. Moreover, certain types of equipment, if exposed to distorted waveforms, lead to further generation of harmonics [1].

1.2.2 Harmonic indices

There are two most common indices to describe content of the harmonics in a time domain signal as one number: *Total Harmonic Distortion* (THD) and *Total Demand Distortion* (TDD).

THD, which usually relates to voltage waveforms, is defined as RMS values (V_{nRMS}) of the harmonics expressed relatively to fundamental components (V_{1RMS}):

$$THD = \frac{\sqrt{\sum_{n=2}^{N} V_{nRMS}^2}}{V_1} \tag{1.3}$$

where n is the harmonic order and N is maximum harmonic order to be considered. For most application, it is sufficient to consider harmonic order range up to 25^{th} harmonic, but most standards recommend up to 50^{th} [1].

Since THD of current waveform can be misleading when load is low and can result in very high THD value, RMS values of harmonic currents can be related to rated or maximum current magnitude rather than to fundamental current (TDD):

$$THD = \frac{\sqrt{\sum_{n=2}^{N} I_{nRMS}^2}}{I_R} \tag{1.4}$$

This reflects distortion in more intuitive way since the electrical power supply systems are design to withstand rated (or maximum) values, while relation to fundamental components when load is far lower from rated value can give impression of much more significant distortion.

In the presented study these indices are also applied to the three-phase systems since for all cases the three-phase balanced system is considered. If the system is not balanced some averaging can be carried out [1].

1.2.3 Sources of harmonics

As mentioned before the sources of harmonic distortions have changed down the years. In early power systems harmonic distortions were mainly caused by saturation of transformers industrial arc furnaces and other arc devices like electric welders. On the other hand, the main concern was the effect of those distortions on electric machines, telephones and on increased risk of failure from overvoltage [2].

Generally speaking, harmonics in power systems are produced due to many phenomena, for example, ferroresonance, magnetic saturation, subsunchronous resonance, and nonlinear and electrically switched loads. These days, harmonic emission from nonlinear loads dominates [3].

In transformers, harmonics appear as result of saturation, switching, high-flux densities, winding connections and grounding. Also, energizing a power transformer generates a high order of harmonics and a DC component [1].

In rotating machines, the construction elements and their limitations of both generators and motors like [1]: armature windings, phase windings, teeth, phase spread etc. affects EMF in the phase windings, therefore rotating machines are also not pure linear elements. Even synchronous machine generates deviated voltage at its terminal, however the voltage is almost sinusoidal.

In presence of system capacitance, some inductive elements like transformers or reactors can lead to so-called ferroresonance phenomena, due to nonlinearity and saturation of reactance. This causes short current surges that generate overvoltages. Moreover, presence of capacitance in sinusoidal circuits can magnify existing harmonics by creating harmonic resonance condition. More about harmonic resonance in Section 1.2.4.

1.2.3.1 Harmonics from power electronics elements

Above classical power system elements described above, static power electronic elements are the main source of harmonics in the power system. We can include in this group devices like: power converters, rectifiers, inverters, diacs, triacs, GTOs and adjustable speed drives [1].

Among the power electronics devices, many of them are controlled with pulse width modulation (PWM). We can distinguish several techniques of PWM: single PWM, multiple PWM, sinusoidal PWM, modified sinusoidal PWM. Inverters which use PWM can be divided into three groups: VSI (voltage source inverters), CSI (current source inverters) and ZSI (impedance source inverters).

These elements usually emit so-called characteristic harmonics which are those produced by power electronic converters during normal operation. They are still integer multiply of fundamental frequency. [1]. Such a device can be viewed as a matrix of static switches that provides an interconnection between input and output nodes of an electrical power system. In rectifying process, current is allowed to pass through semiconductor devices during only a fraction of the fundamental frequency cycle, for which power converters are often regarded as energy-saving devices [2]. Static power electronic devices also produce some non-characteristic harmonics when some non-ideal condition of control occurs (for example unbalanced PWM signal). Then, harmonics emitted will be unbalanced, also interharmonics can appear. Since mitigation of harmonics is usually designed for characteristic harmonics, the non-characteristic harmonics can cause significant problems [1]. In large power converters, generally, there is much higher inductane on the DC than on the AC side. Thus, the DC current is practically constant and the converter acts as a harmonic voltage source on the DC side and as a harmonic current source on the AC side [2].

In the study cases of the thesis, VSI (Voltage Source Inverters) are used in the considered wind power plant. VSIs use switching devices like GTO, IGBT, MTO which have both turn off and turn on control. Because of this, much more accurate control comparing o CSI is possible, also including power flow control. Further details about utilized models of converters and other elements are provided in Section 1.6.

Beyond elements of high power power electronics, there are also many electronic home appliances that are very nonlinear and produce harmonics. These are: fluorescent lights, variable speed air conditioning systems, PCs, microwaves, induction heaters etc.

The harmonics from Wind Power Plants are becoming very important in the power system these days due to increasing number of these sources. As stated in the Introduction, the main subject of this thesis is to analyse harmonics created and possibly emitted to the power system to the grid due to the phenomenon of harmonic resonance in Wind Power Plants inner grid. Further details about Wind Power Plants as a source of harmonics in Section 1.4.

1.2.4 Harmonic Resonance

Harmonic resonance is an important factor affecting the system harmonic levels. Resonant conditions involve the reactance of capacitive elements that at some point in frequency equals the inductive reactance of the inductive elements. These two elements combine to produce series or parallel resonance [2]. Harmonic waveform generated in other part of the grid can be magnified many times due to this phenomenon [1]. For such a harmonic resonance problems, there must be a sufficient level of harmonic source voltages or currents at or near the resonant frequency to excite the resonance [7].

Most of the networks are considered inductive, therefore presence of capacitive elements

can result in local system resonances, which lead in turn to possibly subsequent damage [3]. Depending on the type of the grid these are usually capacitor banks, cables, overhead lines, compensators etc. Since harmonic resonance either amplify existing harmonics or creates new, the negative effects of this phenomenon are very similar to the effects caused by harmonics described in Section 1.2.5. Moreover, it can overload the capacitor and may result in nuisance fuse operation causing severe amplification of the harmonic currents resulting in waveform distortions, which has consequent deleterious effects on the power system components [1].

As circuit theory says, resonance harmonics can occur in series RLC or parallel RLC circuits (the connection type between L and C elements). The resonance frequency depends on values of the inductance and capacitance. The smaller the size of the capacitor, the higher is the resonant frequency [1]. This conclusion we observe in the results presented in Chapter 2.

The resonance problem in power system is a serious potential problem [1]. It leads to many negative (shut-downs, failures). It may appear unexpected at certain operating condition of the power system. Moreover, it can also appear partially or disappear with no negative effect. Due to this problems, prevention may require long-term online measurements to establish the disturbing source in the system [1].

Major concerns about elusive harmonic resonances are: [1]

- the resonant frequency is present in a grid (for example separated industrial grid or inner collection grid of WPP) and depends very strongly on topology of considered network,
- expansion, disconnection of some parts of the network may bring out a resonant condition not existing before (for example switching on the capacitor for power factor improvements),
- even when some elements are designed to prevent from harmonic resonance, after any modification of the topology, immunity from resonant conditions cannot be guaranteed.

In the thesis we describe some methods for monitoring the resonance in the grid and identification of an element responsible for certain emission (Section 1.3). As aforementioned, there are two basic cases of resonance: series and parallel resonance. Following sections describes these two circumstances.

1.2.4.1 Series AC resonance

The simple series connection of resonant element is presented in the Figure 1.1.

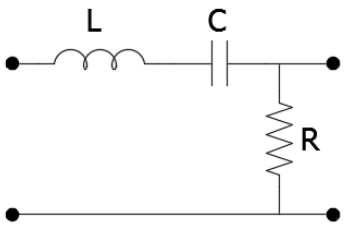

Figure 1.1: Exemplary circuit for series LC resonance.

The impedance of such a circuit is as follows:

$$Z = R + j\omega L + \frac{1}{j\omega C} \tag{1.5}$$

In the case of series resonance, the total impedance at the resonance frequency is reduced exclusively to the resistive circuit component. Assuming $R = 0$, the series resonance occurs at certain resonant frequency f_r, when the impedance is minimum i.e.:

$$j\omega L + \frac{1}{j\omega C} = 0 \tag{1.6}$$

What leads to:

$$\omega_r = \frac{1}{\sqrt{LC}} \tag{1.7}$$

Impedance magnitude of the system from Figure 1.1 and its angle is presented in the in the Figure 1.2.

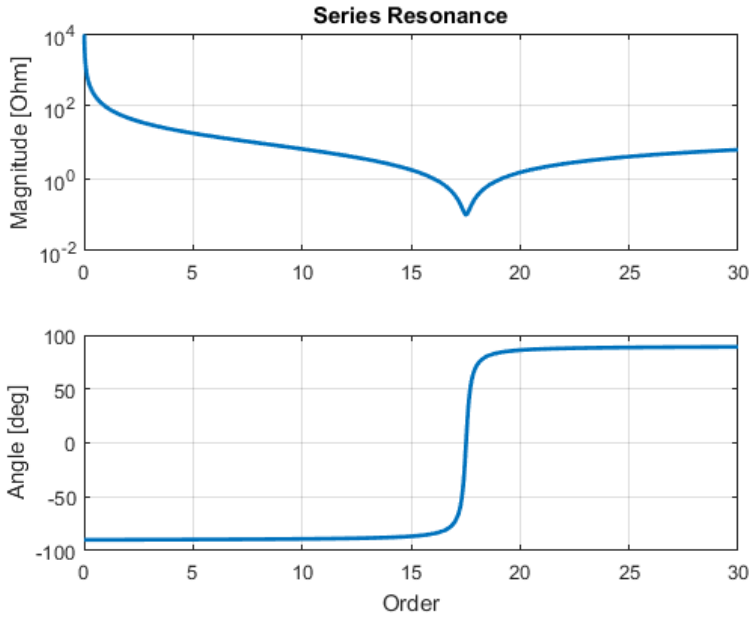

Figure 1.2: Series resonance in LC circuit at frequency 876 Hz ($17^{th} frequency order$).

Since the impedance reduced for resonance frequency, the current can reach very high values:

$$I_r = \frac{V_1}{R} = \frac{V_2}{R} \tag{1.8}$$

Thus, we can see that the current is limited only by resistance. In the pure LC case the currents tends to infinity and if R is very small, current can be high.

1.2.4.2 Parallel AC resonance

The parallel resonance occurs in parallel RLC circuit (see the example circuit in the Figure 1.3) when the total impedance at the resonant frequency is very large (theoretically tends to infinite).

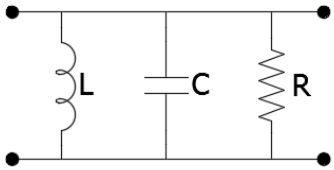

Figure 1.3: Circuit of parallel LC resonance.

$$\frac{1}{Z} = \frac{1}{R} + \frac{1}{j\omega L + j\omega C} \tag{1.9}$$

Thus, the resonant condition is:

$$\omega C - \frac{1}{RomegaL} = 0 \tag{1.10}$$

Then again, the resonant frequency is as follows:

$$\omega_r = \frac{1}{\sqrt{LC}} \tag{1.11}$$

Exemplary impedance magnitude and angle plots of the system from Figure 1.3 are plotted at Figure 1.4.

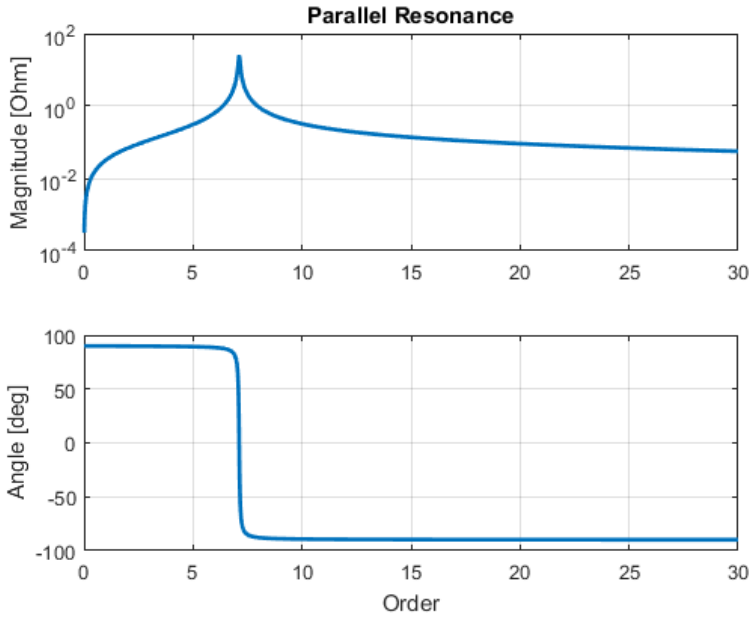

Figure 1.4: Parallel resonance in LC circuit at frequency 356 Hz ($7^{th} frequency order$).

This condition may produce a large overvoltage between the parallel-connected elements, even under small harmonic currents. Therefore, resonant conditions may represent a hazard for solid insulation in cables and transformer windings and for the capacitor bank and their protective devices as well [2].

1.2.4.3 Tank circuit parallel AC resonance

More practical LC circuit i.e. with inductor modelled with non-zero value of resistance and capacitor modelled without resistance is called Tank circuit [1]. Figure 1.5 presents such a circuit.

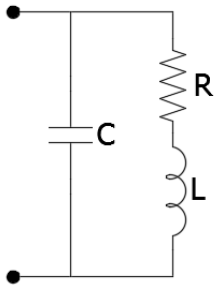

Figure 1.5: Tank circuit of parallel LC resonance.

In this circuit the aggregate admittance seen from the terminals is as follows:

$$Y = j\omega C + \frac{1}{R + j\omega L} \tag{1.12}$$

In other form:

$$Y = \frac{R}{R^2 + \omega^2 L^2} + j\left(\omega C - \frac{\omega L}{R^2 + \omega^2 L^2}\right) \tag{1.13}$$

The plot of exemplary impedance for such a system is presented in the Figure 1.6.

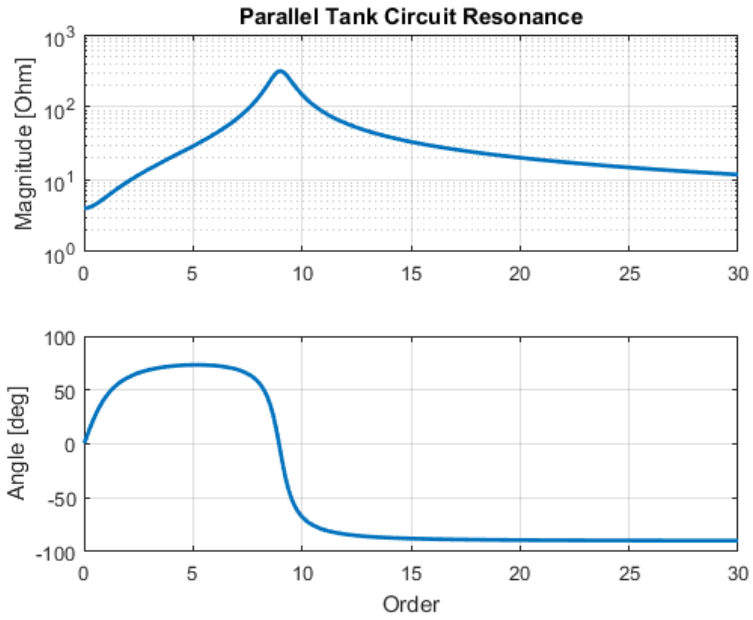

Figure 1.6: Parallel resonance in LC circuit at frequency 447 Hz ($9^{th} frequency order$).

In the circuit with zero-resistance (lossless circuit), resonance occurs if impedance of inductor equals impedance of capacitor i.e. when the circuit works as short-circuited. In this case, resonance occurs in similar situation, even though the resistance stays unchanged in the circuit. In other words resonance occurs when power factor of admittance above equals zero [1].

$$\omega C - \frac{\omega L}{R^2 + \omega^2 L^2} = 0 \tag{1.14}$$

That gives resonance frequency:

$$\omega_r = \sqrt{\frac{1}{LC} - \frac{R^2}{L^2}} \tag{1.15}$$

Moreover, as distinct from the series resonance, where resonance can occur from any value of resistance, in this case resonance occurs only if following equation is true:

$$\frac{R^2}{L^2} \leq \frac{1}{LC} \tag{1.16}$$

In other words, resonance does not occur if:

$$R > \sqrt{\frac{L}{C}} \tag{1.17}$$

1.2.4.4 Factors affecting resonance

Generally speaking, in the power system, the following factors can impact resonance frequency (based on [1]):

- Synchronous and asynchronous sources and loads in the power system. They can absorb some harmonics but also change the resonance points. Correct modelling is crucial.
- Impedance of the utility source. In the models connected to such a source they are given by the three-phase short-circuit current.
- Shunt power capacitors. They are not recommended in presence of devices producing harmonics. They cause also secondary resonance if applied at multi-voltage levels.
- Resistance/resistance loads in power system.
- Single phase loads.
- Already applied harmonic mitigated devices (e.g. passive filters). They does not remove the resonant conditions, but only shift them.
- Topology of the network. Any switching action will change the resonant frequency.

1.2.5 Effects of harmonics

The harmonic resonance in a power system cannot be tolerated and must be avoided. The magnified harmonics will have serious effects on equipment heating, harmonic torque generation, nuisance operation of protective devices, derating of electrical equipment, damage to the shunt capacitors due to overloading, can precipitate shutdowns etc.

Some of the harmonic deleterious effects on electrical equipment are gathered in [4]:

- Capacitor bank failure because of reactive power overload, resonance, and harmonic amplification. Nuisance fuse operation.
- Excessive losses, heating, harmonic torques, and oscillations in induction and synchronous machines, which may give rise to torsional stresses.
- Increase in negative sequence current loading of synchronous generators, endangering the rotor circuit and windings.
- Generation of harmonic fluxes and increase in flux density in transformers, eddy current heating, and consequent derating.
- Overvoltages and excessive currents in the power system, resulting from resonance.
- Derating of cables due to additional eddy current heating and skin effect losses.
- Inductive interference with telecommunication circuits.

- Signal interference in solid-state and microprocessor-controlled systems.
- Relay malfunction.
- Interference with ripple control and power line carrier systems, causing misoperation of the systems, which accomplish remote switching, load control, and metering.
- Unstable operation of firing circuits based on zero-voltage crossing detection and latching.
- Interference with large motor controllers and power plant excitation systems.
- Possibility of subsynchronous resonance.
- Flickers.

1.2.6 Nabe and Akagi instantaneous power theory

Nabe-Akagi instantaneous reactive power pq theory [**?**] is based on Clarks transformations in three phase systems.

The power in electrical circuit is described using instantaneous voltage and current without the use of Fourier series. Usually is used for switching compensators and active filters controls [1].

By linear transformation, the voltages v_a, v_b, v_c and load currents i_a, i_b, i_c are transformed into an $\alpha - \beta$ coordinate system. The instantaneous real power p and the instantaneous imaginary power q are defined on the basis of transformed voltages and currents. The following equations shows the transformations.

$$\begin{vmatrix} v_\alpha \\ v_\beta \end{vmatrix} = \sqrt{\frac{2}{3}} \begin{vmatrix} 1 & -\frac{1}{2} & -\frac{1}{2} \\ 1 & \frac{\sqrt{3}}{2} & -\frac{\sqrt{3}}{2} \end{vmatrix} \begin{vmatrix} v_a \\ v_b \\ v_c \end{vmatrix} \tag{1.18}$$

$$\begin{vmatrix} i_\alpha \\ i_\beta \end{vmatrix} = \sqrt{\frac{2}{3}} \begin{vmatrix} 1 & -\frac{1}{2} & -\frac{1}{2} \\ 1 & \frac{\sqrt{3}}{2} & -\frac{\sqrt{3}}{2} \end{vmatrix} \begin{vmatrix} i_a \\ i_b \\ i_c \end{vmatrix} \tag{1.19}$$

$$\begin{vmatrix} p \\ q \end{vmatrix} = \begin{vmatrix} v_\alpha & v_\beta \\ -v_\beta & v_\alpha \end{vmatrix} \begin{vmatrix} i_\alpha \\ i_\beta \end{vmatrix} \tag{1.20}$$

On the basis of this theory, with further conversions of the equation we obtain the instantaneous active and reactive powers.

$$\begin{aligned} p &= v_\alpha i_{\alpha p} + v_\beta i_{\beta p} \equiv P_{\alpha p} + P_{\beta p} \\ p &= v_\alpha i_{\alpha q} + v_\beta i_{\beta q} \equiv P_{\alpha q} + P_{\beta q} \end{aligned} \tag{1.21}$$

$$
\begin{aligned}
P_{\alpha p} &= \frac{v_\alpha^2}{v_\alpha^2 + v_\beta^2} p \\
P_{\alpha q} &= \frac{-v_\alpha v_\beta}{v_\alpha^2 + v_\beta^2} q \\
P_{\beta p} &= \frac{v_\beta^2}{v_\alpha^2 + v_\beta^2} p \\
P_{\beta q} &= \frac{v_\alpha v_\beta}{v_\alpha^2 + v_\beta^2} q
\end{aligned}
\tag{1.22}
$$

The powers $P_{\alpha p}$ and $P_{\beta q}$ cancels each other. Therefore, one can conclude that in the system of converter connected to source and load on both sides, there is no relationship between the instantaneous reactive power on the source side (between source and converter) and instantaneous reactive power on the load side (between converter and load). Thus, the instantaneous imaginary power on the input side is not equal to the instantaneous imaginary power on the output side. However, the instantaneous real power on the input side is equal to the real output power.

1.2.7 Park Transformation

Park transformation is necessary to obtain the positive and negative impedances for converters equations presented in Section 1.6.4.2.

Park transformation, also called dq0-transformation is a space vector transformation of three-phase time-domain signals from a stationary phase coordinate system (abc) to a rotating coordinate system ($dq0$) as follows [**?**]:

$$
\begin{bmatrix} u_d \\ u_q \\ u_0 \end{bmatrix} = \frac{2}{3} \begin{bmatrix} cos(\Theta) & cos(\Theta - \frac{2\pi}{3}) & cos(\Theta + \frac{2\pi}{3}) \\ -sin(\Theta) & -sin(\Theta - \frac{2\pi}{3}) & -sin(\Theta + \frac{2\pi}{3}) \\ \frac{1}{2} & \frac{1}{2} & \frac{1}{2} \end{bmatrix} = \begin{bmatrix} u_a \\ u_b \\ u_c \end{bmatrix} \tag{1.23}
$$

where $\Theta = \omega t + \delta_A$ is the angle between the rotating and fixed coordinate system at each time t and δ_A is an initial phase shift of the voltage.

The inverse transformation from the $dq0$ frame to the abc frame:

$$
\begin{bmatrix} u_a \\ u_b \\ u_c \end{bmatrix} = \begin{bmatrix} cos(\Theta) & -sin(\Theta) & 1 \\ cos(\Theta - \frac{2\pi}{3}) & -sin(\Theta - \frac{2\pi}{3}) & 1 \\ \cos(\Theta + \frac{2\pi}{3}) & -sin(\Theta + \frac{2\pi}{3}) & 1 \end{bmatrix} = \begin{bmatrix} u_d \\ u_q \\ u_0 \end{bmatrix} \tag{1.24}
$$

1.3 Analysis methods of harmonics propagation

In this study we focus on the methods of analysis in frequency-domain like the ones described below. Therefore methods of harmonic analysis in time-domain like Fourier Series, Discrete Fourier Transform (DFT) or Fast Fourier Transform (FFT) etc. are not included in this description.

The phenomenon of harmonic resonance seems well understood in the literature, however tools available to analyse it are very limited [5]. Method of frequency scan (frequency sweep) is the most general and common method to identify the resonance frequencies in networks [6]. However, this method is limited. The resonance is between two elements (capacitive and inductive) in the system and networks usually consists of many elements. The result of frequency sweep does not indicate which elements exchange energy between each other, causing resonance.

The method of Harmonic Resonance Modal Analysis (HRMA) was developed to face this problem [5]. This method involves only analysis of parallel resonance which is more dangerous in the power system. From HRMA the buses which excite a particular resonances can be identified. Thus, we can observe which components are more involved in a resonance than other. From these results we can conclude where a resonance can be observed more easily or how far the resonance can propagate in the system [5].

1.3.1 Frequency Sweep

Frequency Sweep (or Frequency Scan) analysis is a characterization of the system equivalent impedance at a bus in the system as a function of frequency [7]. As the result, curve of impedance in frequency domain is obtained. The peaks in the curve suggest frequencies when parallel resonance occurs (very high impedance at certain frequency) while dips indicate the frequencies when series resonance occurs (very low impedance at certain frequency).

In Wind Power Plants frequency scans are often done at various grid locations or at the collector bus [7]. The magnitude of computed impedances depends also on the level of equivalent voltage used in the calculations. However, the single value of identified peak impedance does not determine if the resonance occurs. For harmonic problems, there must also be a sufficient level of harmonic source voltages or currents at or near the resonant frequency to excite the resonance [7]. Also, the impedance value itself has to be analysed in particular case to identify the value that causes harm. To do this, the best way is to obtain specific data by measurements, but also data provided by manufacturers of devices in the network.

1.3.2 Harmonic Resonance Modal Analysis

The method is based on analysis of well-known admittance matrix - $\boldsymbol{Y}$. It focuses on the large elements of inverted $\boldsymbol{Y}$. In the extreme case (very large elements) the admittance matrix tends to singularity and element of inverted $\boldsymbol{Y}$ tends to infinity, thus very high voltages can be produced, which is in principle parallel resonance.

The elements are identified on the basis of eigenvalues of $\boldsymbol{Y}$ matrices. Since matrix becomes singular when even one of the eigenvalue becomes zero, the principle can be clearly used. Eigenvalues correspond to certain mode of harmonic resonance, therefore the study consists of identification of critical resonance modes. The equations describing the method including the identification of certain buses and elements are presented below.

The admittance matrix on the network is constructed for certain frequency $\boldsymbol{Y_f}$. Admit-

tance matrix fulfils equation:

$$\boldsymbol{V_f} = \boldsymbol{Y_f^{-1}} \boldsymbol{I_f} \tag{1.25}$$

where: $\boldsymbol{Y_f}$ is the network admittance matrix $\boldsymbol{V_f}$ is the nodal voltage and $\boldsymbol{I_f}$ is the nodal current injection. All matrix values are at frequency f.

To investigate if $\boldsymbol{Y_f}$ approaches singularity, the theory of eigen-analysis is applied. According to [8], matrix $\boldsymbol{Y_f}$ can be decomposed into (index f is neglected in the next equations for simplicity):

$$\boldsymbol{Y} = \boldsymbol{L} \cdot \boldsymbol{\Lambda} \cdot \boldsymbol{T} \tag{1.26}$$

where $\boldsymbol{\Lambda}$ is the diagonal eigenvalue matrix and $\boldsymbol{L}$ and $\boldsymbol{T}$ are the left and right eigenvector matrices.

Defining $\boldsymbol{U} = \boldsymbol{TV}$ as the modal voltage vector and $\boldsymbol{J} = \boldsymbol{TI}$ as the modal current vector, the equation can be derived:

$$\boldsymbol{U} = \boldsymbol{\lambda^{-1}} \boldsymbol{J} \tag{1.27}$$

or

$$\begin{bmatrix} U_1 \\ U_2 \\ ... \\ U_n \end{bmatrix} = \begin{bmatrix} \lambda_1^{-1} & 0 & 0 & 0 \\ 0 & \lambda_2^{-1} & 0 & 0 \\ 0 & 0 & ... & 0 \\ 0 & 0 & 0 & \lambda_n^{-1} \end{bmatrix} = \begin{bmatrix} J_1 \\ J_2 \\ ... \\ J_n \end{bmatrix} \tag{1.28}$$

where each λ^{-1} has the unit of impedance and is named modal impedance Z_m. From matrix Equation 1.26, one can easily identify the location of resonance in the modal domain due to corresponding modal currents and voltage. If $\lambda_1 = 0$ or is very small, a small injection of modal 1 current J_1 will lead to a large modal 1 voltage U_1 [5]. Thus, we can identify that a resonance takes place for specific mode (or modes) and it is not related to a particular bus injection since the values are in modal domain. The smallest eigenvalue is called the critical mode of harmonic resonance and its left and right eigenvectors are the critical eigenvectors.

The modal currents J are a linear projections of the physical currents in the direction of the first eigenvectors by: $\boldsymbol{J} = \boldsymbol{TI}$. Also the physical nodal voltages are related to the modal voltages by: $\boldsymbol{V} = \boldsymbol{LU}$. More details in [5]. In summary, the critical eigenvectors characterize the excitability of the critical mode (right critical eigenvector) and observability of the critical mode (left critical eigenvector). The excitability and observability of modes are characterized with respect to the location.

It is also possible to combine the excitability and observability into a single index according to the theory of selective modal analysis [9]:

$$\boldsymbol{V} = \boldsymbol{L\Lambda^{-1}TI} \tag{1.29}$$

However, this approximation is made possible because $1/\lambda_1$, the critical modal impedance, is much larger than the other modal impedances. If there are more impedances at the similar level as critical impedance, we will observe some inaccuracies in the results.

Assuming one critical modal impedance, much larger than the others, the diagonal elements of the above matrix $\boldsymbol{LT}$ characterize the combined excitability and observability of the critical mode at the same bus. They are called participation factors (PF's) of the bus and are defined as follows [5]:

$$PF_{bm} = L_{bm} \cdot T_{mb} \tag{1.30}$$

where b is the bus number and m is the mode number.

From the calculation on the basis of admittance matrix and the approximation above (Equations 1.26 - 1.30) we obtain: the set of participating factors for each bus for each critical mode (the modes when the modal impedance peaks), which occurs for certain frequency at certain number of mode. Moreover, if approximation of only one critical impedance is right, the participation factors of all buses sum up to 1, therefore the comparison of participation factors between buses is simple and we express them in percentage values.

Critical Modes and Resonance Condition comparison between FS and HRMA As mentioned, resonant conditions identified in this method depends on the value of eigenvalue, which is very small if resonance occurs. This is equal in other words to very high modal impedance. As seen from comparison with frequency scan impedance curves, the sharp peaks occur for the same frequencies. One has to remember that in frequency scan method, the impedance curves are seen from the certain point in the grid, while in HRMA the impedance curves are divided into modes, which does not correspond exactly to the physical buses, even though the number of modes and the number of buses is the same.

Moreover the values of maximum impedances at peak point from both methods are different. The reason is again due to comparison between *real* impedance and *modal* impedance. Modal impedance should be investigated referring to every specific case in order to identify the threshold value or the range, above which the harmful resonance occurs. In this study, values of interests identified by both methods are the frequencies when resonances occurs, therefore the harmful impedance, neither real nor modal are not identified.

1.4 Harmonics in Wind Power Plant

Wind Power Plants, due to intermittency of the wind, are usually supported by great number of power electronic converters which enable effective operation of WPP. These non-linear devices are sources of significant amounts of harmonics in Wind Farms.

Harmonics produced by converters first of all are introduced into inner grid of WPP. Before any waveform produced by wind turbines and converted by wind turbines converters is introduced into the power system (through PCC between WPP and external grid), it is exposed to dangerous phenomenon of harmonic resonance in inner grid of WPP.

Internal harmonic resonance depends essentially on the elements that the inner grid consists of (including possible HVDC link converter) and the way of their connection (topology). As described in Section 1.2.4 harmonic resonance contributes to amplification

of existing harmonics and is able to create new harmonic components.

As the result, overall external emission of harmonics (to the power system) from Wind Power Plants, if the WPP is not decoupled by HVDC link, first of all depends on [1] (1) converter topology, (2) applied harmonic filters and (3) short-circuit current at PCC. These three features has to be completed by the above problem of (4) internal harmonic resonance in the WPP inner grid. If the wind farm is connected by HVDC link, then the emission of harmonics to the external grid depends on the DC/AC conversion at the PCC behind HVDC connection. Even though, the emission to the grid of such a WPP is not a problem, harmonic phenomena still creates a many issues in the inner WPP AC grid.

Main focus of the thesis is understanding and description harmonic resonance appearing in inner grids of Wind Power Plants. Moreover, stability issues due to the harmonic resonance are put forward. As mentioned in the Section 1.1, the analysis of these problems has recently become very important due to serious problems observed in first HVDC connected offshore wind farm during its first years of operation. For future implementation of HVDC connected offshore WPP the problem is currently investigated.

1.4.1 Converter topology in WPP

Topology of WT-converters in WPP's is partially determined by the electrical machine that is used in wind turbine to generate electricity. According to the level of power that flows through a converter, full scale converter can be distinguished. It provides control over total power produced in generator. On the other hand, there are also Wind Turbine application where only part of the power produced can flows through converter. The ratings of the converter, so also its costs, are reduced, however control of the power produced in wind turbine is limited.

Within the full-scale converters, the most popular utilized in these days in wind turbines are: 2-level converters, 3-level NPC converters, multi-level converters, also matrix converters and tandem converters [10].

Regarding the harmonics propagation problem from each WT-converter, when it comes to the scale of the wind farm, as stated in [1], the greater the number of turbines the lower is the magnitude of the harmonics and subharmonics, especially of the lower order.

In this study, only models of full rate wind turbine converters are considered. On the other hand, HVDC link converter is modelled with respect to principles described in the Section 1.6.4.

1.4.2 Control of harmonics and harmonic resonance

The two main methods for controlling harmonics in WPP are avoiding producing of harmonics and implementing filters to mitigate them [7]. To avoid the production of harmonics, network of WPP has to be designed properly, however implementation of harmonic filters anyway can be necessary due to topology changes or even very insignificant modifications which change resonance levels. The designing of filters should be based on measurements and simulations in order to control resonance properly.

Second method - implementation of filters - is the most common approach to the harmonic resonance [7]. The design and implementation of filters is not considered in this study, however the HRMA method presented is crucial for identification of the buses which are potentially more appropriate for filters implementation.

1.4.3 Short circuit current at PCC

From the main grid side, the short circuit level at the point of application is also not fixed. It varies with operational condition in the grid. The weaker the external grid, the more it varies usually, therefore the resonant frequency can float around. These fluctuations are not considered in the thesis.

1.4.4 Internal WPP resonance

The phenomenon of electrical resonance is described in section 1.2.4. As mentioned, if the resonance is not properly controlled, it leads to failures, instabilities, shut-downs or even damage of components. If the internal grid of WPP is separated from external grid for example by HVDC connection, electrical behaviour of the WPP grid can be different from the main grid.

In such a WPP inner grid there is no rotating mass that establishes physical binding of power and frequency [11]. Thus, the frequency of internal WPP and the infeed from the WTs can and should be completely controlled by converters. Moreover, every converter has its own control schemes that can have a bandwidth of several hundred hertz. Thus, converters are able to amplify oscillations which are in the system [11].

The resonance in Wind Power Plant is the main reason of the instability in first HVDC connected offshore WPP, described in motivation part of the thesis (section 1.1).

1.5 Stability of WPP

In VSC converters the bandwidth of control signals are several times of the fundamental frequency. Such high-frequency control introduces dynamics above fundamental frequency, creating potential for high frequency instabilities and resonances that are not present in CSC [12]. Since the VSC does not need reactive power support, has higher controllability and the ability of black start the system, this type of converter is getting more popular in new Wind Farms.

In the offshore WPP Bard Offshore 1 VSC converters are utilized [11]. However the problem of grid resonances caused by these converters was not considered during planning phase of the WPP. Therefore, stability problems due to converters interactions were not considered.

As stated in [13] and [12] converters could go into resonance with the grid causing instabilities if the grid impedance exceed the input impedance of the converter. On the basis of this statement, the analysis of stability is performed. The essence of the method is presented in [14]. Stability problems happen due to more advanced nonlinear power electronics included in the converters. The problem of modelling converter impedance

nonlinear behaviour is described in Section 1.6.4.2. This sort of problems does not occur between, for example, synchronous generators since power electronic elements influence in these elements is limited.

1.5.1 Harmonic Stability

The stability criterion based on Nyquist stability criterion is described in [13] and is still under development [11]. The main advantage of this method is that it does not require all details about converter which are always considered as intellectual property of manufacturers. Due to this advantage it could be right choice at the planning phase of an investment. Only frequency dependent impedances of converter are needed [11]. The method also avoids the need to remodel each inverter and repeat its loop stability analysis when the grid impedance changes [13].

In contrast to EMT simulations and eigenvalue analysis only relatively simple stability criterion is developed. Thus, this method is very fast and can evaluate new topology if any switching action occurs [11]. The simplicity is achieved by aggregation of all wind farms with their controllers into one element. Then, the aggregated system is evaluated by Nyquist stability criterion that provides information about gain and phase margin. As mentioned, the manufacturers have to provide only frequency dependent impedance of their generation unit (converter), including passive elements impedance and impedance changes due to active controls. In other words, the main advantage of this approach is that the frequency dependent impedance can be calculated with analytic model (providing appropriate data from manufacturer) or calculated with an EMT-tool but also measured at a real generation unit [11].

1.5.2 Stability evaluation model

With the proper data and assumptions described above, we use the simple model to evaluate the stability consisting of voltage source with internal impedance and the impedance of the grid (Figure 1.7) [11, 13].

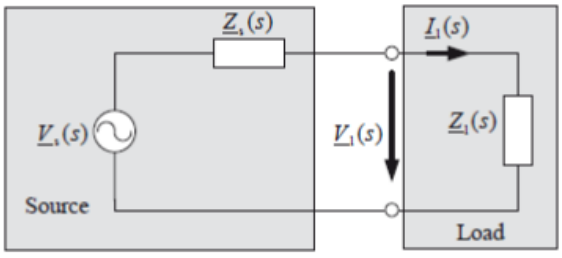

Figure 1.7: Stability analysis first model.

In such a network the current I_g depends on both Z_s and Z_g impedances:

$$I_g = \frac{V_s(s)}{Z_s(s) + Z_g(s)} = \frac{V_s(s)}{Z_g(s)} \frac{1}{1 + \frac{Z_s(s)}{Z_g(s)}} \tag{1.31}$$

The equation of the network $_Ig$ current (Eq. 1.31) can be expressed in as loop gain for the system in the Figure 1.8.

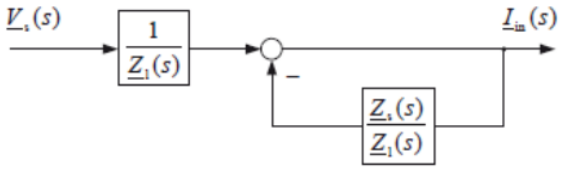

Figure 1.8: Loop gain corresponding to the stability model.

On the basis on the equation (Eq. 1.31) we conclude that the system is stable if the source has a zero and the load an infinite output impedance. For stability, the value of ratio $|Z_s(s)/Z_g(s)|$ has to be at least below 1 to for all frequencies [13] in other words the system is table if $Z_s(s)/Z_g(s)$ satisfies the Nyquist stability criterion [14].

The first problem with the model above is the point division between Z_s and Z_l. The best point of division is still under investigation [11]. In this study the network is divided behind the HV transformer from the HVDC link point of view (Bus 2) (see Figure 2.2).

There is also other conceptual problem with the presented approach. As either the inverter of WT of HVDC inverter could be treated as the source, the results about stability conclusions are very different [13]. In this study we perform only one approach where the aggregated WT converter is treated as source and HVDC link converter as grid and the point of division is always as described above.

Finally, the stability criterion requires frequency impedances of converters which could be modelled as either voltage or current sources. The problems and details about these two models are explained in [13]. The source part and the grid part of the network can be modelled by its Thevenin equivalent circuit (voltage source) or Norton equivalent circuit (current source). The Thevenin model for stability criterion was presented above. However, it is also possible to represent converters by current source [13] (Figure 1.9).

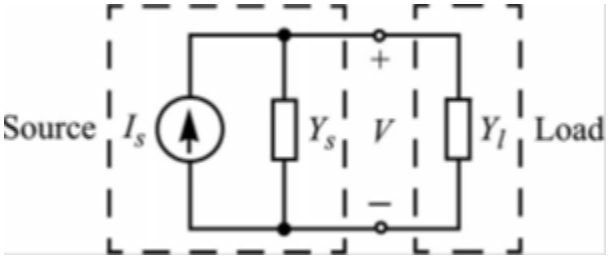

Figure 1.9: Stability analysis second model.

The stability criterion is, analogically to (Eq. 1.31), based on the system equation:

$$V(s) = I_s(s)Z_g(s)\frac{1}{1 + Z_s(s)/Z_g(s)} \tag{1.32}$$

where, for stability, the ratio of the load input impedance to the source output impedance should meet the Nyquist stability criterion.

Comparing (Eq. 1.31) to (Eq. 1.32) one can see that stability requirement for CS system is opposite to that for VS system. The distinction between these models is described

in [13]. The author states also that the most common grid model is hybrid system combining current and voltage sources (Figure 1.10). Applying hybrid model to the case of this study, the wind turbine inverter is modelled as a current source while, the HVDC rectifier is modelled as voltage source.

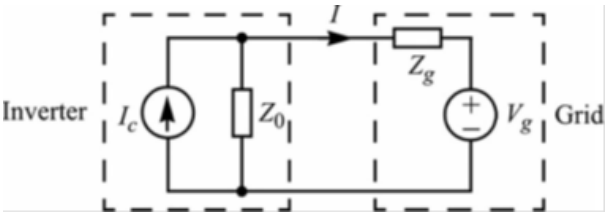

Figure 1.10: Stability analysis hybrid model.

The assumptions of the stable system without the inverter and the stable inverter when grid impedance is zero are still applicable.

Then, the current in the system is:

$$I(s) = \left[I_s(s) - \frac{V_g(s)}{Z_s(s)} \right] \cdot \frac{1}{1 + Z_g(s)/Z_s(s)} \tag{1.33}$$

And the Nyquist stability criterion of this system is: $Z_g(s)/Z_s(s)$.

1.5.3 Stability assessment

From the examples and assumptions described above, we assess the stability *source* and *grid* are plotted in a Bode diagram for positive and negative sequences. From Bode diagram, each intersection of grid curves with source curves could be critical and has to be investigated. For each intersection, phase margin between appropriate curves (curves that intersects) will be calculated according to:

$$\phi_m = 180^\circ - \Delta\phi \tag{1.34}$$

where $\Delta\phi$ is the phase difference between curves in degree. If the phase margin calculated in such a way is below 30° the system can be instable [11]. As aforementioned the stability assessment is performed for specified point of division and specified *source* and *grid* sides.

1.6 Modelling of elements

1.6.1 Transformers

For harmonics modelling of transformers in electrical grid models for very high frequencies a generally not necessary. For higher frequencies resistance increases, while the leakage inductance reduces [1]. In this study, two- and three- winding transformers impedances will be represented simply by its resistance and inductance as follows:

$$Z_{tr}(f) = R_{tr} + jX_{tr}(f_h/f_1) \tag{1.35}$$

where R_tr and X_tr correspond to fundamental frequency resistance and reactance. The skin effect and eddy currents effect the resistance at higher frequencies, therefore we do not consider these effects.

1.6.2 Cables

Modelling of cables is important in harmonic analysis since they are very significant source of capacitance in considered grids. For harmonic frequencies up to 3000Hz the resistance of cables will increase. The slight effect of decrease in inductance and shunt capacitance can be ignored [1]. PI models are considered as appropriate for frequency scan analysis, but not for transient analysis. Usually, exact frequency-dependent model is obtained by Finite Element analysis [1], however in this study exact methods of cable models are not considered. Elements of Pi model of the cables is described by:

$$\begin{aligned} Z_{cable}(\omega_f) &= R_{cable} + j(\omega_f/\omega_1)L_{cable} \\ Y_{cable}(f) &= j(\omega_f/\omega_1)C_{cable} \end{aligned} \tag{1.36}$$

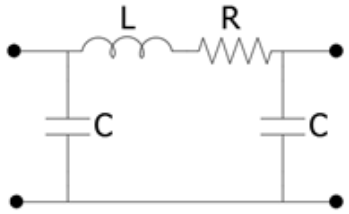

Figure 1.11: PI model circuit of the cables.

1.6.3 Filter reactors

Filter reactors modelling is important since it significantly affects the tuning of whole system. Resistance of the filters at high frequencies can be calculated as follows:

- For aluminium reactors: $R_h = \left[\frac{0.115h^2+1}{1.15}\right] R_f$
- For copper reactors: $R_h = \left[\frac{0.015h^2+1}{1.055}\right] R_f$

In the models presented, series resistance of LCL filters and resistance of phase reactor is neglected (equals zero).

1.6.4 Power converters

Modelling of power converters is the most crucial and challenging within all elements. Power converters devices are very nonlinear and their impedance behaviour strongly

depends on many factors. The exact model should be derived on the basis of control codes, ideally also on the basis of measurements on the real device.

Control codes are very unique and never published by the manufacturers. Control codes are considered their intellectual property and thus the determination of the exact frequency is very difficult [11]. There are also more simple approaches to face the problem of converter modelling. The principles presented below are considered for frequency domain analysis. EMT (electromechanical transient) analysis is not considered.

1.6.4.1 Voltage Source (VS) and Current Source (CS) models

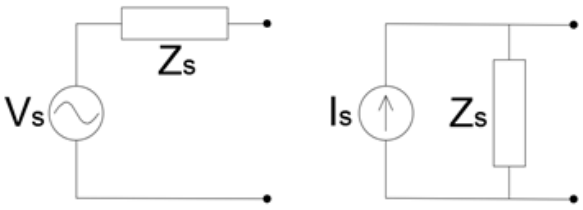

Figure 1.12: Ideal voltage and current source models.

It is common to approach modelling of converters as either current or voltage source. As stated in [11], current sources should be only used if the grid impedances are similar. Otherwise it leads to very inaccurate harmonic current values and wrong results. Therefore, voltage sources should be modelled instead and the input impedance should be considered.

There is very important fact to be considered for both approaches in frequency domain analysis. According to circuit theory, ideal voltage source internal resistance is zero (short-circuit). On the other hand, the ideal current source internal resistance is infinite (open-circuit).

In this study, models with either ideal current source or voltage sources are considered for comparison in FS method and HRMA method. For those models, internal impedance of source (VS or CS) Z_s is zero or infinite, respectively. The third model of converter is described in the following section and is based on voltage source with nonzero, nonlinear internal impedance Z_s (nonideal VS). For stability study the principles of converters modelling and stability assessment are described in Sections 1.5.2-1.5.3.

1.6.4.2 Frequency dependent impedance model Z(s)

The models of either voltage source or current source described in the previous section are very important, however for the resonance analysis the value of series impedance (in case of voltage source) or parallel impedance (in case of current source) is crucial. The voltage and current sources themselves should be open-circuited or short-circuited, respectively. The approach developed in [12] and [15] of frequency dependent impedance of converters is introduced to this study and described below.

The authors, by applying appropriate modelling method, such as harmonic linearization presented in [**?**, 16], obtain impedance models valid below and above the fundamental frequency [12]. Each converter is described by positive- and negative-sequence impedances

without cross coupling [17]. The Park's transformation, described in Section 1.2.7 is also crucial to derive the converters impedances equations.

The assumed converters modelled are [12]: 2-level VSC Wind Turbine DC/AC inverter and the same type of HVDC AC/DC rectifier. Models of these converters are then used in the simulation.

Wind turbine converter (inverter) For the control purposes, wind turbine converter is controlled as current source. Due to this fact, the device behaves more like current source and the control will be modelled in this way. Reactive power supply and voltage regulation of the model is not considered. A phase-locked loop (PLL) is included in the model for AC bus synchronisation [12].

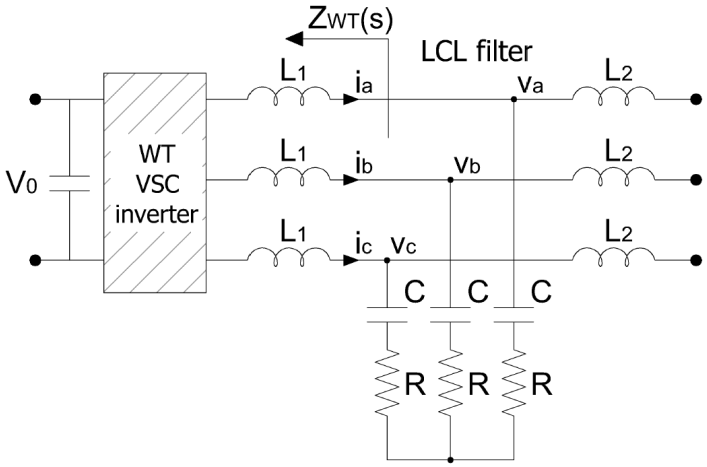

Figure 1.13: Aggregated wind turbine converter impedance model.

The wind turbine model is described in dq-frame. As mentioned, the current control scheme is used. The reference value is the current provided be the DC link voltage regulator. The current compensator transfer function is given:

$$H_i(s) = K_p + \frac{K_i}{s} \tag{1.37}$$

The PLL is implemented using PI regulator. Including the integrator to convert frequency into angle, the PLL compensation transfer function becomes:

$$H_p(s) = \left(K_p + \frac{K_i}{s}\right)\frac{1}{s} \tag{1.38}$$

The values of parameters are specified in Chapter II.

For the stability study, the wind turbines are lumped into one device (one impedance). The output impedance of WT inverter is developed using the harmonic linearization method described in [16]. As the result, converters are represented by positive-sequence and negative-sequence impedances without cross coupling [17]. Providing constant DC bus voltage (as the reference) the impedances become:

$$Z_p(s) = \frac{H_i(s - j\omega_1)V_0 + (s - j\omega_1)L}{1 - T_pll(s - j\omega_1)[1 + H_1(s - j\omega_1)I_1V_0/V_1]}$$
$$Z_n(s) = \frac{H_i(s - j\omega_1)V_0 + (s - j\omega_1)L}{1 - T_pll(s - j\omega_1)[1 + H_1(s - j\omega_1)I_1V_0/V_1]} \quad (1.39)$$

where ω_1 is fundamental angular frequency, $T_pll(s)$ is the loop gain of dq-frame PLL defined by:

$$T_pll(s) = \frac{V_1H_p(s)}{2[1 + V_1H_p(s)]} \quad (1.40)$$

and H_i and H_p are the current an PLL compensator transfer functions, as defined before.

HVDC link converter (rectifier) In case of HVDC converter, the device is controlled to behave as a voltage source at the ac terminals [18]. Figure 1.14 demonstrate the model for HVDC converter impedance calculation.

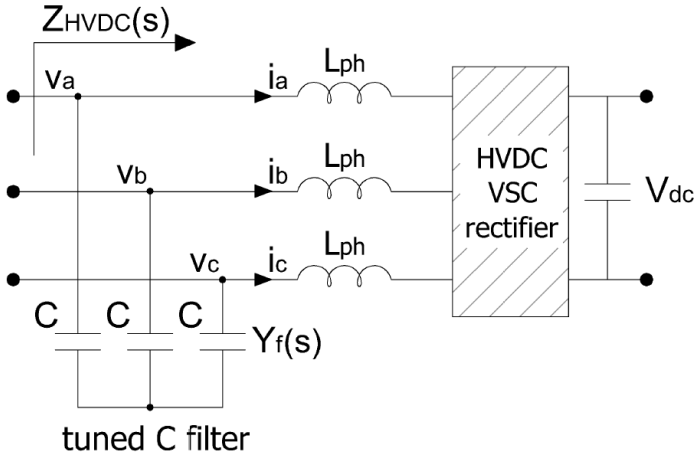

Figure 1.14: HVDC-link converter impedance model.

The HVDC rectifier voltage control is performed by a PI regulator in the dq-reference frame [12]:

$$H_v(s) = K_p + \frac{K_i}{s} \quad (1.41)$$

A current loop is embedded within the voltage loop and the current compensator transfer function is defined as:

$$H_i(s) = K_p + \frac{K_i}{s} \quad (1.42)$$

Other control approaches could be incorporated but are not considered. The values of parameters are included in Chapter II.

Again, the assumption of constant DC-link voltage (V_dc) is made. The resulting positive- and negative-sequence input impedance are given by:

$$Z_p(s) = \frac{H_i(s - j\omega_1)V_dc + sL}{1 + Y(s)[H_i(s - j\omega_1)V_dc + sL] + T_p(s)}$$
$$Z_p(s) = \frac{H_i(s + j\omega_1)V_dc + sL}{1 + Y(s)[H_i(s + j\omega_1)V_dc + sL] + T_n(s)} \quad (1.43)$$

where ω_1 is fundamental angular frequency, $Y(s)$ is admittance of the ac filter, $T_p(s)$ and $T_n(s)$ are defined as:

$$T_p(s) = [H_i(s - j\omega_1) + jK_id]H_v(s - j\omega_1)V_dc$$
$$T_n(s) = [H_i(s + j\omega_1) - jK_id]H_v(s + j\omega_1)V_dc \quad (1.44)$$

and $H_i(s)$ and $H_v(s)$ are the current and voltage compensator transfer functions defined before.

As described in [Sun 2014],... Why do we ignore the frequencies around fundamental...?

1.7 Harmonics and power quality regulations

In this chapter the harmonic distortion limitations according to some standards are described. It is worth of mentioning that harmonics are not the only problem of power quality in power system. Power quality includes more electromagnetic phenomena which are categorized on the basis of duration (from nanoseconds, like lightning strokes) to steady state disturbances (e.g. harmonics and interharmonics) [1]. The other than harmonic frequency power quality issues are not of concern in this study.

Moreover, considered HVDC connected off-shore WPP is not directly connected to the external grid. The connection is realized through HVDC link, therefore the harmonic phenomena occur before PCC i.e. within the inner WPP grid. Before being emitted to the main grid distorted waveforms are converted to DC waveforms. However, the harmonic content of the inner WPP grid influences the performance of the HVDC converter, therefore the limits should also be considered.

One of the standard that provides information about harmonics and interharmonics and is internationally accepted is [19] IEC Standard Series 61000. Moreover, there are EN standards like [20] EN 50160 approved by European standardization body CENLEC. EN standards are official standards for European Union. In North America, the harmonic limits are described in [21] IEEE 519. All three mentioned standard are internationally accepted [1].

These standards establish emission requirements such as harmonics, voltage fluctuations, radio frequency disturbance, immunity requirements etc. Some of these requirements are summarized in the sections of this chapter. However, most of the information included would not be utilized in further analysis, even if applicable to the inner WPP networks, since the EMT simulations are not performed in this study. In other words the waveforms for which the harmonic content is assessed do not appear in this study.

The important concept for harmonic emission is point of common coupling (PCC). PCC is the point of metering of power supply for both utility and consumer or any point where both parties can access the point for direct measurement, also for harmonic indices

measurements. It is usually also the point where another consumer can be served from the same system [1].

To be developed...

1.8 Environmental impact

To be developed...

1.9 Temporary planning and cost of the thesis development

To be developed...

Chapter 2

Simulations

2.1 System description

In most of the simulations for harmonic resonance study we consider offshore wind power plant with VSC-HVDC connection to the onshore grid. Total amount of installed wind turbines power is 400MW. The WPP considered has a radial topology consisting of four-branch network. It is assumed that each string (branch) of wind turbines has the same parameters. The layout of the 400MW WPP is presented in the Figure 2.1.

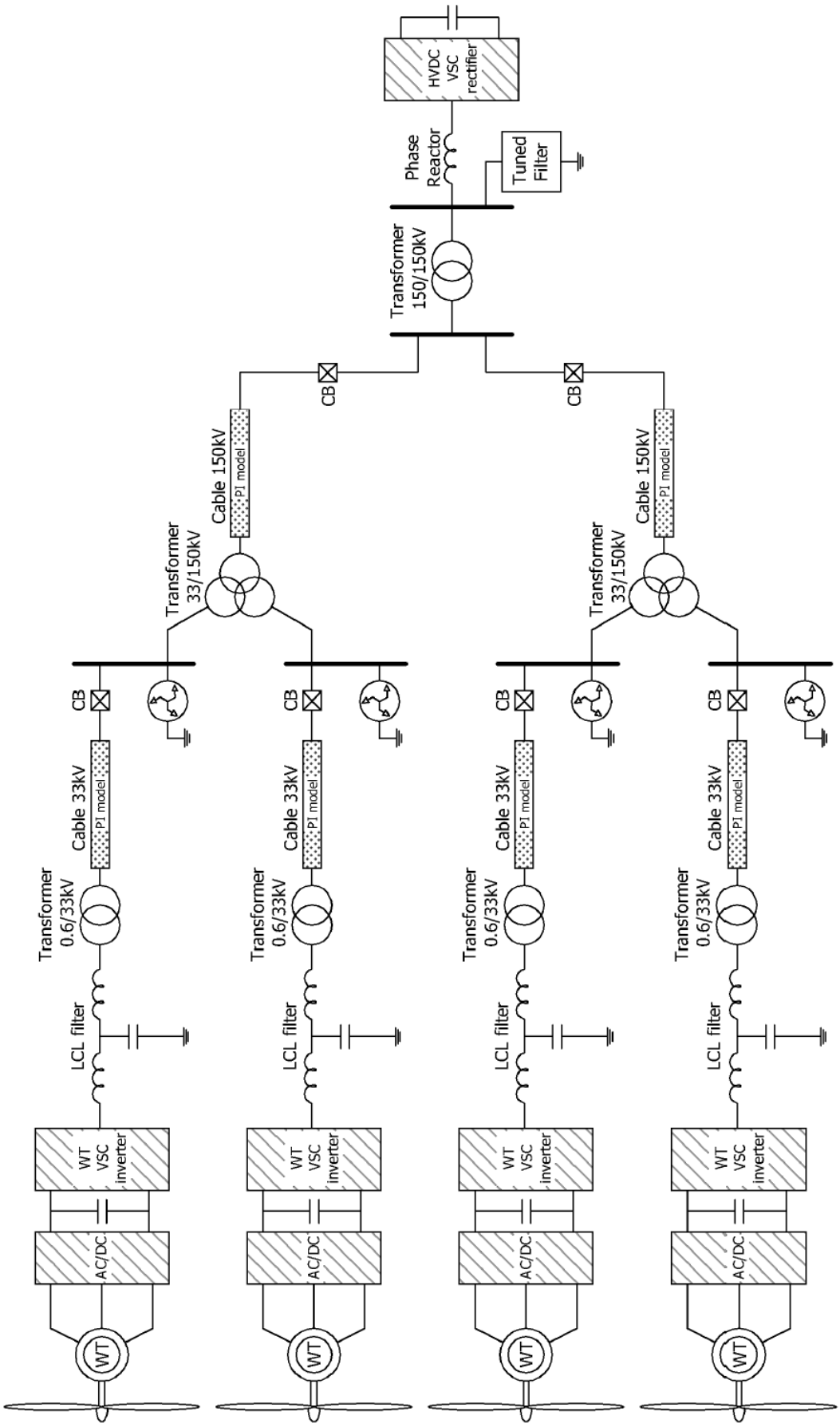

Figure 2.1: Considered 400MW Wind Power Plant

Each of four branch is formed by ten 10-MW wind turbines with a terminal voltage of 690V. The aggregated model of each branch is used where each set of ten turbines is lumped and modelled as a single aggregated turbine, represented by a 100 MW turbine. Each aggregated turbine is connected to the LCL filter. Behind the LCL filter there are elements of collection grid: 690V/33kV transformer and an 8km underground collector cable (33kV). 33kV cable is linked to the 150kV transmission cable with a length of 58km via a 150kV/33kV/33kV three winding transformer with YN-dd configuration. The 150kV transmission cable is tied to the VSC-HVDC rectifier through a 150kV/150kV transformer and a phase reactor with an tuned shunt capacitor filter.

2.1.1 Network impedance model

Equivalent impedance diagram of WPP AC system is shown in the Figure 2.2. All of the parameters are converted to the 150kV equivalent voltage level. Table 2.1 presents the values of parameters in the network. The impedances of VSC-WT inverters and VSC-HVDC rectifier are calculated on the basis of three different methods presented in Section 1.6.4. The resulting impedances are presented in Section 2.1.3.

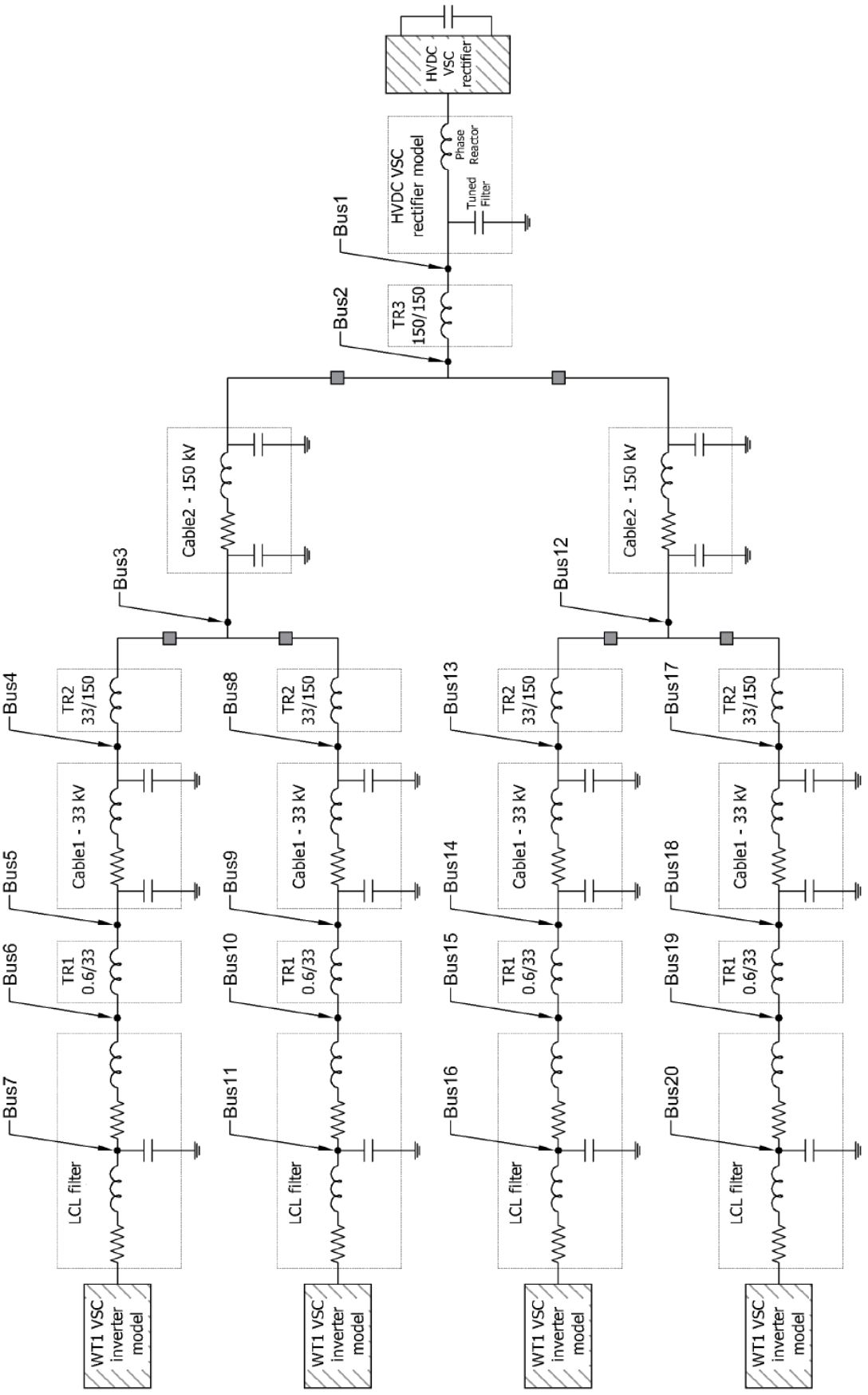

Figure 2.2: Impedance diagram of the WPP network.

Table 2.1: Basic data of the system element at the equivalent voltage level of 150 kV.

Component	Symbol	Value at 150 kV
Phase reactor	L_{ph}	19.3 mH
Tuned C filter	C_f	5.658 μF
Converter transformer	L_{tr3}	19.338 mH
Cable 150 kV	R_{cab2}	0.056 Ω
	L_{cab2}	1 mH
	C_{cab2}	0.52 μF
MV/HC three-winding transformer	L_{tr2}	38.676 mH
Cable 33 kV	R_{cab1}	0.372 Ω
	L_{cab1}	18.181 mH
	C_{cab1}	57.09 nF
LV/MV wind turbine transformer	L_{tr1}	51.568 mH
LCL filter	L_{LCL1}	1.2 H
	L_{LCL2}	149.1 nF
	C_{LCL}	0.641 H

2.1.2 Topology cases

In the study, we approach comparison between different topologies. There are three topology cases examined. In principle, the difference between three topology depends on the number of included branches with aggregated wind turbines (1, 2 or 4 branches). The buses in the figures have assigned numbers which we employ in further analysis.

- Case 1 model consist of one aggregated WT. In this case only one out of four branches is connected. The other three branches are disconnected by circuit breakers at the lower side of the three-winding transformers. Both branches connected to the lower other 150kV cable are disconnected, therefore this line is also disconnected. The topology of this system is presented in the Figure 2.3.

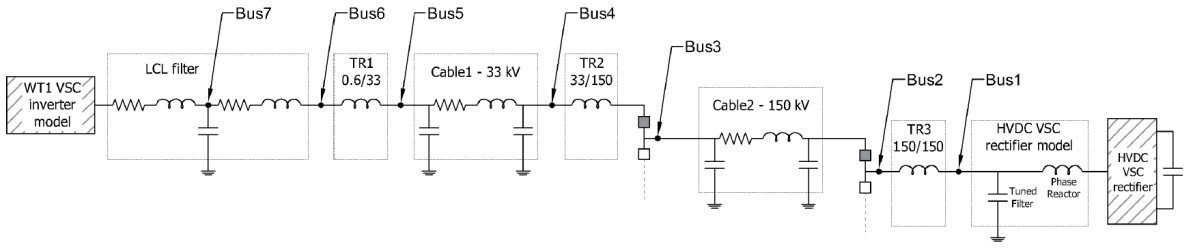

Figure 2.3: Case 1 impedance diagram.

- Case 2 includes one more aggregated turbine branch than Case 1. The second WT branch is connected to the first three-winding transformer. The second 150kV line is still disconnected. The topology of this system is presented in the Figure 2.4.

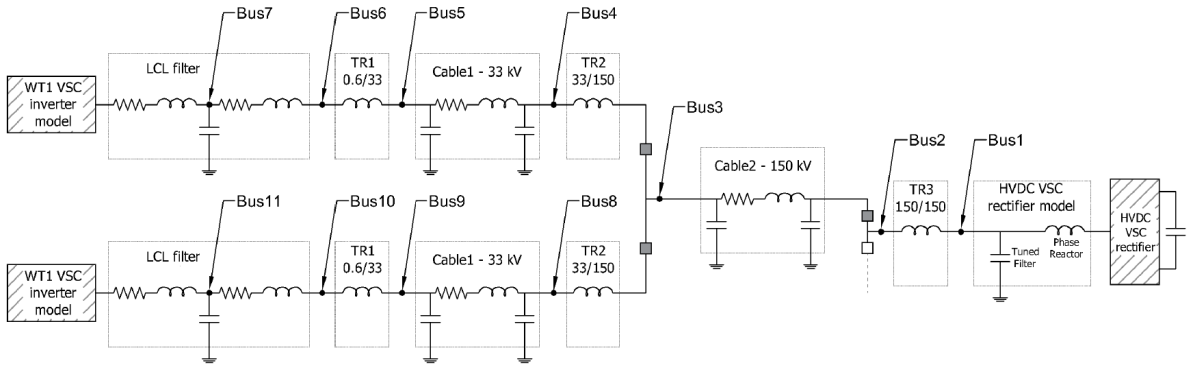

Figure 2.4: Case 2 impedance diagram.

- Case 3 consists of all elements in the networks. All branches are activated, therefore all elements are included in analysis. This topology is presented in the previous section, in the Figure 2.2.

2.1.3 Power converters models

All of the elements excluding converters are modelled as the RLC elements. The principles of modelling of the elements are described in Section 1.6. This section explains also the three different approaches to model converters (Section 1.6.4). In whole Chapter II of the thesis containing results of simulation, for simplicity, we refer to the different models of converters as follows: VS the model where both WT and HVDC converters are modelled as voltage sources (Section 1.6.4.1), $CS - WT$ or CS where WT converter is modelled as a current source and HVDC converter is still represented by voltage source (Section 1.6.4.1), $Z(s)$ where both converters are represented by non-linear impedance models (Section 1.6.4.2).

Following tables (Table 2.2 and Table 2.3) present the values of parameters which are implemented to the models described by equations (1.39) and (1.43). The values are obtained from [12] and [15], however the we rescale values of voltages and currents to the 150 kV equivalent voltage level. These changes are done in order to align the values of obtained impedance to further analysis where we combine the converter models with the other elements of the network which values are also recalculated to the equivalent 150 kV model (Table 2.1).

Table 2.2: WT converter nonlinear impedance model data.

Parameter	Symbol	Value
Dc Bus Voltage	V_0	1500 V
Phase Voltage Amplitude	V_1	563 V
Phase Current Amplitude	I_1	236 kA
Phase Inductance	L	0.526 µH
Output Filter Inductance	L_f	0.5 µH
Output Filter Capacitance	C_f	0.207 F
Output Filter Damping Resistance	R_f	2.75 mΩ
Current Control Compensator $H_i(s)$	K_p	0.44×10^{-6}
	K_i	0.55×10^{-3}
Current Decoupling Coefficient	K_{id}	22.5×10^{-6}
Current Control Bandwidth	f_i	250 Hz
PLL Compensator $H_p(s)$	K_p	0.239
	K_i	45
PLL Bandwidth	f_{pll}	30 Hz

Table 2.3: HVDC converter nonlinear impedance model data.

Parameter	Symbol	Value
HVDC Dc Link Voltage	V_{dc}	300 kV
Phase Voltage Amplitude	V_m	122 kV
Phase Inductance	L	17.9 mH
Ac Filter Inductance	L_f	0.43 µH
Ac Filter Capacitance	C_f	17.7 µF
Ac Filter Resistance	R_f	10 Ω
Current Control Compensator $H_i(s)$	K_p	0.075×10^{-3}
	K_i	0.094
Current Decoupling Coefficient	K_{id}	23×10^{-6}
Current Control Bandwidth	f_i	250 Hz
Voltage Control Compensator $H_v(s)$	K_p	11.1×10^{-3}
	K_i	8.388
Voltage Decoupling Coefficient	K_{vd}	5.56×10^{-3}
Voltage Control Bandwidth	f_v	100 Hz

The results of impedance of both converters for Z(s) model are demonstrated in the Figure 2.5 for WT-converter and in the Figure 2.6 for HVDC converter. Both plots include curves of impedance magnitude and impedance angle for positive-sequence and negative-sequence in the domain of frequency.

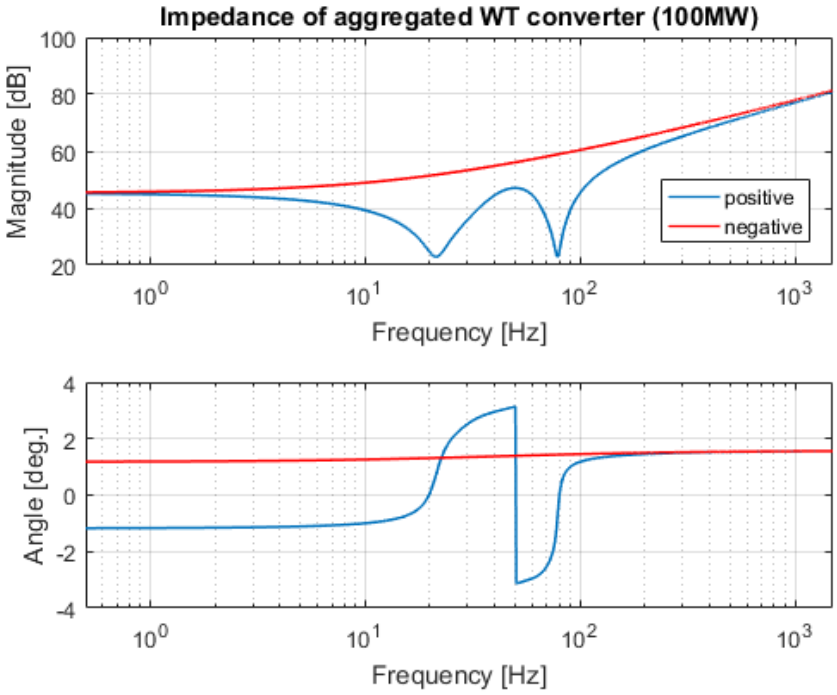

Figure 2.5: WT converter nonlinear impedance model.

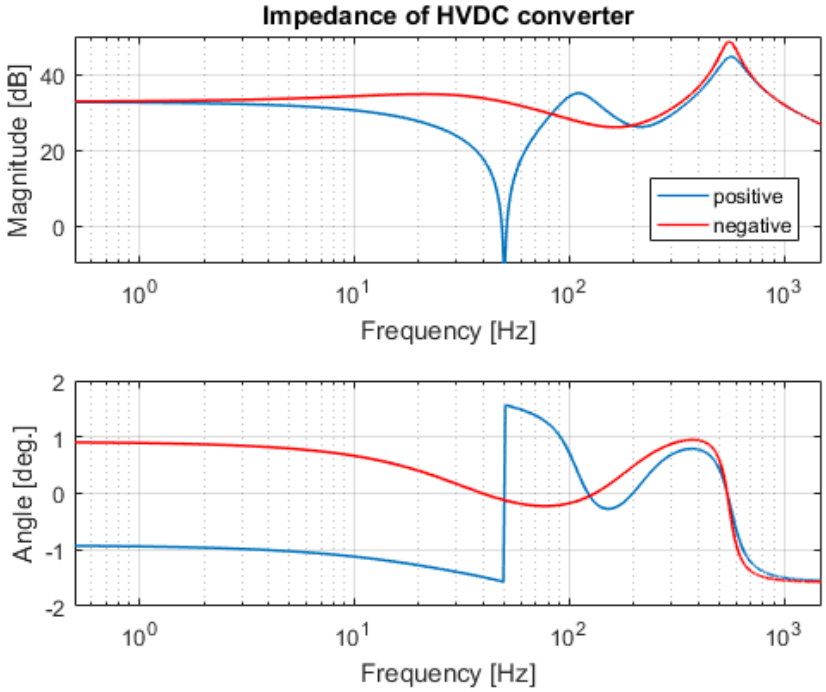

Figure 2.6: HVDC converter nonlinear impedance model.

For both converters, we note sharp changes in the values of positive-sequence impedance angle at the fundamental frequency. On the other hand, the values of magnitudes and angles of negative-sequence are quite smooth for both converters. Moreover, we observe that above second frequency order the curves of positive- and negative-sequences are very close to each other for all four plots.

The results obtained correspond to the results obtained in [12].

2.2 Comparison of resonance frequencies between different topology cases and converter models

The objective of this section is to compare results of harmonic resonances frequencies for three topology cases (Section 2.1.2). The description of modelling converter as VS, CS and Z(s) model can be found in Section 1.6.4. Secondly, on the basis of Harmonic Resonance Modal Analysis, we identify the resonant frequencies again and additionally we spot the buses that have the most significant influence on the particular resonance frequencies. This identification is very useful for further study of implementation of tuning filters, however it is not investigated in this study.

2.2.1 Case 1

Frequency Sweep Figure 2.7 presents implementation of the frequency sweep method. All three models are included. The frequency sweep always refers to the particular node in the network. For this study, the bus number 7 (see Figure 2.3) is the bus of observation. In other words, the impedance is seen from that point in the network.

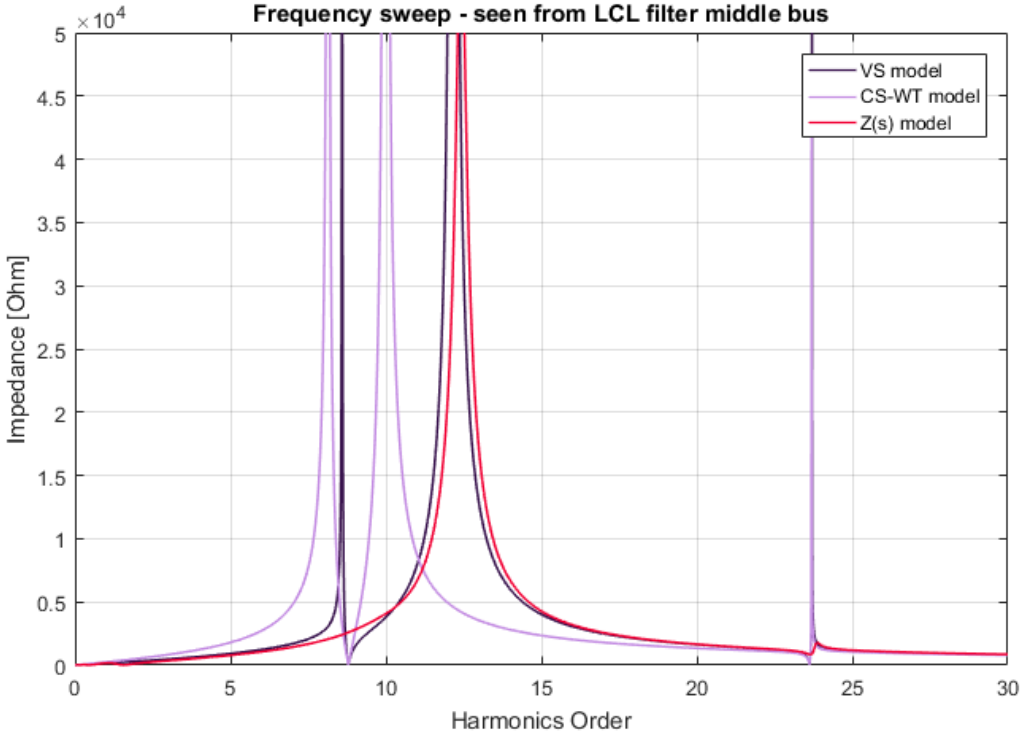

Figure 2.7: Impedance curves from FS - linear.

For the better visibility, the Figure 2.8 presents the same data but with logarithmic vertical axis.

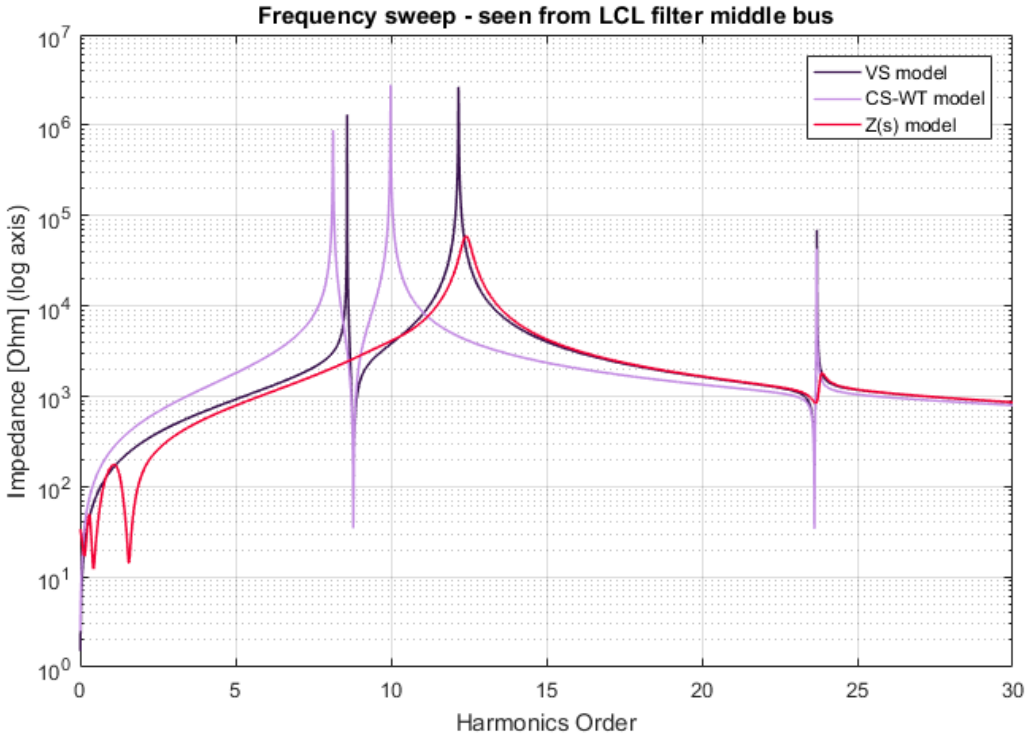

Figure 2.8: Impedance curves from FS - log.

We can clearly see that the resonance frequencies vary for different models of converters. Table 2.4 presents approximate resonance frequencies values. The values of frequencies are identified when impedance reaches local extreme values.

Table 2.4: Results of frequency sweep.

Converter model	Frequency order [-]	Peak impedance [Ω]
VS	8.59	1304 k
	12.17	2655 k
	23.7	69 k
CS-WT	8.14	880 k
	9.99	2787 k
	23.69	43 k
Z(s)	12.42	59 k
	23.87	2 k

Due to the issues with the Z(s) model presented in Section 2.1.3, the result of resonance around fundamental frequency is ignored.

For VS model, within the observed scope, we observe three resonance frequencies. Similarly, in case of CS model there are three resonance frequencies. For the Z(s) model of converters only two resonance frequencies are detected (the lowest resonance is ignored due to the inaccuracies mentioned before).

Moreover, the values of impedance for Z(s) model are reduced comparing to the VS and CS models. The principles of modelling converters by this method leads to higher values of damping. The detailed description is provided in Section 1.6.4.2 and in [12, 15] Why

lower values for Z(s)?

Harmonic Resonance Modal Analysis We compare the results of frequency sweep to the results of Harmonic Resonance Modal Analysis. As mentioned in section 1.3.2, with this method we obtain the values of participation factors which suggest probable buses and thus the elements which influence resonance more than others. The Figures 2.9, 2.10 and 2.11 present the curves of modal impedance in domain of harmonic order.

The Figure 2.9 illustrates the modal impedance for three models. Only maximum modal impedance for each harmonic order is selected and plotted.

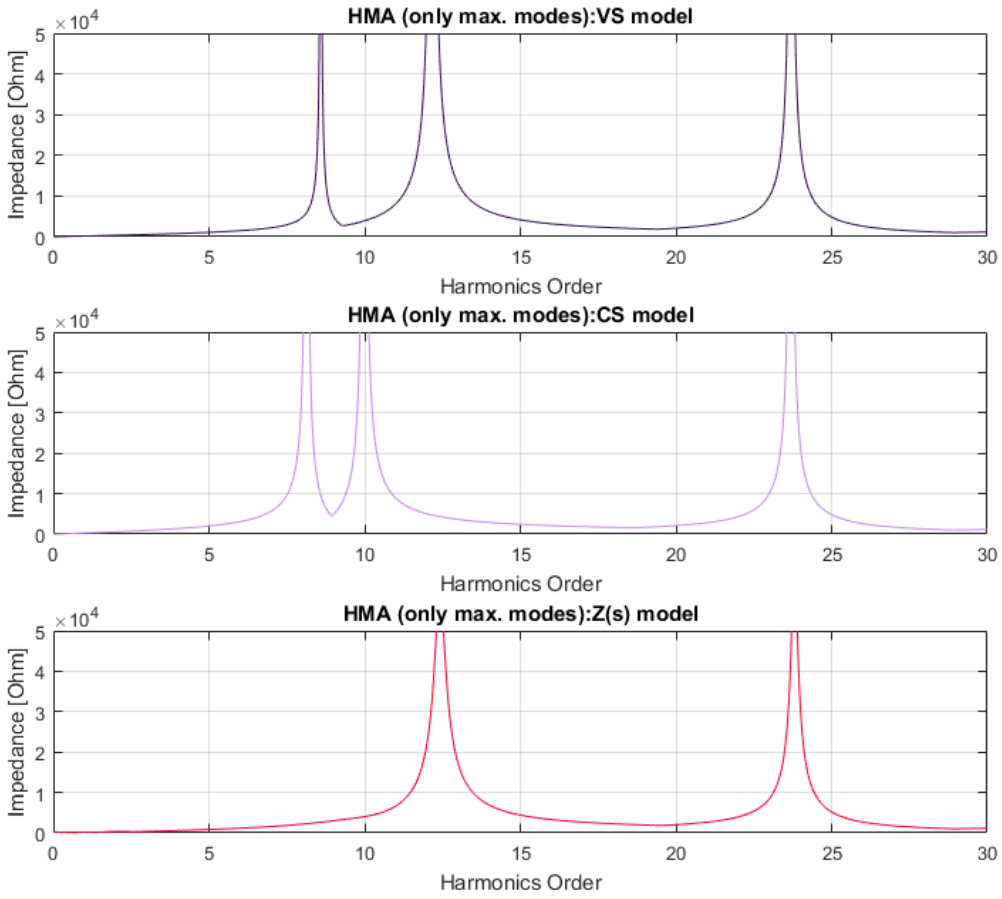

Figure 2.9: Case 1 - HRMA method. Maximum modal impedance curves.

In the Figure 2.10, we can observe the very similar shapes of curves, however, this time all the modes are drawn. Most of the modes are barely visible since they equals zero or very small values for all frequencies.

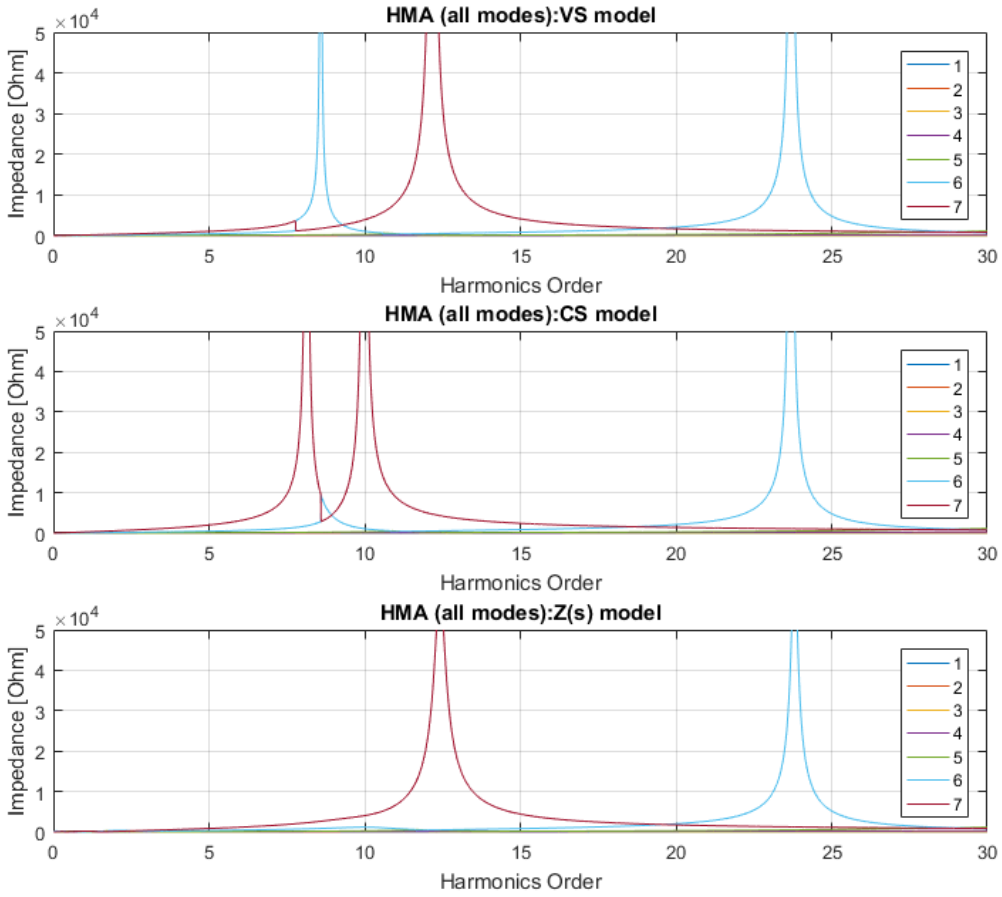

Figure 2.10: Case 1 - HRMA method. Impedance curves of all modes.

The graphs above feature two modes without a doubt - modes 6. and 7. Modal impedance for these modes reaches much higher value at the frequencies of resonance. The modes that determine the resonances are called critical modes. The critical modes impedances are plotted in the Figure 2.11.

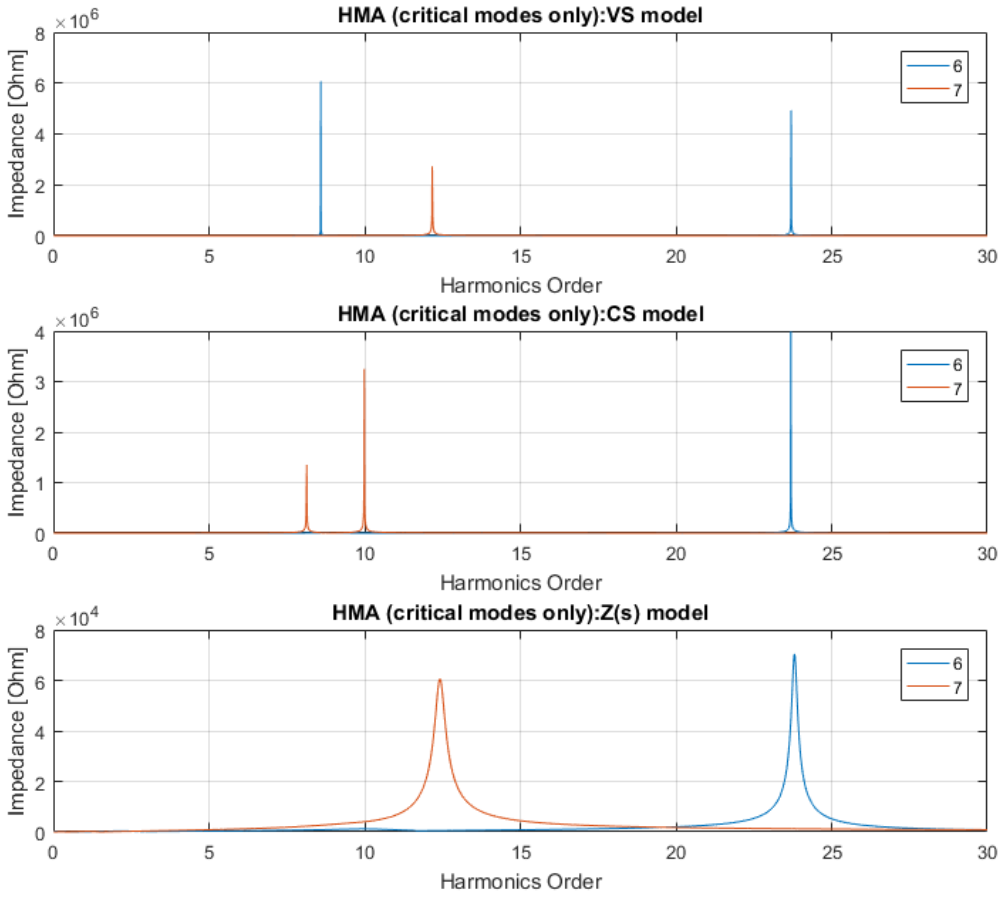

Figure 2.11: Case 1 - HRMA method. Impedance curves of critical modes.

Even though the total number of modes equals the number of buses in the network, these modes do not correspond to each other exactly. Their correlation is reported by the participation factors presented in Table 2.6. Before, Table 2.5 presents the critical modal impedance values and the harmonic orders for frequencies when the critical modal impedances occur.

Table 2.5: Case 1 - HRMA method results.

Order	Critical mode	Critical impedance magnitude [Ω]	Angle [°]
VS model			
8.59	6	6072 k	-79.9
12.17	7	2727 k	-81.3
23.7	6	4928 k	-20.5
CS-WT model			
8.14	7	1351 k	84.6
9.99	7	3252 k	74.5
23.69	6	3992 k	-40.5
Z(s) model			
12.42	7	61 k	5.5
23.81	6	70 k	2.0

Table 2.6: Case 1 - HRMA method results - PFs.

Order	Participation factors [%] for the buses							PF's sum
	1	2	3	4	5	6	7	
VS-model								
8.59	8.8	12.8	13.0	14.2	14.6	15.1	**21.5**	1.000
12.17	0.1	0.0	0.0	0.2	0.4	1.8	**97.4**	1.000
23.7	0.9	14.6	15.7	23.1	**24.3**	20.0	1.4	1.000
CS-WT model								
8.14	2.6	4.4	4.4	6.2	7.0	9.3	**66.0**	1.000
9.99	1.1	1.0	0.9	0.2	0.0	0.3	**96.5**	1.000
23.69	0.9	14.6	15.6	23.2	**24.4**	20.2	1.1	1.000
Z(s) model								
12.42	0.2	0.1	0.1	0.2	0.5	1.8	**97.8**	1.007
23.81	1.0	14.5	15.6	23.1	**24.3**	20.1	1.4	1.000

The study of participation factors is very relevant for localization of the best nodes in a network for filter implementation. The participation factors express the significance of a bus in resonance creation. Therefore, the modification of capacitance/inductance at the point of the network with the highest participation factor should trigger to the most powerful change of the resonance frequency. The details about participation factors in Section 1.3.2 and [5].

In the study of Case 1, from the values of participation factors, one can easily diagnose that the buses number 5 and 7 are the two buses which contribute to the resonance frequencies more than the others. As we can see, these two buses play the lead role in all three different models what indirectly confirms the accuracy of the method. From the values of the participation factors, one can conclude about the different number of resonance frequencies in the last model Z(s) presented. Since the two resonance frequencies from the first two models are mostly correlated to the bus 7 and similarly for the one of the resonance frequencies from the last model (higher PF at bus 7), in the last Z(s) model, the two resonance frequencies could have been merged into one resonance

frequency. Otherwise, due to the higher resistance of the Z(s) model, one of the resonance frequency could have been shaved to the insignificant value.

DIgSILENT Power Factory model In this simulation, we use the Power Factory model presented in the Figure 2.12. The model is combined of basic RLC elements.

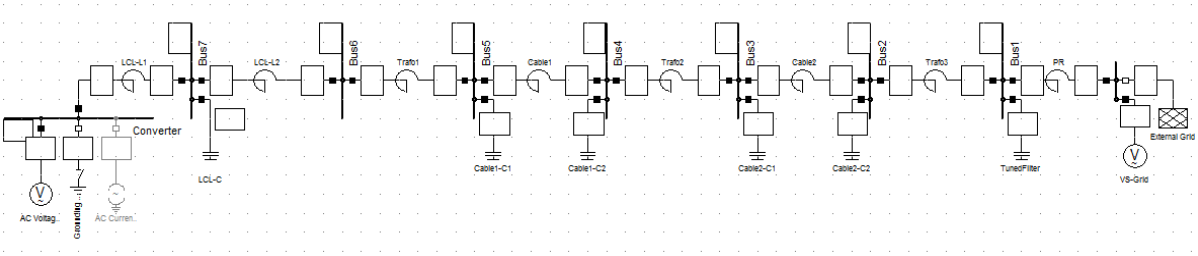

Figure 2.12: Case 1 - Power Factory model.

The two models: VS and CS-WT are simulated. The software performs Impedance Frequency Characteristic calculations. Figures 2.13 and 2.14 show the results of frequency sweep for VS and CS-WT model, respectively.

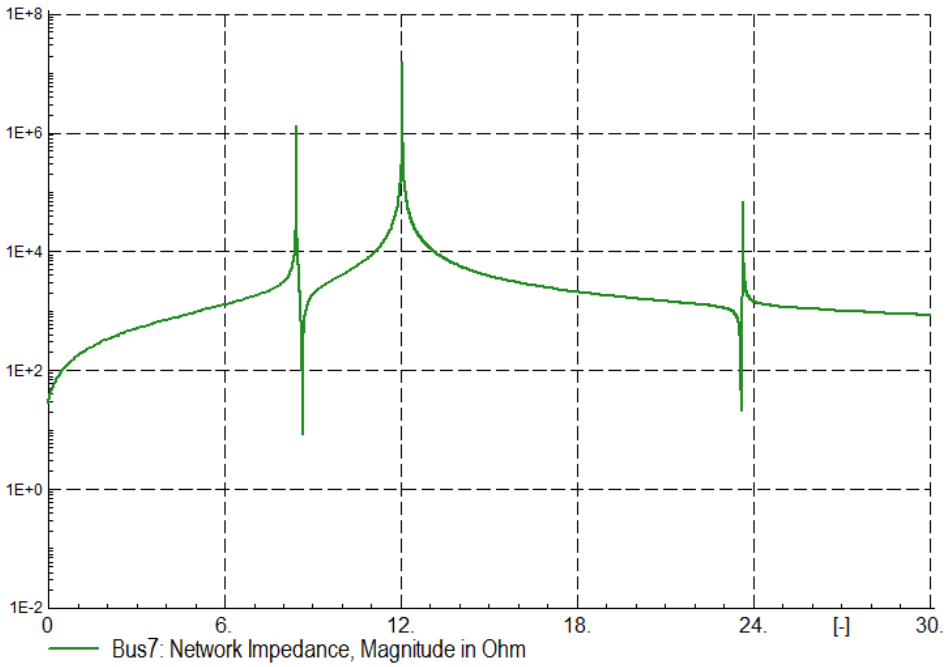

Figure 2.13: Case 1 - Power Factory VS model results

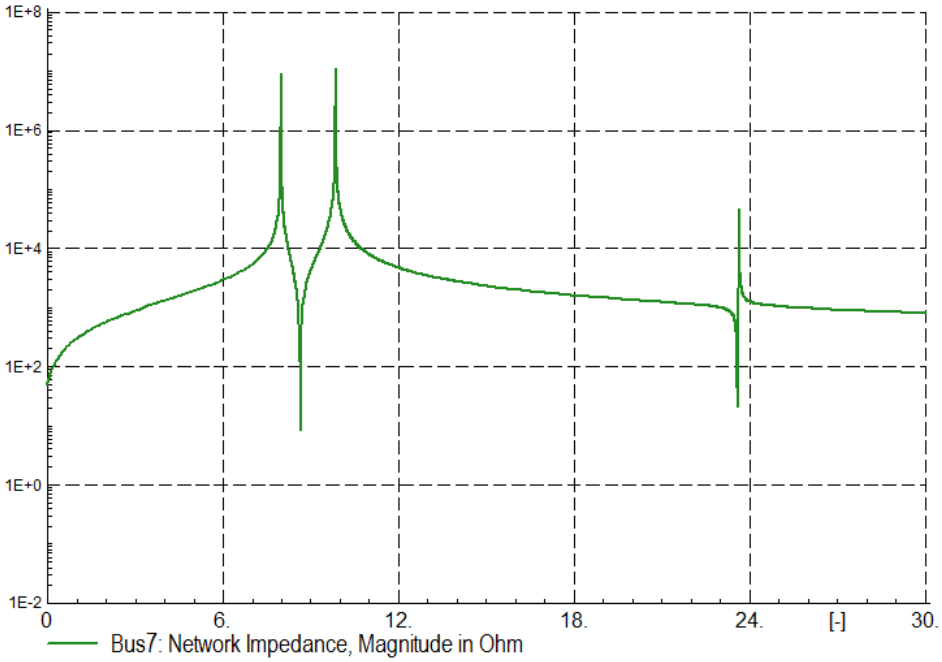

Figure 2.14: Case 1 - Power Factory CS model results

We can examine the figures obtained from the Power Factory software and conclude that they are coincident with the ones received from detail analysis in MATLAB. However, the peak values of impedances are different. The differences probably sources in the settings of Impedance Calculation for Frequency Sweep analysis. The step size of the simulation was set at the value of 0.1 Hz; furthermore the Automatic Step Size Adaptation was selected. Hence, difference in the values of impedance occurs. The dependence of the peak values from the value of step size was checked through similar simulation with different step sizes. The observation confirms that the step size influences the peak values.

What is more important in this study are the values of the resonance frequencies. The values obtained by Power Factory confirms the values gained from MATLAB analysis of both frequency sweep and modal analysis.

Table 2.7: Case 1 - Power Factory frequency results.

	Order [-]		
VS model	8.59	12.17	23.7
CS-WT model	8.14	9.99	23.69

As aforementioned, the observation of network impedance (frequency sweep) is performed from the specified bus in the network (bus 7). Due to the Power Factory software, we can performed the observation of impedance from each of the bus in the considered case. The results of frequency sweep seen from all 7 buses is presented in the Figure 2.15 and 2.16, for VS model and CS model, respectively.

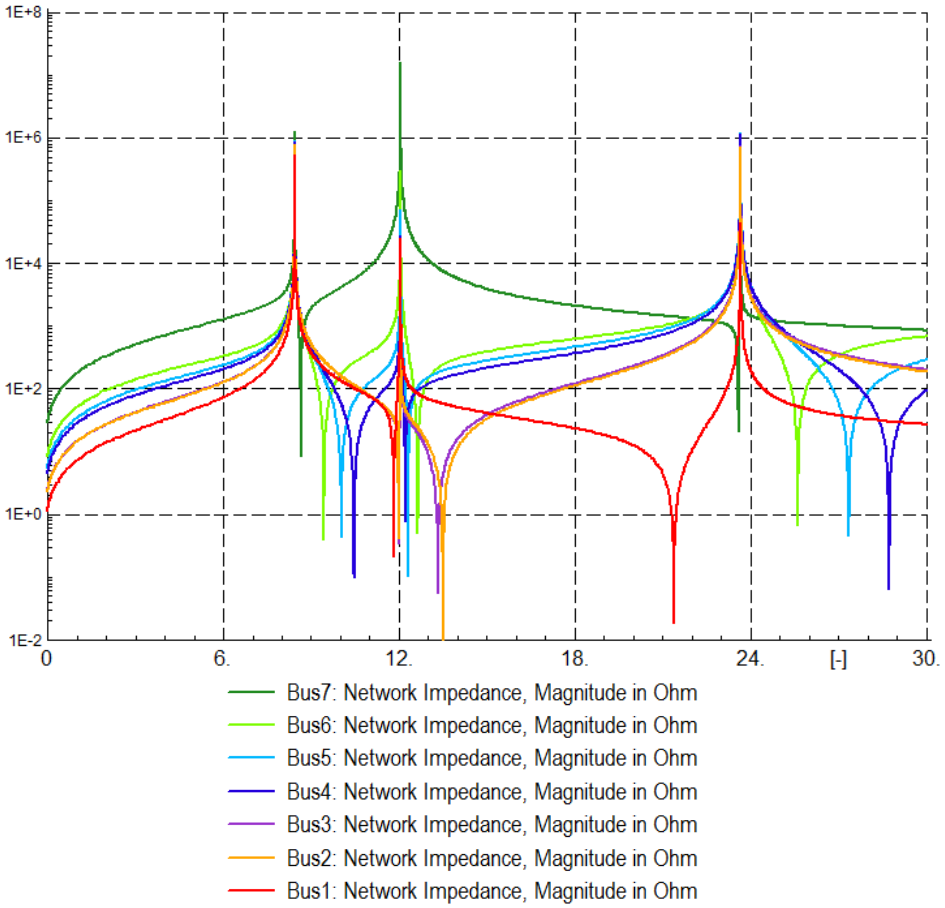

Figure 2.15: Case 1 VS - all buses - Power Factory resonance results.

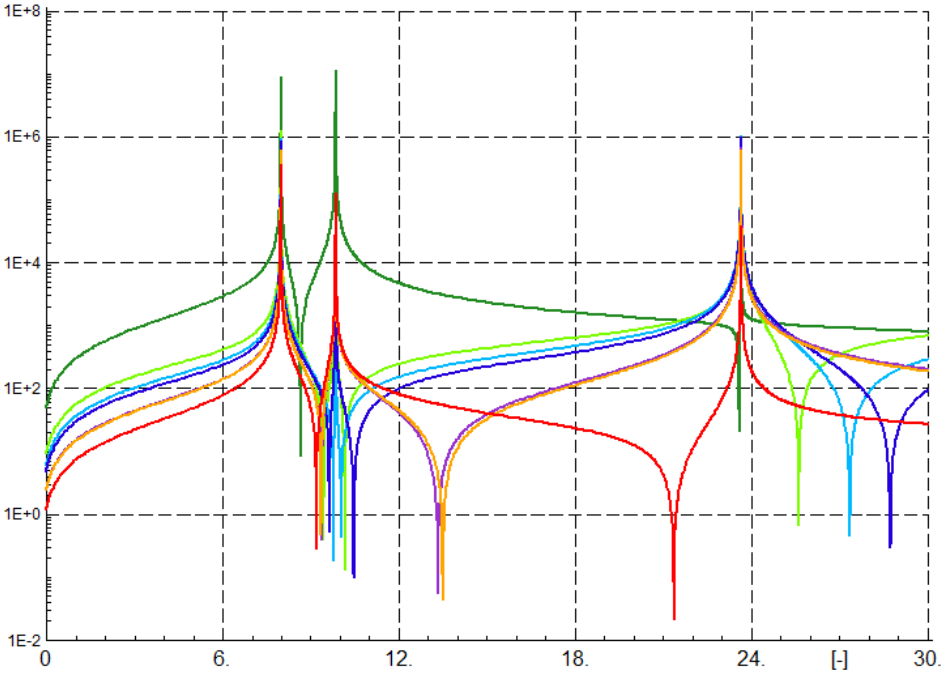

Figure 2.16: Case 1 CS - all buses - Power Factory resonance results.

The examination of the curves above demonstrates that the peaking impedances for both models occurs at the same frequencies, regardless the bus of observation. On the other hand, the dips of impedance undoubtedly depend on the bus where the observation is performed from. Coupled with the principles of parallel and series resonance, we can draw the two conclusions. Firstly, the series resonance frequency depends on the bus in the network i.e. series resonance frequency is different at the different points in the network. Secondly, since the peaks of the impedance, so the parallel resonance frequencies, are the same regardless the bus of observation, we conclude that the parallel resonance frequencies do not depend on the point of observation. The confirmation of the latter statement we recognize in the HRMA method. As described in Section 1.3.2, the method is utilized in order to investigate the parallel resonance and is not performed for particular bus, but for entire network. The frequencies collected from that method are exactly the frequencies obtained for every different case of observation bus in the frequency sweep method.

Results comparison In the three previous sections the results of frequency sweep analysis, harmonic resonance modal analysis, both performed in MALAB were presented. Moreover these results we couple with Frequency sweep tool in Power Factory software. The values of resonance frequencies obtained ambiguously confirms the correspondence of these three approaches to the problem. The values of parallel resonant frequencies are the same for the considered accuracy.

The difference of the impedance peak values are not considered very deeply in this study. However, as aforementioned, these values very often depends on the step size of the calculation. Moreover, the threshold impedance values above which the impedance level is defined as dangerous should be assigned individually for each case. Furthermore, the values of modal impedance from HRMA method does not exactly correspond to the real impedance value and should not be compared directly to the values of impedances obtained from frequency sweep or Power Factory tool.

2.2.2 Case 2

The topology Case 2 was presented in Section 2.1.2. In this case, the Wind Power Plant consists of two branches. There is one aggregated Wind Turbine in each branch. The total power of connected Wind Turbines is 200 MW.

Frequency Sweep In the Figures 2.17 and 2.18 the results of frequency sweep method are presented with linear and logarithmic impedance scale, respectively. Again, all three models of converters are included. The impedance of the grid is seen again from the bus number 7 i.e. middle bus of LCL filter in the first branch. Since the branch 1 is equal to the branch 2, we can obtain the same curves for impedance observed from bus 11.

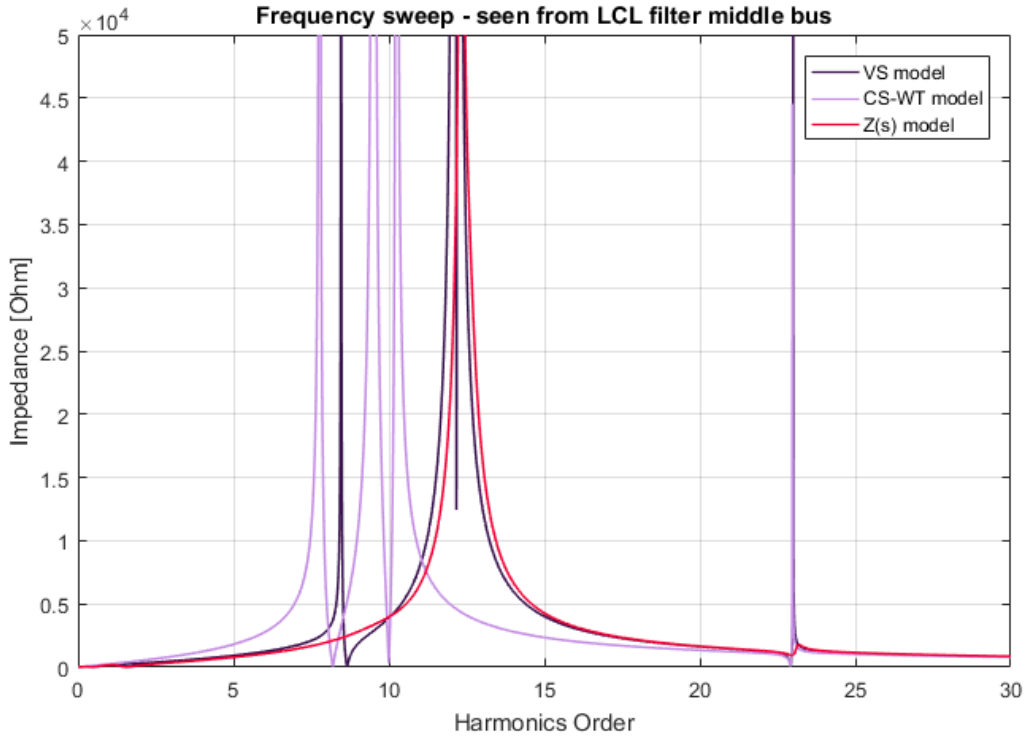

Figure 2.17: case 2 Impedance curves from FS - linear.

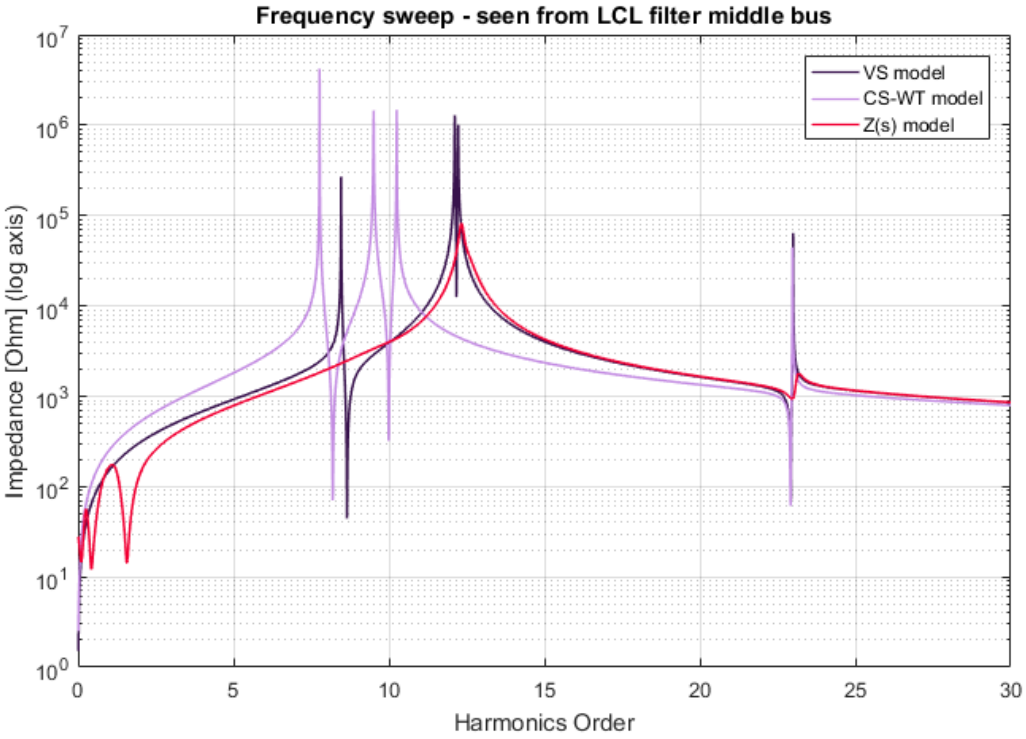

Figure 2.18: case 2 Impedance curves from FS - log.

Table 2.8 presents approximate resonance frequencies values. The values of frequencies are identified when impedance reaches local extreme values.

Table 2.8: Case 2 FS results.

Converter model	Frequency order [-]	Peak impedance [Ω]
VS	8.46	269 k
	12.12	1289 k
	12.23	1007 k
	23.00	64 k
CS-WT	7.77	4217 k
	9.51	1455 k
	10.25	1475 k
	22.98	45 k
Z(s)	12.33	82 k
	23.18	2 k

Again, due to the issues with the Z(s) model presented in Section 1.6.4.2, the results of resonance around fundamental frequency are ignored.

This time we can note that undoubtedly there are four resonant frequencies for Current Source model. The curve of VS model consists surely of three peaks, however the last one is very close to the one around 12^{th} order therefore is harder to notice it from the graph. The Z(s) model comprises two impedance rises, excluding ones around fundamental frequency. The value of impedance of Z(s) model is significantly lower than in other models, similarly to the Case 1. We carry on further conclusions and contemplations about the resonant frequencies after presentation of HRMA results for this case.

Harmonic Resonance Modal Analysis The Figures 2.19-2.21 illustrate the HRMA result curves. Similarly to the previous case, the following graphs shows the curves of maximum modal impedances for each harmonic order, modal impedances with respect to the each mode separately and critical modes only i.e. the modes that are assigned to the modal impedance peaks.

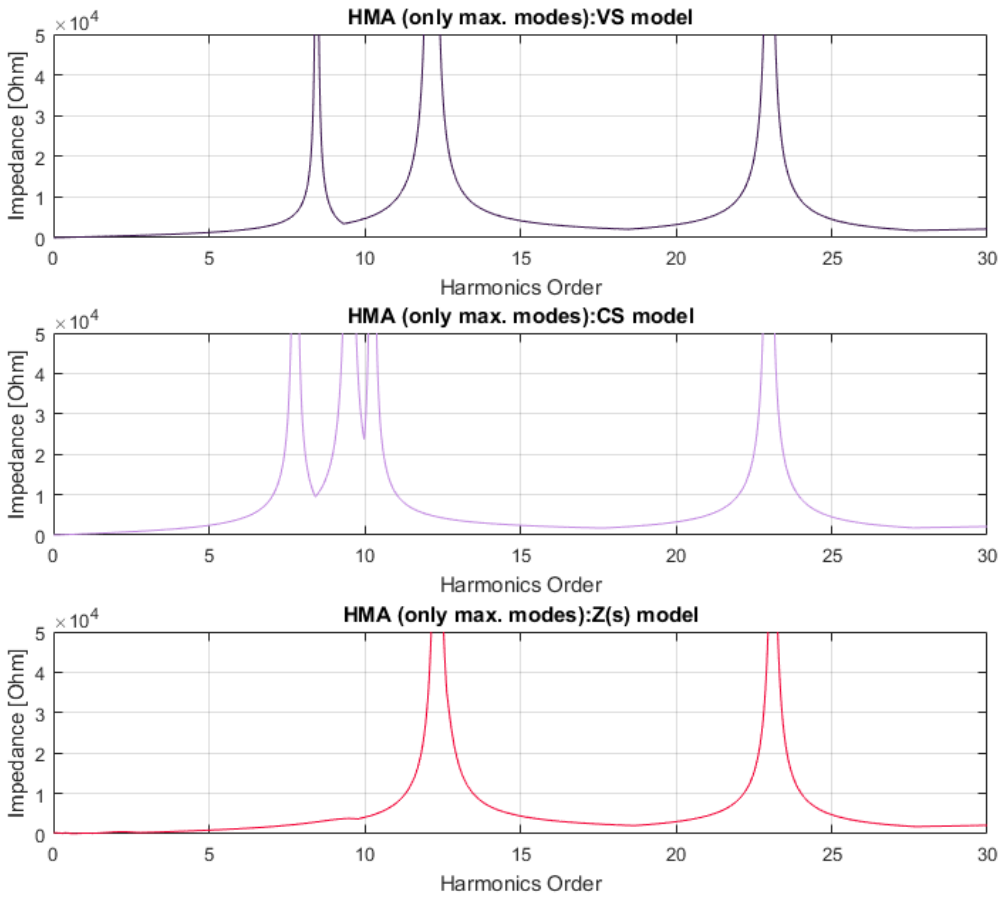

Figure 2.19: Case 2 - HRMA method. Maximum modal impedance curves.

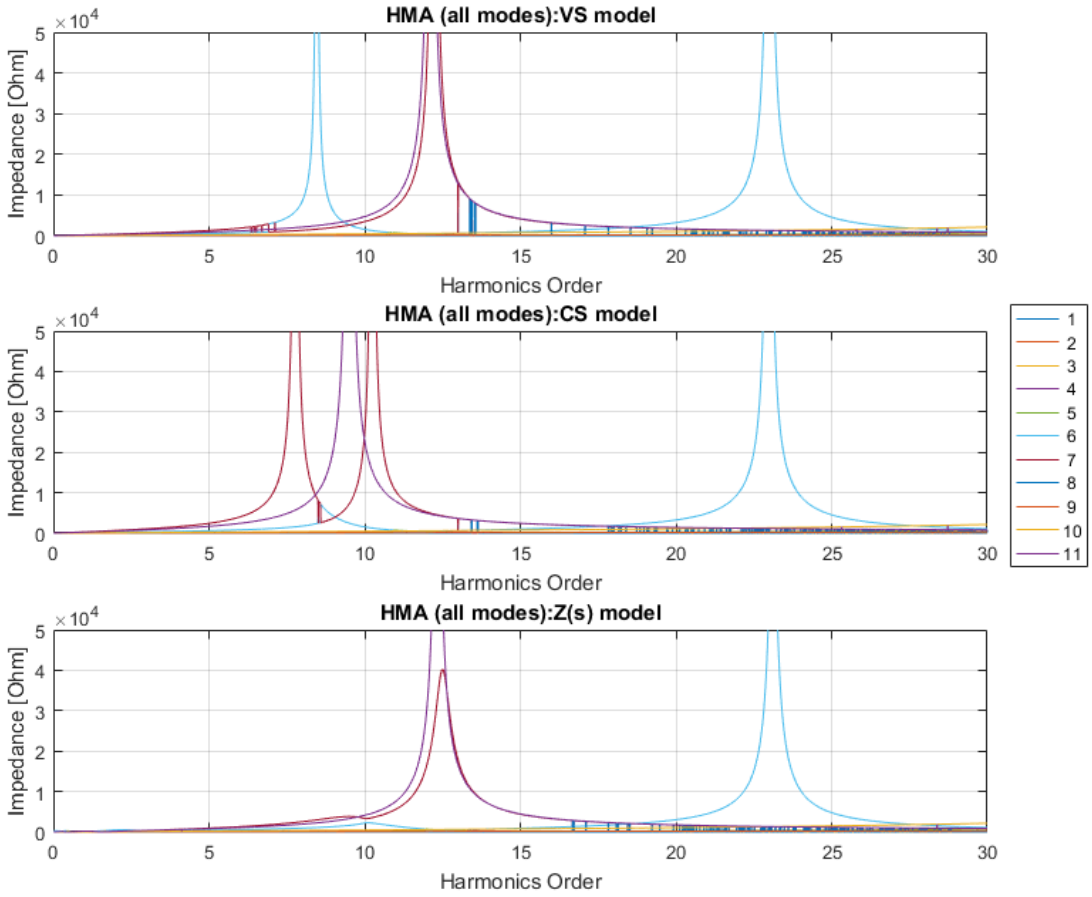

Figure 2.20: Case 2 - HRMA method. Impedance curves of all modes.

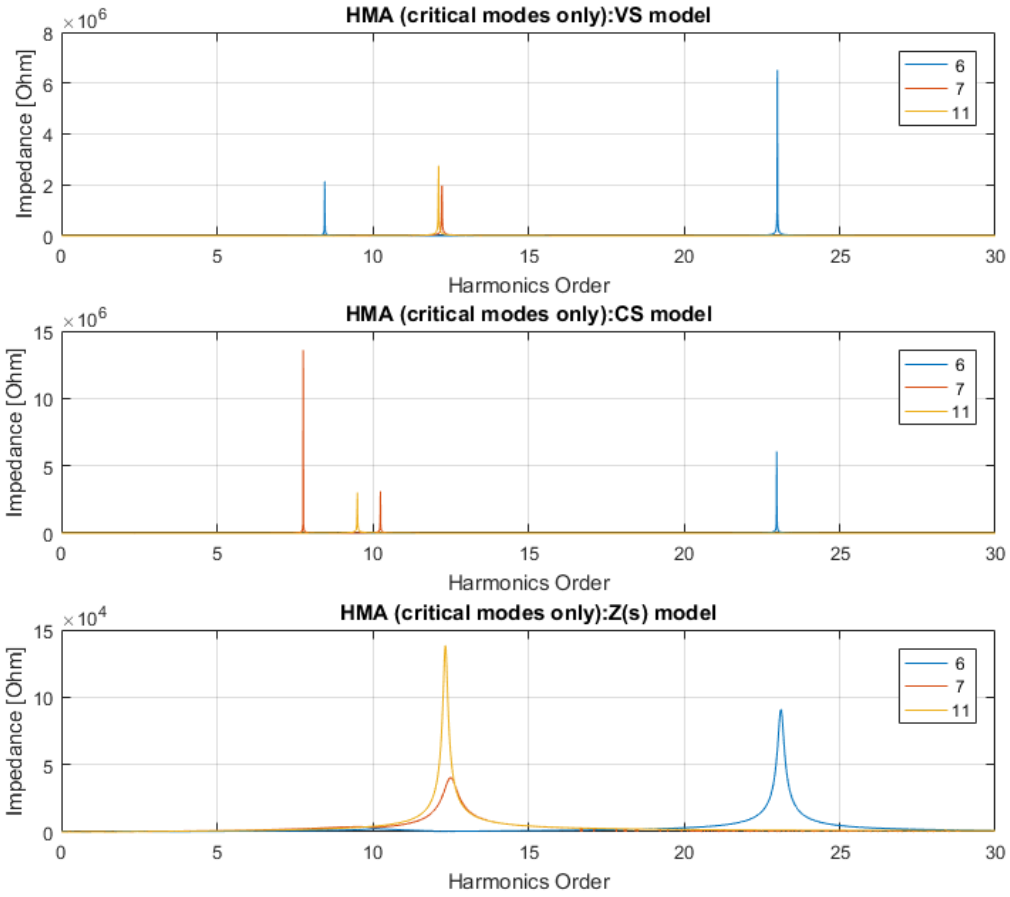

Figure 2.21: Case 2 - HRMA method. Impedance curves of critical modes.

Again, the participation factors point out the connotation of each mode to the real buses in the network. Table 2.10 presents the participation factors for the detected resonant frequencies i.e. frequencies at which the modal impedance rises occur. The values of critical impedances are gathered in Table 2.9.

Table 2.9: Case 2 - HRMA method results.

Order	Critical mode	Critical impedance magnitude [Ω]	Angle [°]
VS model			
8.46	6	2140 k	-86.7
12.12	11	2753 k	82.4
12.23	7	1965 k	83.0
23	6	6517 k	20.3
CS-WT model			
7.77	7	13.6 M	10.6
9.51	11	3008 k	76.8
10.25	7	3098 k	74.2
22.98	6	6062 k	-28.5
Z(s) model			
9.51	7	4 k	-52.3
12.34	11	138 k	3.3
23.11	6	91 k	-1.5

Table 2.10: Case 2 - HRMA method results - PFs.

Order	Participation factors [%] for the buses											PF's sum
	1	2	3	4	5	6	7	8	9	10	11	
VS-model												
8.46	5.3	7.9	8.0	8.7	9.0	9.2	**12.5**	8.7	9.0	9.2	**12.5**	1.000
12.12	0.0	0.0	0.0	0.2	0.3	1.1	**48.4**	0.2	0.3	1.1	**48.4**	1.000
12.23	0.3	0.0	0.0	0.0	0.1	0.8	**48.9**	0.0	0.1	0.8	**48.9**	1.000
23	0.6	8.9	9.6	13.6	**14.2**	11.7	1.0	13.6	**14.2**	11.7	1.0	1.000
CS-WT model												
7.77	1.7	3.2	3.2	4.2	4.6	5.8	**31.3**	4.2	4.6	5.8	**31.3**	1.000
9.51	0.0	0.0	0.0	0.1	0.3	1.1	**48.5**	0.1	0.3	1.1	**48.5**	1.000
10.25	1.5	1.1	1.1	0.4	0.2	0.0	**47.4**	0.4	0.2	0.0	**47.4**	1.000
22.98	0.6	8.9	9.6	13.7	**14.3**	11.8	0.7	13.7	**14.3**	11.8	0.7	1.000
Z(s) model												
9.51	2.8	5.4	5.5	7.1	7.8	9.3	**45.5**	7.1	7.8	9.3	**45.5**	1.533
12.34	0.0	0.0	0.0	0.2	0.3	1.1	**48.4**	0.2	0.3	1.1	**48.4**	1.000
23.11	0.7	8.8	9.5	13.6	**14.2**	11.7	1.0	13.6	**14.2**	11.7	1.0	1.000

This time we observe one significant difference between the frequency sweep curves and HRMA curves. For Z(s) model, one of the frequency missing in the frequency sweep method appears in the HRMA curves. To investigate and interpret this we look at the value of the modal impedance for this resonant frequency or at the figures. The value of critical impedance of critical module is much smaller than the other modal critical impedances (for other resonant frequencies). Since the resonant frequencies are recognized as the extreme points of impedance curves, peak value are identified in this way. However, in order to exclude this frequency from the results, further investigation of minimum dangerous impedance is necessary.

Besides this difference, the results of frequencies converge completely.

From the values of participation factors we derive couple of conclusions. First of all, the values of participation factors for buses of branch 1 (4-7) correspond to the buses of branch 2 (8-11) with the same values. That shows that from the modal analysis point of view the wind turbine branches are the same and the participation factor is distributed to the two analogical buses for both branches. Secondly, comparing the results of participation factors for Case 1 and Case 2 we can observe some similarities in apparition of the new resonant frequency. For both VS and CS-WT model, the lowest resonant frequency stays approximately at the same level, to be more precise is slightly shifted down to the lower value. The value of participation factor is divided equally into two analogical buses. The second frequency from Case 1 seems to appear in Case 2 as two resonant frequencies, one greater and the other less than the frequency from Case 1. The values of participation factors for both cases for these frequencies appear to confirm this assumption since their value is again distributed equally and the values are very similar for the new two frequencies.

On the contrary, in the Z(s) model, the two frequencies stay at approximately the same level and the new resonance frequency appears independently after adding new branch.

Analysing the third model Z(s) we have to have in mind the new resonant frequency which appears in this analysis. As stated before, the value of critical impedance is very low. From the curves of modal impedances with regards to each single node, we observe that the values of two modes are at the similar level of modal impedance for this value of resonance mode 7 and mode 11. This condition disturbs the assumption settled in Section 1.3.2 that one within the modal impedances is much greater than the others. As the result, we obtain inaccurate participation factors. The easiest way to check if the that assumption is fulfilled is to sum all the participation factors for particular frequency. If the results is around 1 the assumption is achieved. For the new frequency, the sum of participation factors reaches 1.533 therefore all participation factors are is considered as inaccurate.

DIgSILENT Power Factory model Furthermore, the results of FS and HRMA are compared with the curves acquired from Power Factory software. Figure 2.22 presents the diagram of the network used for calculation.

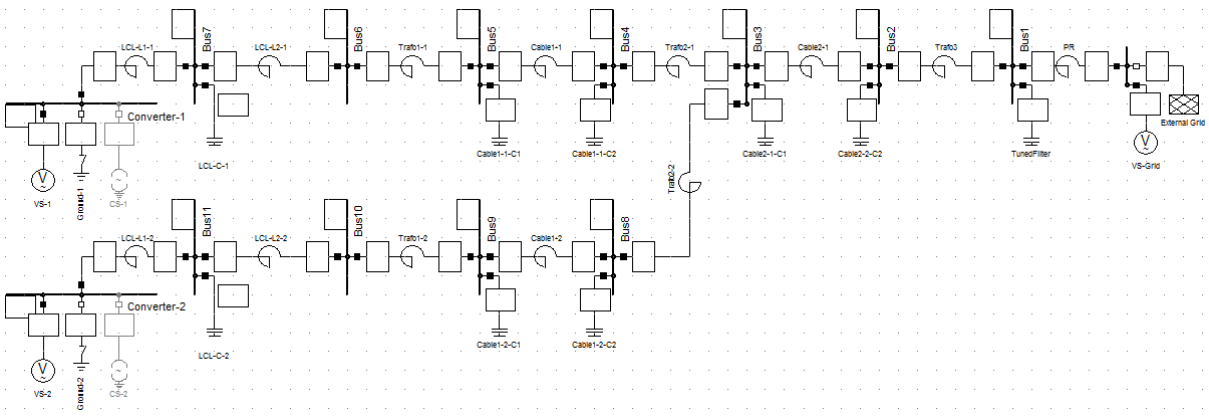

Figure 2.22: Case 2 - Power Factory model.

Again, the models of VS and CS-WT are simulated for Impedance Frequency Characteristic calculations. Figures 2.23 and 2.24 present the results of frequency sweep for VS and CS-WT model, seen from the middle LCL filter bus i.e. the same bus as for MATLAB model bus 7.

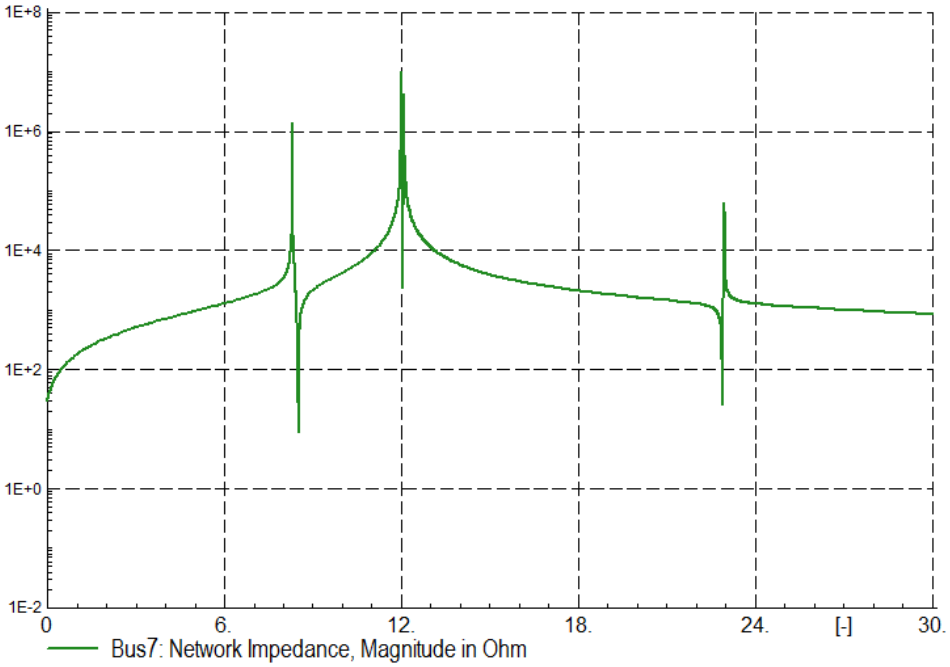

Figure 2.23: Case 2 - Power Factory VS model results

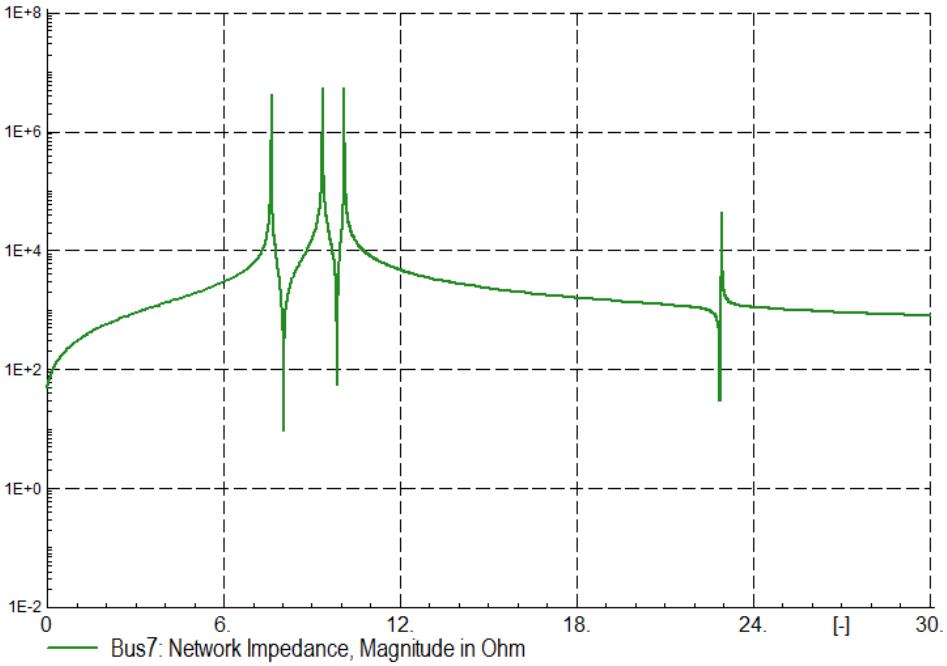

Figure 2.24: Case 2 - Power Factory CS model results

The resonant frequencies for peak impedances are measured in the software tool and presented in the Table 2.11.

Table 2.11: Case 2 - Power Factory frequency results.

	Order [-]			
VS model	8.46	12.12	12.23	23.00
CS-WT model	7.77	9.51	10.25	22.98

The values of resonant frequencies are consistent with the values obtained both in FS and HRMA in MATLAB. Again, we present the impedance curves seen from other buses. The buses where the impedance is observed are buses 1-7. Since the two branches with wind turbines are the same, we know that the impedance curves seen from buses 4-7 are the same as seen from respective buses 8-11. Therefore the presentation of impedance curves for one branch is sufficient. The Figure 2.25 shows the curves for buses 1-7 for the VS model, while the Figure 2.26 illustrate the same curves but for model CS-WT.

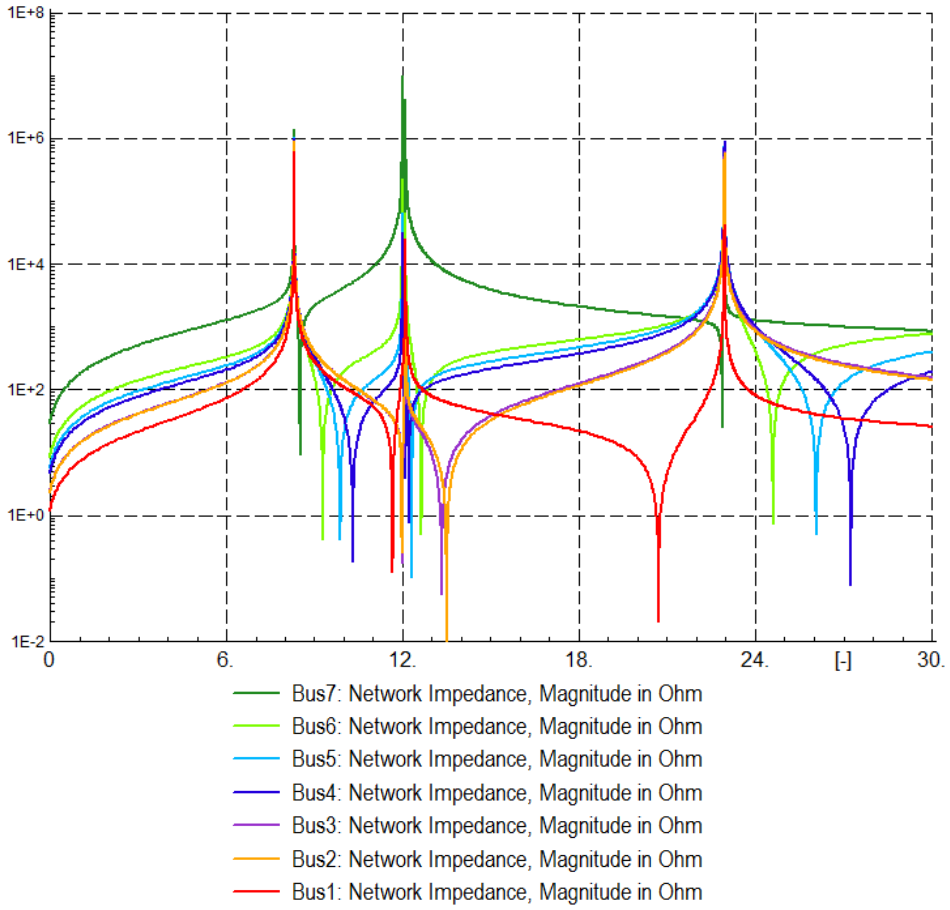

Figure 2.25: Case 2 VS - all buses - Power Factory resonance results.

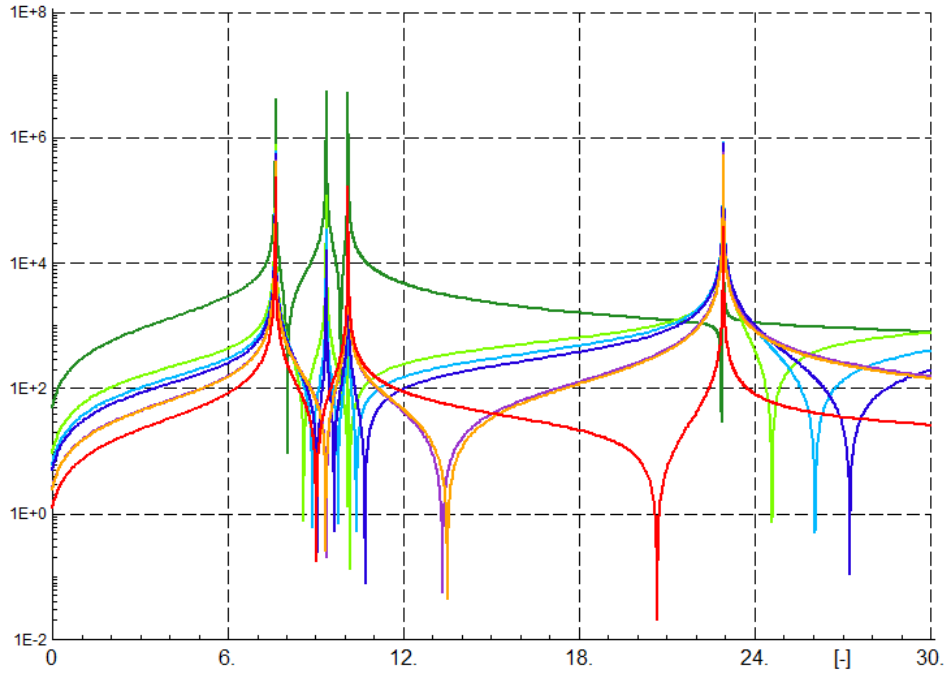

Figure 2.26: Case 2 CS - all buses - Power Factory resonance results.

The shapes of the curves indicate the same conclusions like for Case 1 i.e. the series and parallel resonance does and does not depend on the point in the network, respectively. The previous section presenting results of Case 1 describes these principles in details.

Results comparison Similarly to the first case, the results of FS, HRMA and from Power Factory are very similar. For the considered accuracy, the values of corresponding frequencies are the same. The important fact to highlight is that we obtain one resonance frequency more for HRMA comparing to FS in the Z(s) model. Even though the value of modal impedance is quite low comparing to the other resonance points, the level of impedance dangerous for the network is not identified and could apparently be already dangerous in this range of frequency. The situation suggests the conclusion that we should always consider both methods together and compare their outputs. Since the amount of data necessary for both methods is very similar, this does not pose a problem.

2.2.3 Case 3

The last topology case is described in Section 2.1.2. All installed power (400 MW) and all elements of Wind Power Plant are considered.

Frequency Sweep Figures 2.27 and 2.28 present the frequency sweep curves for linear and logarithmic scales, respectively. All three models are included. The bus of observation is again bus 7. All four wind turbine branches are equal therefore the features of those branches are symmetrical to each other. The groups of equal bus numbers at the wind turbine branches are: (4, 8, 13, 17), (5, 9, 14, 18), (6, 10, 15, 19), (7, 11, 16, 20). Moreover bus 3 and bus 12 are also symmetrical, installed at the end of two symmetrical cables connecting pairs of wind turbine branches.

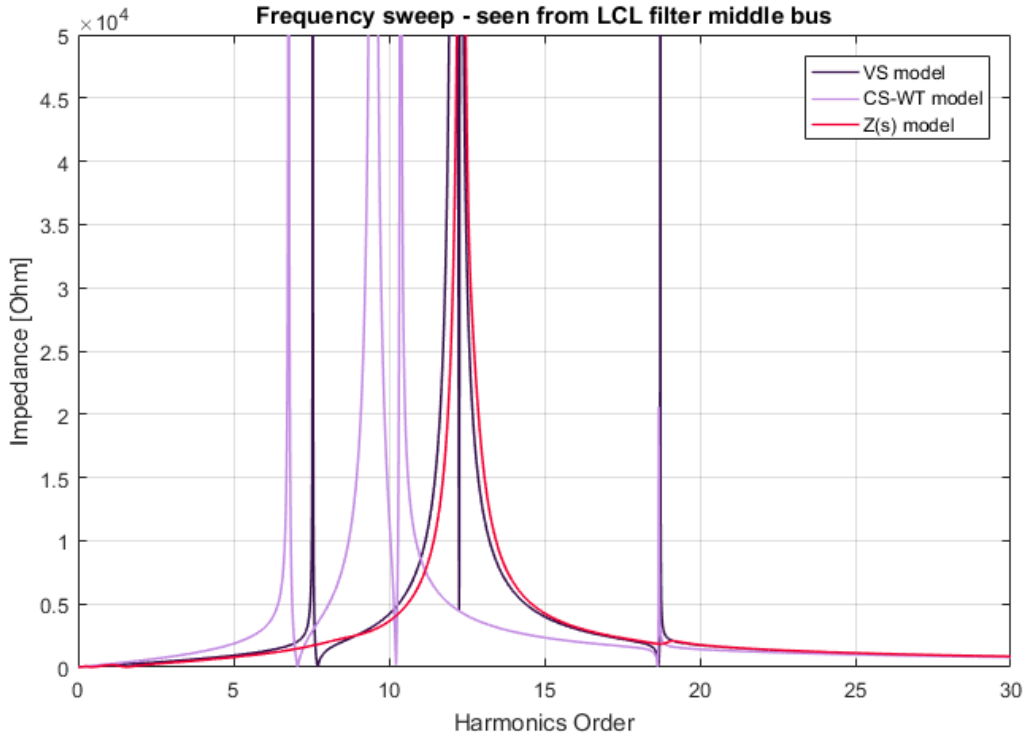

Figure 2.27: case 3 Impedance curves from FS - linear.

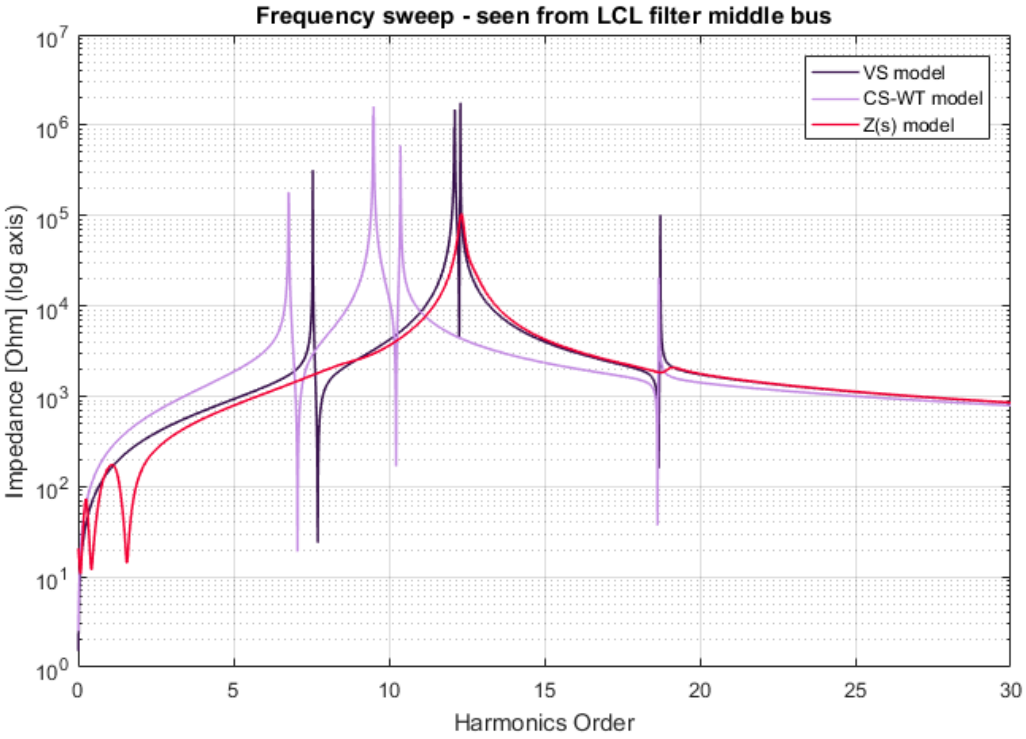

Figure 2.28: case 3 Impedance curves from FS - log.

Table 2.12 presents approximate resonance frequency values and the peak values of corresponding peaking impedance. The values around the fundamental frequency for Z(s) model are ignored.

Table 2.12: case 3 FS results.

Converter model	Frequency order [-]	Peak impedance [Ω]
VS	7.55	318 k
	12.1	941 k
	12.12	1491 k
	12.3	1769 k
	18.73	102 k
CS-WT	6.78	180 k
	9.49	1288 k
	9.51	1606 k
	10.37	595 k
	18.68	21 k
Z(s)	12.33	104 k
	19.13	2 k

We can observe one additional resonance frequency for each of the VS and CS-WT models. However, pair of frequencies for each model have very similar values therefore can be considered as the one resonant frequency. Further examination and comparison of the frequency sweep results for all considered topology cases is presented in Section 2.2.4.

Harmonic Resonance Modal Analysis Following Figures 2.29, 2.30 and 2.31 shows the HRMA results. Again, the graphs present maximum modal impedances, modal impedances curves for all modes separately and critical modes curves alone.

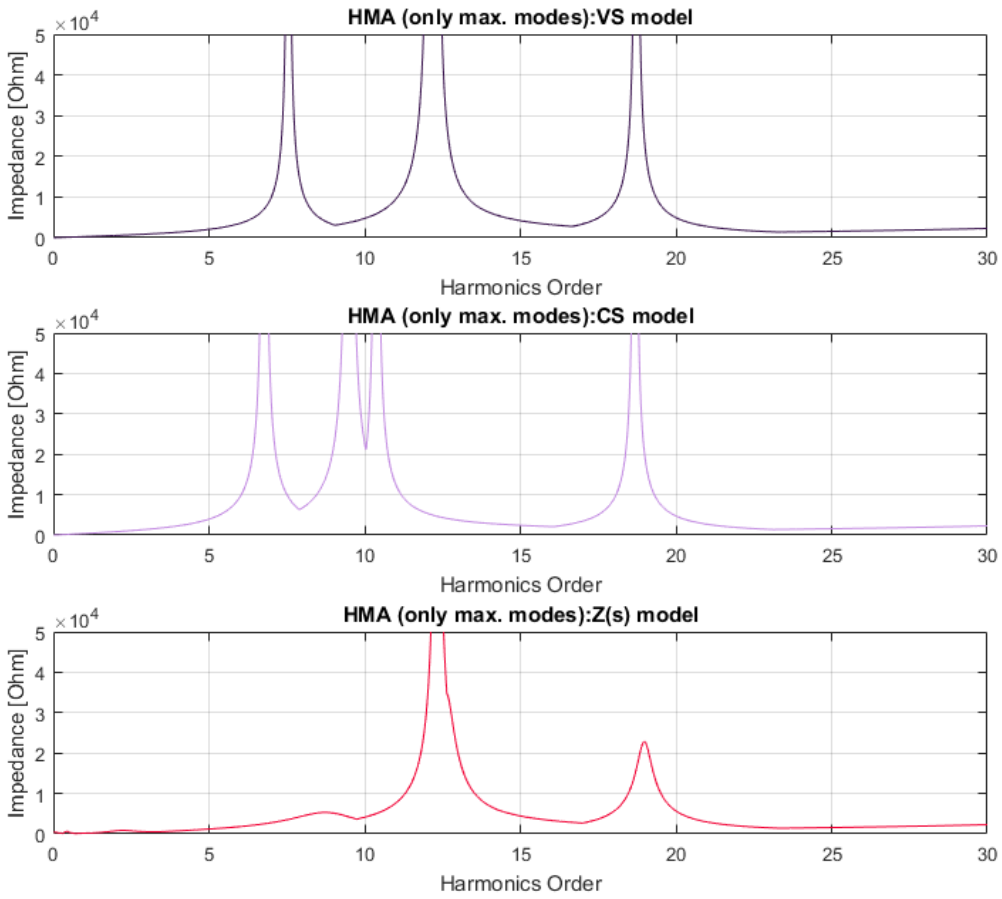

Figure 2.29: Case 3 - HRMA method. Maximum modal impedance curves.

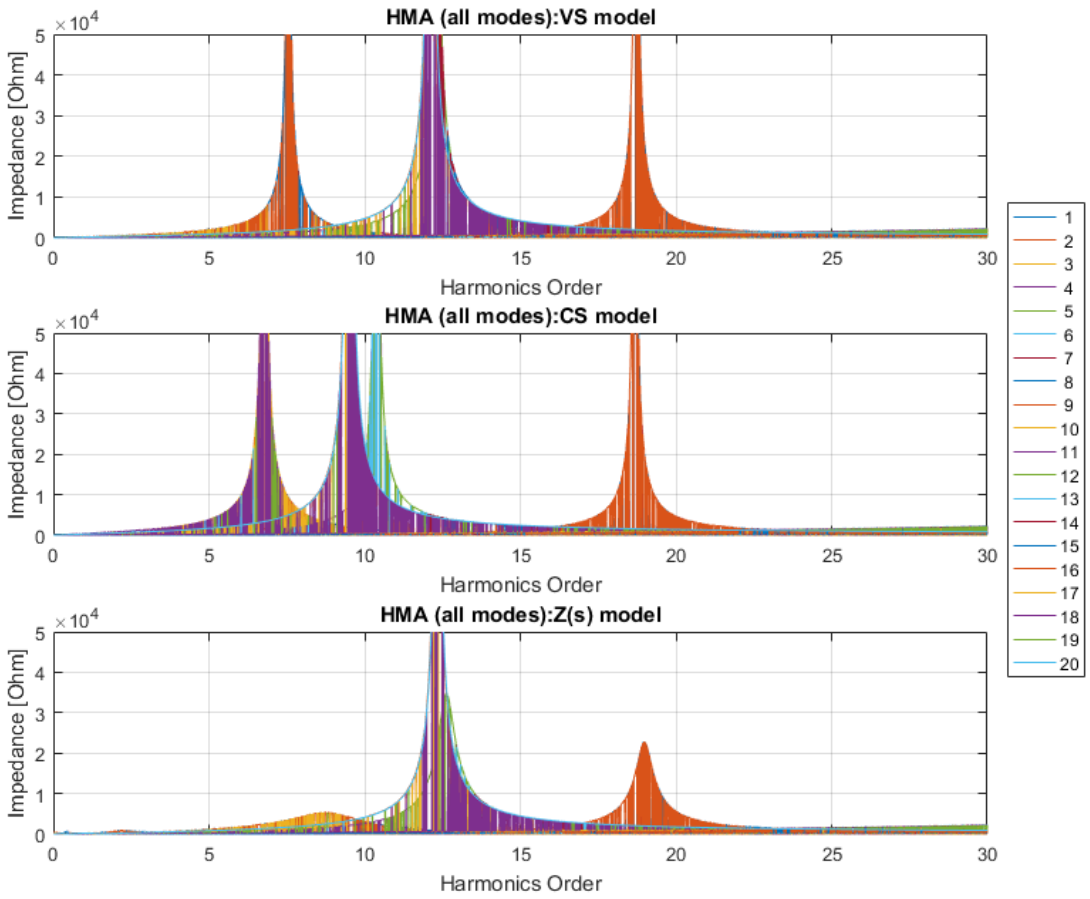

Figure 2.30: Case 3 - HRMA method. Impedance curves of all modes.

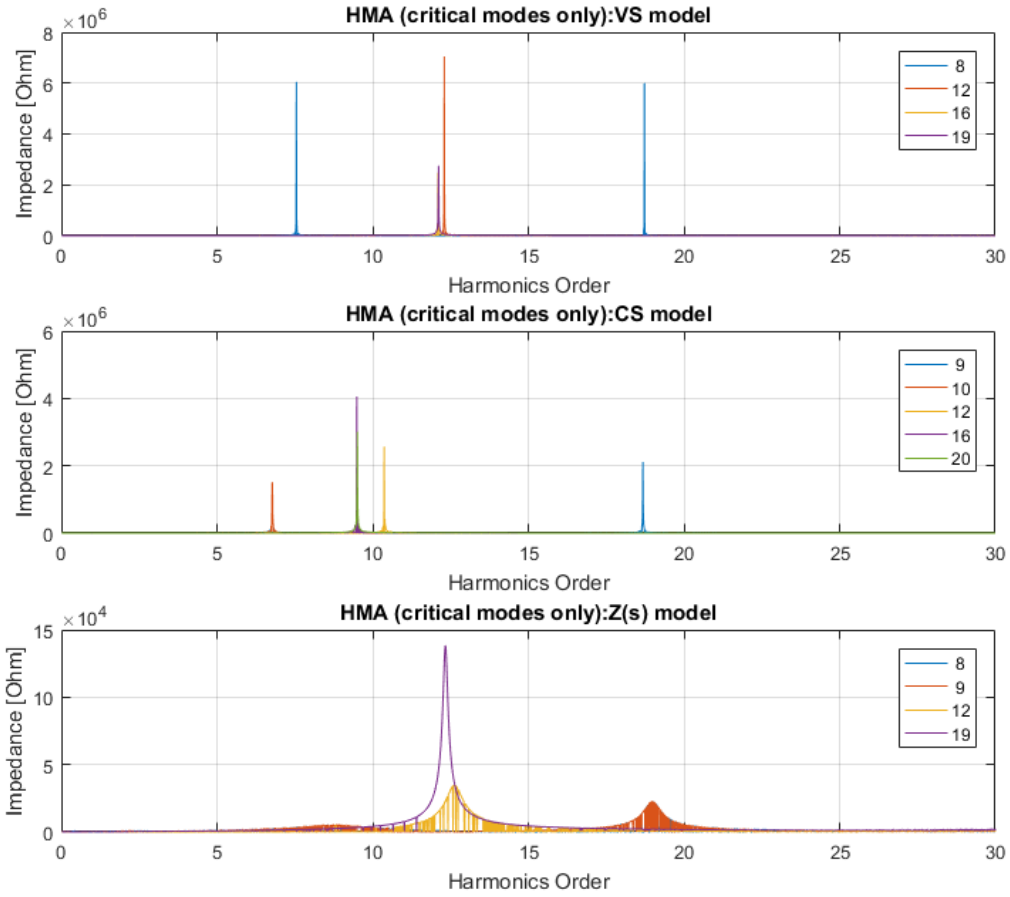

Figure 2.31: Case 3 - HRMA method. Impedance curves of critical modes.

With these results in mind, the values of critical impedances and values of participation factors for Case 3 are presented for each resonance frequency in Table 2.13 and 2.14, respectively.

Table 2.13: Case 3 - HRMA method results.

Order	Critical mode	Critical impedance magnitude [Ω]	Angle [°]
VS model			
7.55	8	6050 k	-83.4
12.1	16	2484 k	-80.8
12.12	19	2753 k	82.4
12.3	12	7050 k	64.5
18.73	8	5997 k	57.5
CS-WT model			
6.78	10	1511 k	85.4
9.49	16	4054 k	-66.1
9.51	20	3008 k	76.8
10.37	12	2567 k	-77.3
18.68	9	2114 k	-78.7
Z(s) model			
8.73	9	5 k	-13.6
12.34	19	138 k	3.3
18.98	9	23 k	4.0

Table 2.14: Case 3 - HRMA method results - PFs.

Order	Participation factors [%] for the buses										
	1	2	3	4	5	6	7	8	9	10	
VS-model											
7.55	2.5	4.8	4.9	5.1	5.2	5.2	**5.2**	5.1	5.2	5.2	
12.1	0.0	0.0	0.0	0.1	0.2	0.6	**24.2**	0.1	0.2	0.6	
12.12	0.0	0.0	0.0	0.2	0.3	1.1	**49.5**	0.2	0.3	1.1	
12.3	0.4	0.1	0.1	0.0	0.0	0.3	**24.5**	0.0	0.0	0.3	
18.73	1.7	5.6	5.8	**6.7**	6.7	5.2	1.7	**6.7**	6.7	5.2	
	11	12	13	14	15	16	17	18	19	20	PF's sum
7.55	**5.2**	4.9	5.1	5.2	5.2	**5.2**	5.1	5.2	5.2	**5.2**	1.000
12.1	**24.2**	0.0	0.1	0.2	0.6	**24.2**	0.1	0.2	0.6	**24.2**	1.000
12.12	**49.5**	0.0	0.0	0.0	0.0	1.9	0.0	0.0	0.0	1.9	1.063
12.3	**24.5**	0.1	0.0	0.0	0.3	**24.5**	0.0	0.0	0.3	**24.5**	1.000
18.73	1.7	5.8	**6.7**	6.7	5.2	1.7	**6.7**	6.7	5.2	1.7	1.000
CS-WT model											
6.78	1.2	2.8	2.8	3.2	3.4	3.9	**12.1**	3.2	3.4	3.9	
9.49	0.0	0.0	0.0	0.1	0.2	0.5	**24.2**	0.1	0.2	0.5	
9.51	0.0	0.0	0.0	0.0	0.0	0.1	4.3	0.0	0.0	0.1	
10.37	1.1	0.8	0.8	0.4	0.2	0.0	**23.6**	0.4	0.2	0.0	
18.68	1.8	5.6	5.9	**6.8**	6.8	5.5	1.0	**6.8**	6.8	5.5	
	11	12	13	14	15	16	17	18	19	20	PF's sum
6.78	**12.1**	2.8	3.2	3.4	3.9	**12.1**	3.2	3.4	3.9	**12.1**	1.000
9.49	**24.2**	0.0	0.1	0.2	0.5	**24.2**	0.1	0.2	0.5	**24.2**	1.000
9.51	4.3	0.0	0.1	0.3	1.0	**44.4**	0.1	0.3	1.0	**44.4**	1.005
10.37	**23.6**	0.8	0.4	0.2	0.0	**23.6**	0.4	0.2	0.0	**23.6**	1.000
18.68	1.0	5.9	**6.8**	6.8	5.5	1.0	**6.8**	6.8	5.5	1.0	1.000
Z(s) model											
8.73	1.9	4.7	4.7	5.2	5.3	5.4	**7.3**	5.2	5.3	5.4	
12.34	0.0	0.0	0.0	0.1	0.3	1.1	**47.9**	0.1	0.3	1.1	
18.98	2.0	5.5	5.8	**6.7**	6.7	5.3	1.6	**6.7**	6.7	5.3	
	11	12	13	14	15	16	17	18	19	20	PF's sum
8.73	**7.3**	4.7	5.2	5.3	5.4	**7.3**	5.2	5.3	5.4	**7.3**	1.089
12.34	**47.9**	0.0	0.0	0.0	0.0	1.2	0.0	0.0	0.0	1.2	1.012
18.98	1.6	5.8	**6.7**	6.7	5.3	1.6	**6.7**	6.7	5.3	1.6	1.002

Similarly to the Case 2, for Z(s) model we obtain one more resonance frequency from HRMA comparing to frequency sweep. Besides this frequency, the values of equivalent ones are the same or very similar. Again, the modal impedance value of critical mode for new frequency is very low.

Furthermore, the participation factors for new frequency are probably inaccurate since the sum of them for the new frequency exceeds unity. Finally, we note that the participation factors are not completely symmetrical in some cases. The symmetry remains between the pair of branches 1 and 2 or 3 and 4 (the pairs connected to the same three-winding transformer) but symmetry of participation factors between pair branches connected to different three-winding transformers fades away.

DIgSILENT Power Factory model Analogically, we compare the results of FS and HRMA with the curves from Power Factory model. The model used in this case is presented in the Figure 2.32.

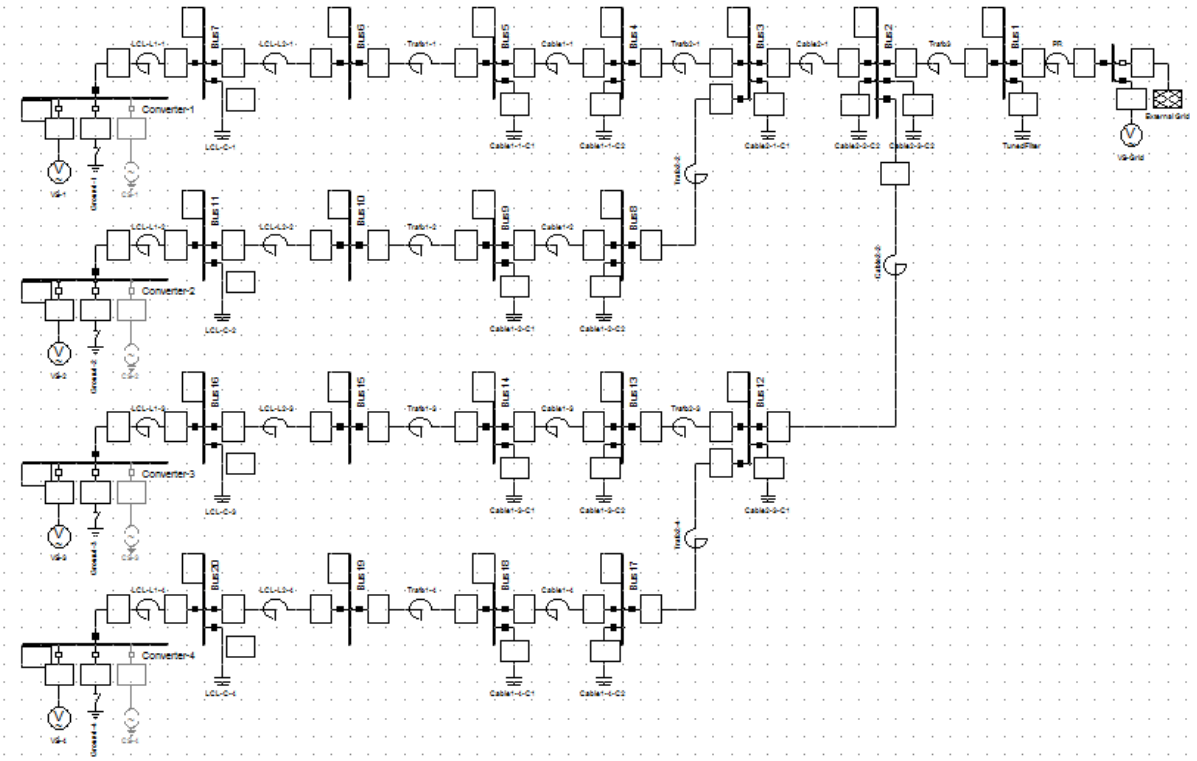

Figure 2.32: Case 3 - Power Factory model.

The models of VS and CS-WT are simulated for Impedance Frequency Characteristic calculations. Figures 2.33 and Figures 2.34 present the results of frequency sweep for VS and CS-WT model, seen from the middle LCL filter bus i.e. the same bus as for MATLAB model bus 7.

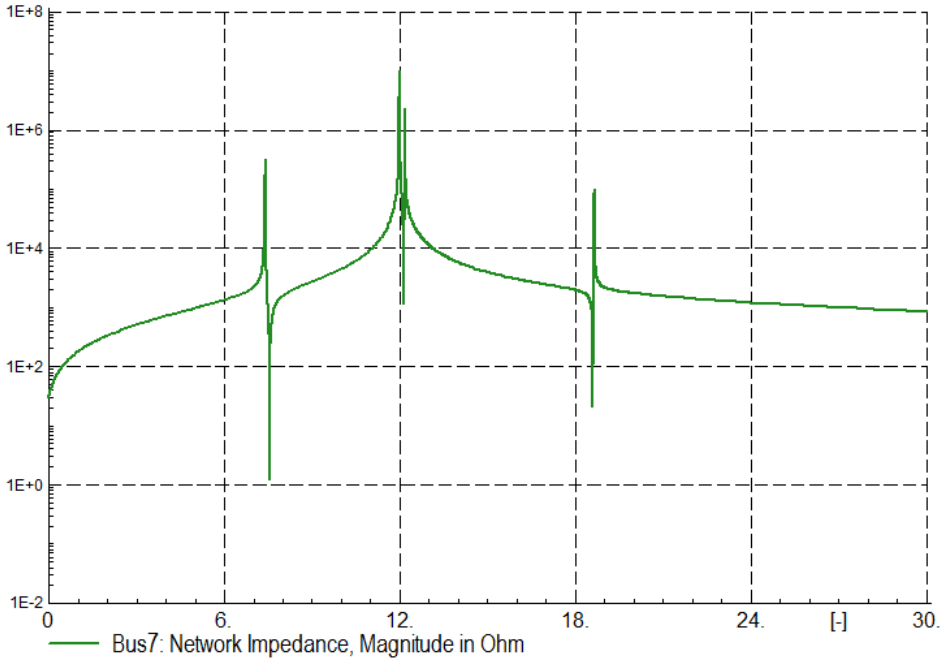

Figure 2.33: Case 3 - Power Factory VS model results

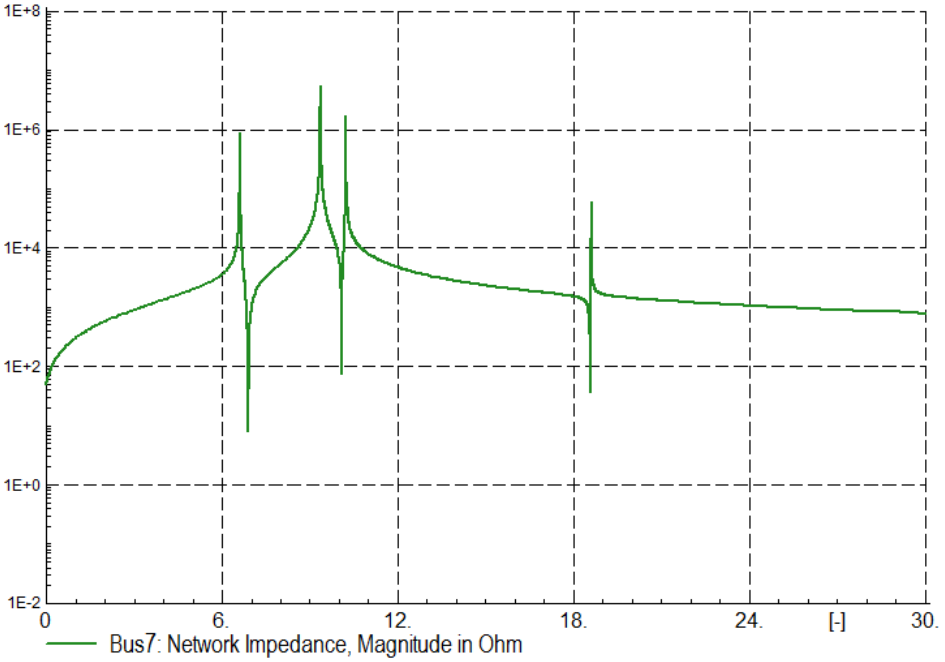

Figure 2.34: Case 3 - Power Factory CS model results

The resonant frequencies for peak impedances are measured in the software tool and presented in the Table 2.15.

Table 2.15: Case 3 - Power Factory frequency results.

	Order [-]				
VS model	7.55	12.10	12.12	12.30	18.73
CS-WT model	6.78	9.49	9.51	10.37	18.68

One more time, the values obtained from Power Factory converge with those we collected from frequency sweep analysis in MATLAB. Similarly to the Case 2 analysis, the Figures 2.35 and 2.36 show the curves for buses 1-7 for the VS model and CS-WT model, respectively.

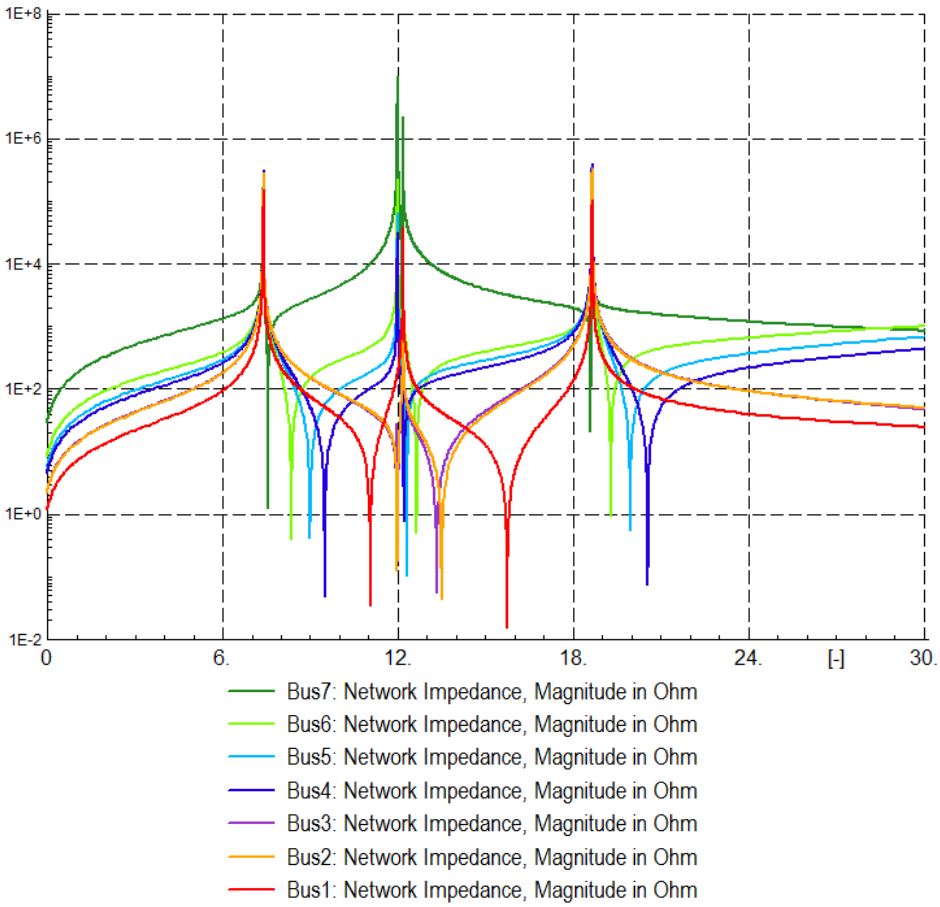

Figure 2.35: Case 3 VS - all buses - Power Factory resonance results.

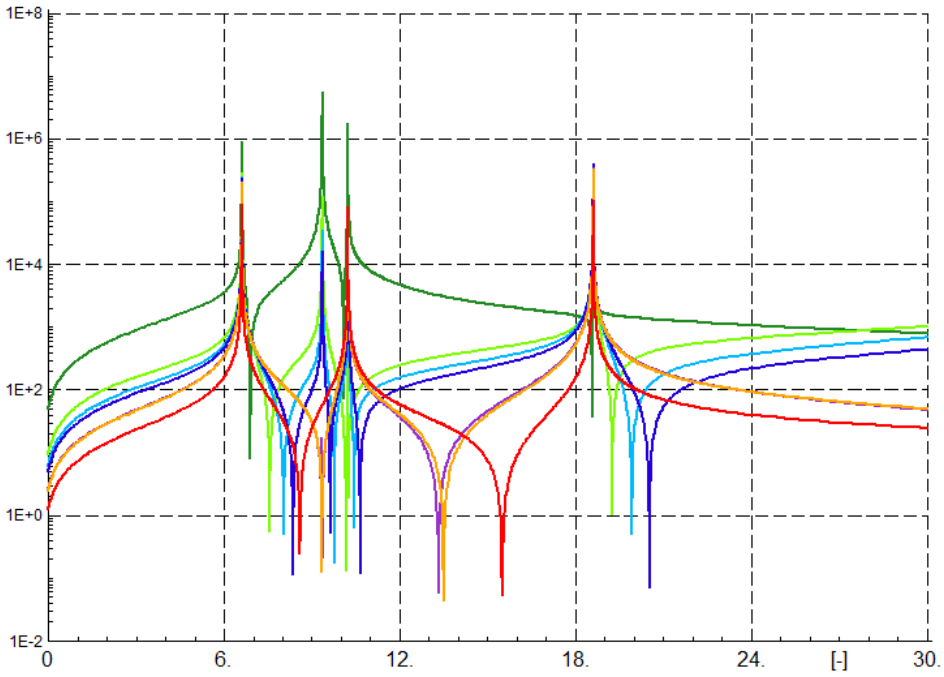

Figure 2.36: Case 3 CS - all buses - Power Factory resonance results.

The shapes of the curves indicate the similar conclusions like for Case 1 and Case 2.

Results comparison Similarly to the first and second case, the values of received frequencies from all three approaches are similar. Once again, we obtain one more resonant frequency from HRMA comparing to frequency sweep. Again we observe similar behavior of resonances with regard to the bus of observation.

2.2.4 Comparison between topology cases

2.2.4.1 VS model

In this section we compare the results obtained in three previous sections jointly. The following figures and tables demonstrate the behaviour of frequency sweep curves for VS model, CS-WT model and Z(s) model. Each model is considered separately but for all three topology cases jointly. In tables the results of resonance frequencies for all topology cases (parallel resonance) are gathered. The aim of this section is to identify patterns and any similarities between the topology cases and the models.

Frequency sweep The following figure presents the frequency sweep curves for all three topology cases. We had a try to group the frequencies in the three groups like indicated in the figure.

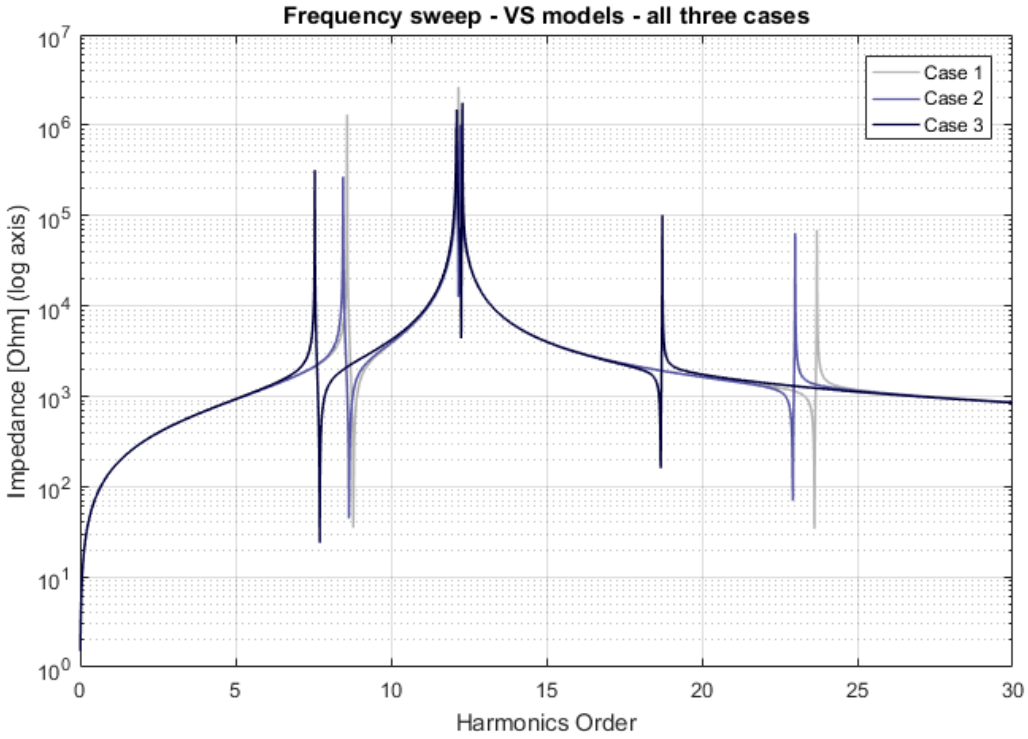

Figure 2.37: Caption FS

Table 2.16: Caption FS table

Method / model	Frequency order [-]		
	Case 1	**Case 2**	**Case 3**
FS / VS	8.59	8.46	7.55
	12.17	12.12	12.1
		12.23	12.12
			12.3
	23.7	23.00	18.73

We observe clearly that that in each next case, the frequencies of first and third group are shifted downward. The second group (around 12th harmonic order) is becoming more numerous for the cases with multiple branches, whereas the values stay at the similar level.

Harmonic Resonance Modal Analysis

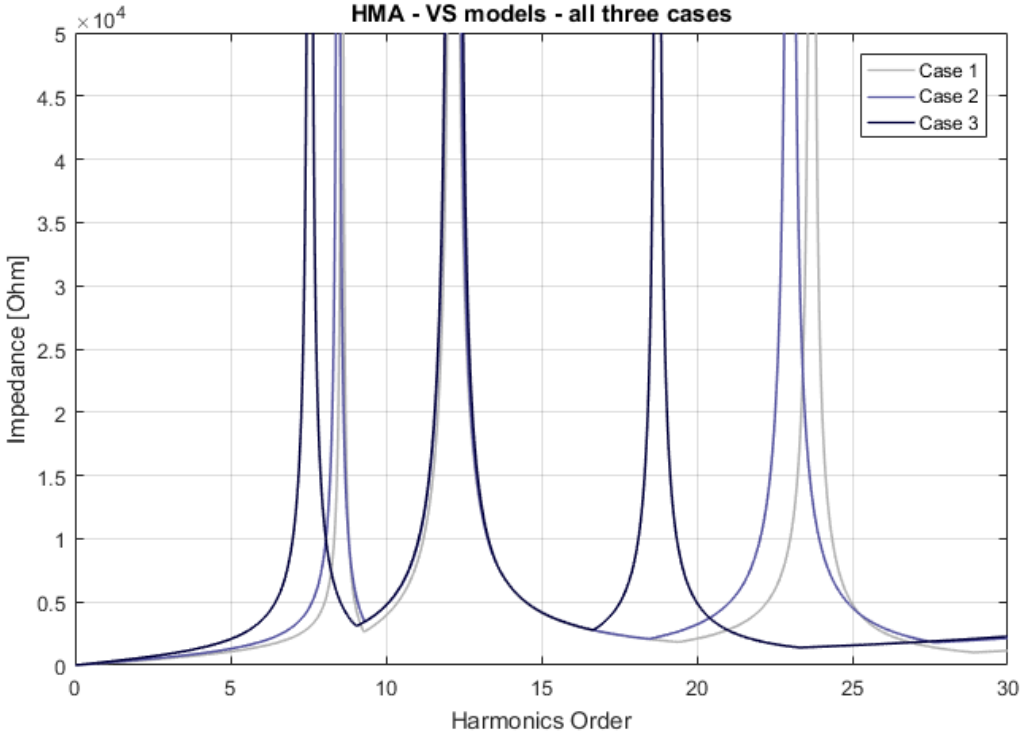

Figure 2.38: Caption hrma

Since the frequencies calculated in HRMA are the same to those obtained from frequency sweep, we do not draw more observations. However, we also have at our disposal the values of participation factors indicating the excitability and observability of the buses in the network. The values of PFs for three topology cases for VS mode are gathered in the Table 2.17.

Table 2.17: Caption hrma pf table

Frequency order [-]	Participation factors [%] for the buses							
	Case 1							
	1	2	3	4	5	6	7	PF's sum
8.59	8.8	12.8	13.0	14.2	14.6	15.1	**21.5**	1.000
12.17	0.1	0.0	0.0	0.2	0.4	1.8	**97.4**	1.000
23.7	0.9	14.6	15.7	**23.1**	**24.3**	20.0	1.4	1.000

Frequency order [-]	Participation factors [%] for the buses											
	Case 2											
	1	2	3	4	5	6	7	8	9	10	11	PF's sum
8.46	5.3	7.9	8.0	8.7	9.0	9.2	**12.5**	8.7	9.0	9.2	**12.5**	1.000
12.12	0.0	0.0	0.0	0.2	0.3	1.1	**48.4**	0.2	0.3	1.1	**48.4**	1.000
12.23	0.3	0.0	0.0	0.0	0.1	0.8	**48.9**	0.0	0.1	0.8	**48.9**	1.000
23	0.6	8.9	9.6	**13.6**	**14.2**	11.7	1.0	**13.6**	**14.2**	11.7	1.0	1.000

Frequency order [-]	Participation factors [%] for the buses										
	Case 3										
	1	2	3	4	5	6	7	8	9	10	
7.55	2.5	4.8	4.9	5.1	5.2	5.2	**5.2**	5.1	5.2	5.2	
12.1	0.0	0.0	0.0	0.1	0.2	0.6	**24.2**	0.1	0.2	0.6	
12.12	0.0	0.0	0.0	0.2	0.3	1.1	**49.5**	0.2	0.3	1.1	
12.3	0.4	0.1	0.1	0.0	0.0	0.3	**24.5**	0.0	0.0	0.3	
18.73	1.7	5.6	5.8	**6.7**	**6.7**	5.2	1.7	**6.7**	**6.7**	5.2	
	11	12	13	14	15	16	17	18	19	20	PF's sum
7.55	**5.2**	4.9	5.1	5.2	5.2	**5.2**	5.1	5.2	5.2	**5.2**	1.000
12.1	**24.2**	0.0	0.1	0.2	0.6	**24.2**	0.1	0.2	0.6	**24.2**	1.000
12.12	**49.5**	0.0	0.0	0.0	0.0	1.9	0.0	0.0	0.0	1.9	1.063
12.3	**24.5**	0.1	0.0	0.0	0.3	**24.5**	0.0	0.0	0.3	**24.5**	1.000
18.73	1.7	5.8	**6.7**	**6.7**	5.2	1.7	**6.7**	**6.7**	5.2	1.7	1.000

From the values of PFs we can see the pattern that confirms our assumption created with respect to resonant frequencies from frequency sweep only. The first group of harmonics seems to mark the bus 7 (and symmetrical buses of other branches) as the source of this group of resonances. It touches all topology cases. We have to notice that the values of the PFs could be also considered as spread quite evenly between the buses. In case of the second group of resonant frequency (around 12th harmonic order), the bus that is surely indicated by the PFs is the bus 7 (and symmetrical ones). For the third group of resonances, we identify two buses (bus 4 and bus 5) indicated by PFs as the two participating the most in the excitation of the resonance. Bus 4 and bus 5 are the terminals of 33 kV collection cable. The observations described above are encapsulated in the Table 2.18.

Table 2.18: Caption hrma table

Method / model	Frequency order [-]			Dominant bus
	Case 1	**Case 2**	**Case 3**	
HRMA / VS	8.59	8.46	7.55	Middle LCL buses (7) or evenly
	12.17	12.12	12.1	Middle LCL buses (7)
		12.23	12.12	
			12.3	
	23.7	23.00	18.73	Cable 33 kV terminal buses (4, 5)

2.2.4.2 CS-WT model

Frequency sweep

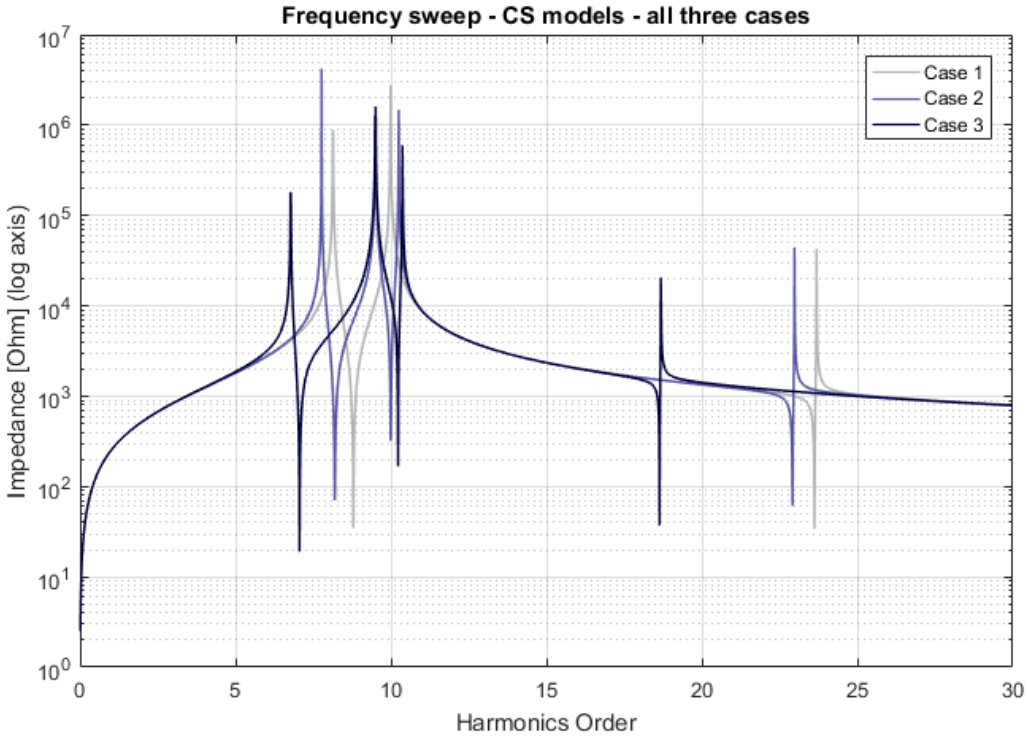

Figure 2.39: Caption FS

Table 2.19: Caption FS table

Method / model	Frequency order [-]		
	Case 1	**Case 2**	**Case 3**
FS / CS-WT	8.14	7.77	6.78
	9.99	9.51	9.49
		10.25	9.51
			10.37
	23.69	22.98	18.68

Similarly to the observations drawn for the Voltage Source model we can conclude for the model with aggregated WT converters modelled as Current Sources. On the basis of FS only, we divide the values of resonance frequencies into three groups. Again, we detect that the values of each group are shifted downwards when the number of branches is increased. All of the values of the frequencies are lower comparing o the first topology case. For each group, these changes differ.

Harmonic Resonance Modal Analysis

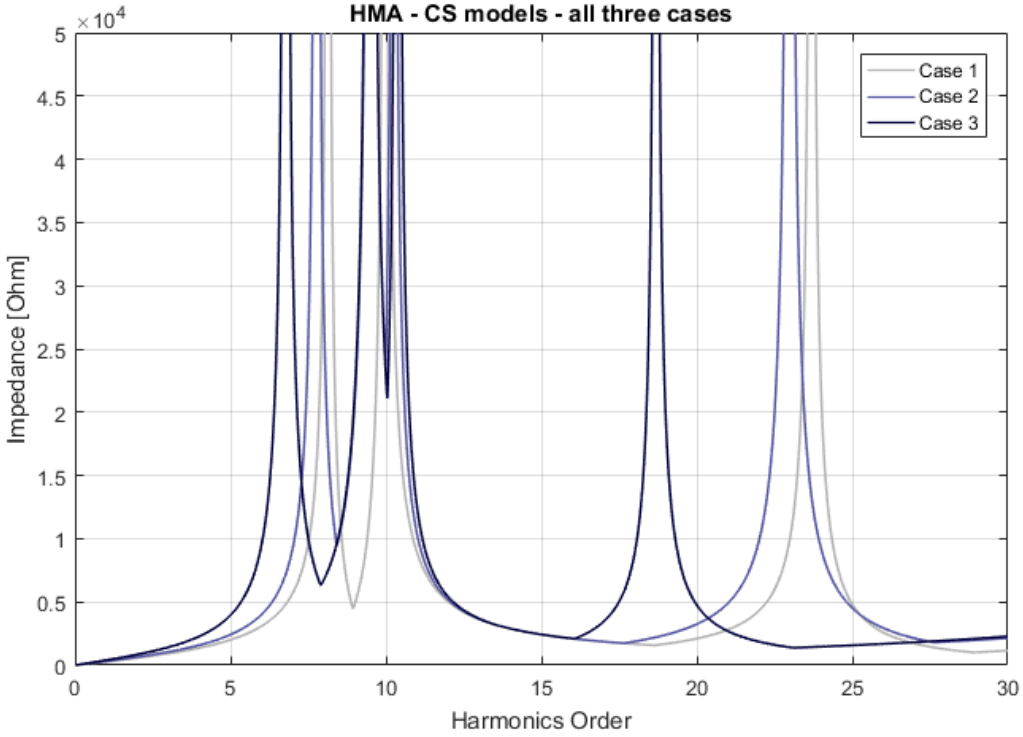

Figure 2.40: Caption hrma

The values of frequency orders are the same for FS and HRMA. Again, we include participation factors to our conclusions and try to identify some patterns. The values of PFs for all cases are presented first in Tables 2.20.

Table 2.20: Caption hrma pf table

Frequency order [-]	Participation factors [%] for the buses							
	Case 1							
	1	2	3	4	5	6	7	PF's sum
8.14	2.6	4.4	4.4	6.2	7.0	9.3	**66.0**	1.000
9.99	1.1	1.0	0.9	0.2	0.0	0.3	**96.5**	1.000
23.69	0.9	14.6	15.6	**23.2**	**24.4**	20.2	1.1	1.000

Frequency order [-]	Participation factors [%] for the buses											
	Case 2											
	1	2	3	4	5	6	7	8	9	10	11	PF's sum
7.77	1.7	3.2	3.2	4.2	4.6	5.8	**31.3**	4.2	4.6	5.8	**31.3**	1.000
9.51	0.0	0.0	0.0	0.1	0.3	1.1	**48.5**	0.1	0.3	1.1	**48.5**	1.000
10.25	1.5	1.1	1.1	0.4	0.2	0.0	**47.4**	0.4	0.2	0.0	**47.4**	1.000
22.98	0.6	8.9	9.6	**13.7**	**14.3**	11.8	0.7	**13.7**	**14.3**	11.8	0.7	1.000

Frequency order [-]	Participation factors [%] for the buses										
	Case 3										
	1	2	3	4	5	6	7	8	9	10	
6.78	1.2	2.8	2.8	3.2	3.4	3.9	**12.1**	3.2	3.4	3.9	
9.49	0.0	0.0	0.0	0.1	0.2	0.5	**24.2**	0.1	0.2	0.5	
9.51	0.0	0.0	0.0	0.0	0.0	0.1	4.3	0.0	0.0	0.1	
10.37	1.1	0.8	0.8	0.4	0.2	0.0	**23.6**	0.4	0.2	0.0	
18.68	1.8	5.6	5.9	**6.8**	**6.8**	5.5	1.0	**6.8**	**6.8**	5.5	
	11	12	13	14	15	16	17	18	19	20	PF's sum
6.78	**12.1**	2.8	3.2	3.4	3.9	**12.1**	3.2	3.4	3.9	**12.1**	1.000
9.49	**24.2**	0.0	0.1	0.2	0.5	**24.2**	0.1	0.2	0.5	**24.2**	1.000
9.51	4.3	0.0	0.1	0.3	1.0	**44.4**	0.1	0.3	1.0	**44.4**	1.005
10.37	**23.6**	0.8	0.4	0.2	0.0	**23.6**	0.4	0.2	0.0	**23.6**	1.000
18.68	1.0	5.9	**6.8**	**6.8**	5.5	1.0	**6.8**	**6.8**	5.5	1.0	1.000

On the basis of PFs, we draw the similar observations for CS-WT model than from VS model. The PFs for the first two groups of harmonic orders indicates bus 7 (and symmetrical buses at other branches) as the bus with highest participation to the harmonic excitation. In the same manner as for VS model, the PFs of harmonic orders of third group mark the buses 4 and 5 as the buses exciting the resonance. These observations are gathered in the Table 2.21.

Table 2.21: Caption hrma table

Method / model	Frequency order [-]			Dominant bus
	Case 1	**Case 2**	**Case 3**	
HRMA / CS-WT	8.14	7.77	6.78	Middle LCL bus (7)
	9.99	9.51	9.49	
		10.25	9.51	
			10.37	
	23.69	22.98	18.68	Cable 33 kV terminal buses (4, 5)

2.2.4.3 Z(s) model

Frequency sweep Figure 2.41 shows the FS curves for all topology cases derived for Z(s) model.

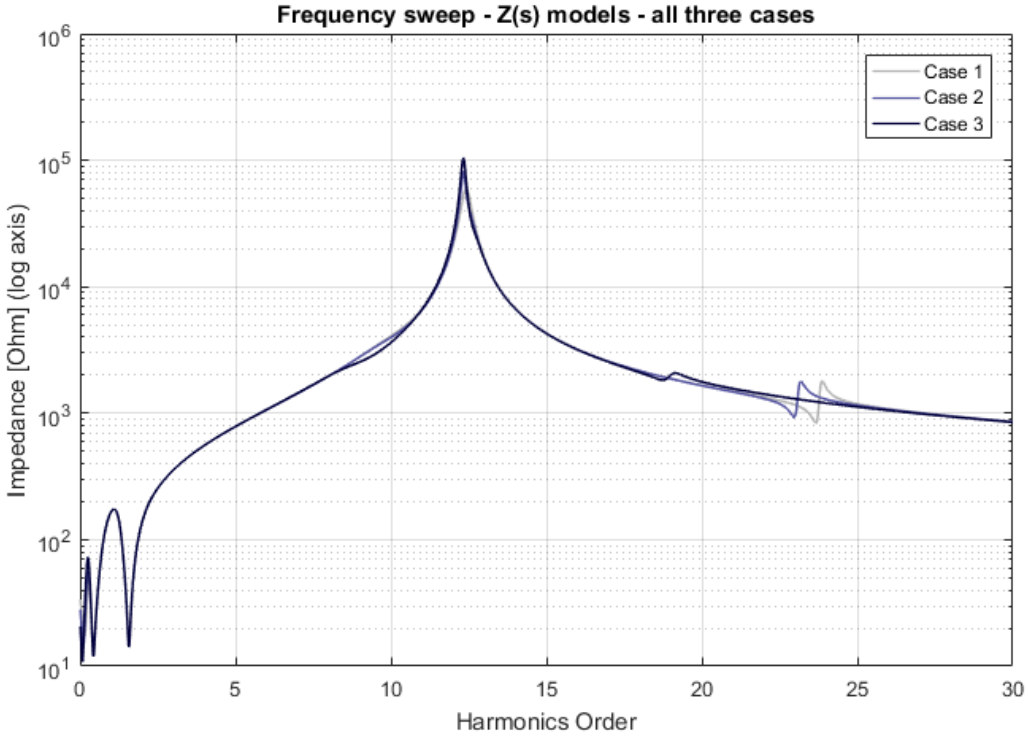

Figure 2.41: Caption FS

Table 2.22: Caption FS table

Method / model	Frequency order [-]		
FS / Z(s)	**Case 1**	**Case 2**	**Case 3**
	12.42	12.33	12.33
	23.87	23.18	19.13

This time, FS method does not detect resonance frequencies analogical to the lowest orders group for VS and CS-WT model. The number of peaking impedance points around 12th order also does not increase for multiple branches cases. However, we observe the equivalent resonances for two groups with values very close to the VS model. Also, we mark the downward shift for multiple branches what was the same for the other models.

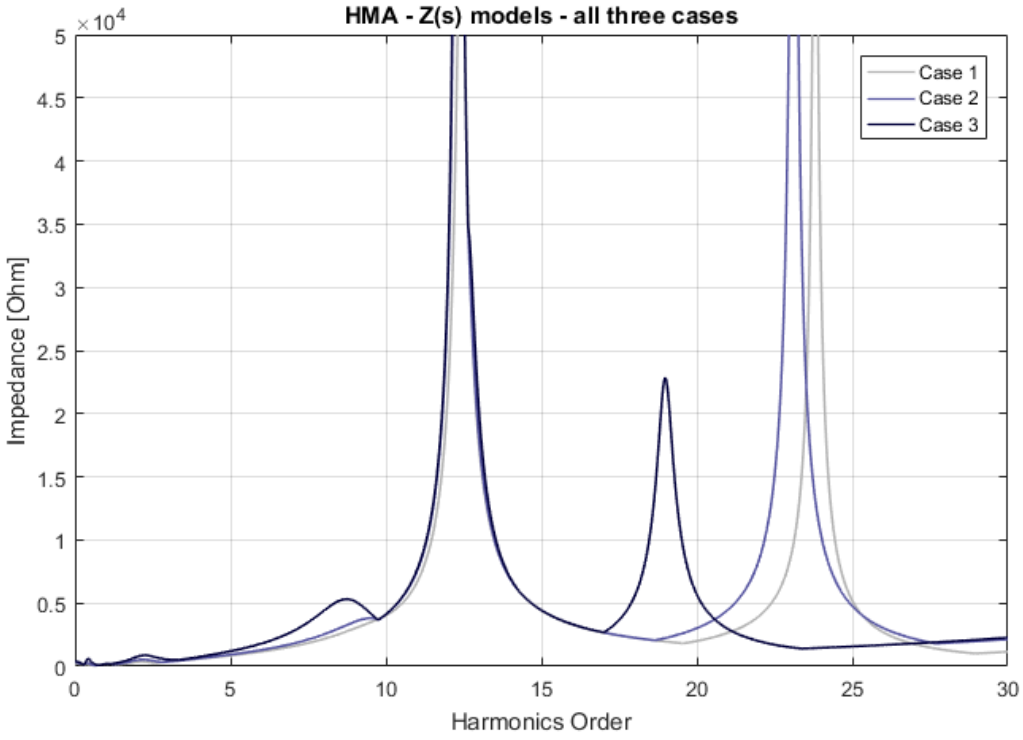

Figure 2.42: Caption hrma

Harmonic Resonance Modal Analysis As pointed out in previous section, for Z(s) model HRMA detects additional resonant frequency comparing to FS, but at the low level (relatively to the other critical impedances). These new frequencies corresponds accurately to the first group of frequencies detected in VS and CS-WT model.

Again, we include PFs in the analysis and we identify the buses with the highest values of PFs. The Table 2.23 presents PFs values for all topology cases.

Table 2.23: Caption hrma pf table

Frequency order [-]	Participation factors [%] for the buses							
	Case 1							
	1	2	3	4	5	6	7	PF's sum
12.42	0.2	0.1	0.1	0.2	0.5	1.8	**97.8**	1.007
23.81	1.0	14.5	15.6	**23.1**	**24.3**	20.1	1.4	1.000

Frequency order [-]	Participation factors [%] for the buses											
	Case 2											
	1	2	3	4	5	6	7	8	9	10	11	PF's sum
9.51	2.8	5.4	5.5	7.1	7.8	9.3	**45.5**	7.1	7.8	9.3	**45.5**	1.533
12.34	0.0	0.0	0.0	0.2	0.3	1.1	**48.4**	0.2	0.3	1.1	**48.4**	1.000
23.11	0.7	8.8	9.5	**13.6**	**14.2**	11.7	1.0	**13.6**	**14.2**	11.7	1.0	1.000

Frequency order [-]	Participation factors [%] for the buses									
	Case 3									
	1	2	3	4	5	6	7	8	9	10
8.73	1.9	4.7	4.7	5.2	5.3	5.4	**7.3**	5.2	5.3	5.4
12.34	0.0	0.0	0.0	0.1	0.3	1.1	**47.9**	0.1	0.3	1.1
18.98	2.0	5.5	5.8	**6.7**	**6.7**	5.3	1.6	**6.7**	**6.7**	5.3
	11	12	13	14	15	16	17	18	19	20	PF's sum
8.73	**7.3**	4.7	5.2	5.3	5.4	**7.3**	5.2	5.3	5.4	**7.3**	1.089
12.34	**47.9**	0.0	0.0	0.0	0.0	1.2	0.0	0.0	0.0	1.2	1.012
18.98	1.6	5.8	**6.7**	**6.7**	5.3	1.6	**6.7**	**6.7**	5.3	1.6	1.002

With respect to PFs, we observe the very similar results to the models VS and CS-WT. The PFs of harmonic orders of the first group and the medium one indicates bus 7 as the one participating the most in the resonances. For the highest order group, similarly, the buses 4 and 5 are identified.

Table 2.24: Caption hrma table

Method / model	Frequency order [-]			Dominant bus
	Case 1	**Case 2**	**Case 3**	
HRMA / Z(s)		9.51	8.73	Middle LCL bus (7)
	12.42	12.34	12.34	
	23.81	23.11	18.98	Cable 33 kV terminal buses (4, 5)

2.2.4.4 Comparison between topology cases and conclusions

On an axis...?

2.3 Stability study with respect to topology cases

This section presents the results of stability analysis for the three different already described topology cases. The principles of stability analysis are described in Section 1.5.2 in the theoretical part of the thesis. In this part, only the last model of the network is used i.e. the model containing the nonlinear impedances of the converters Z(s) model. This model is considered as the most polished within all presented in this thesis. In short, the stability is evaluated on the basis of Nyquist stability criterion plotted in the Bode diagrams. The method is considered as still under development [11]. The question that has not been struck in the literature is the use of both WT converter nonlinear model and HVDC-link converter nonlinear model at the same time for stability study.

The sections below present the results separately for each topology case, also comparing the values obtained to the previous results from FS and HRMA methods.

2.3.1 Case 1 stability

The Figure 2.43 present the Bode diagram of the considered model used for stability study. As described in detail in theoretical part, the network is divided into two elements: the source and the grid. The point of division is behind the HV transformer, looking from the grid side. The positive and negative sequences of grid and source segments are presented in domain of frequency.

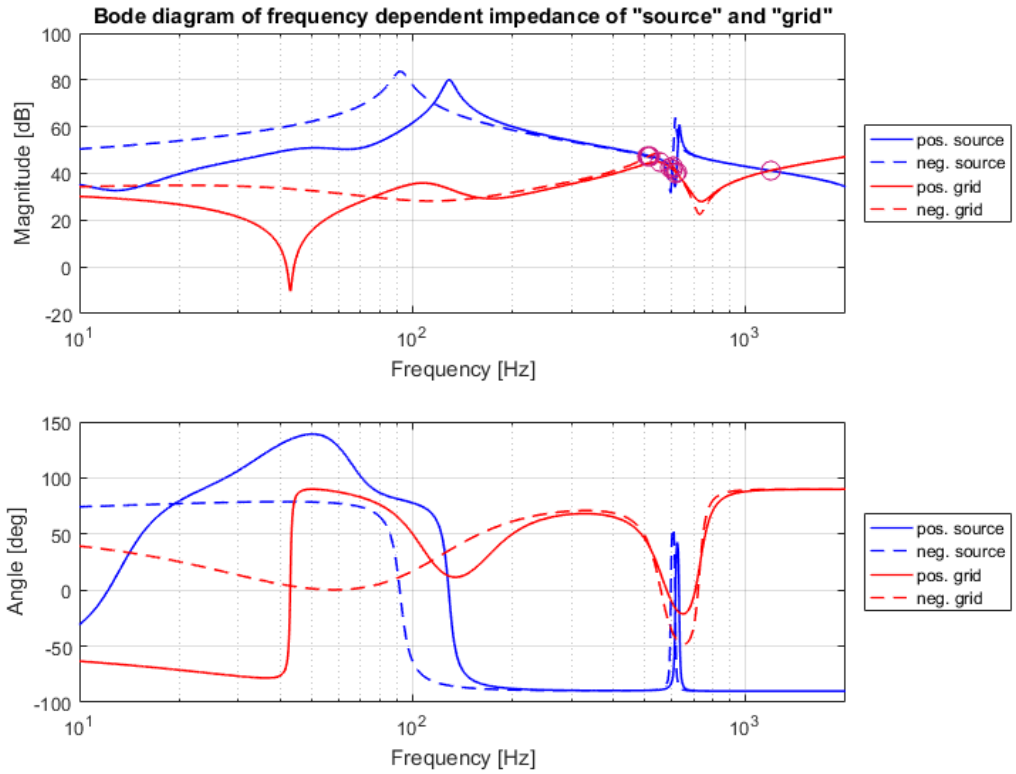

Figure 2.43: Caption bode

The points of attention where the instabilities may occur are the crossings of the grid and the source impedances, regardless the positive or negative sequence. All of them are investigated and the possible instabilities identified. In the Figure 2.43 the intersections are marked with purple circles. Figure 2.44 presents the source and grid curves zoomed in the area of high density of intersections.

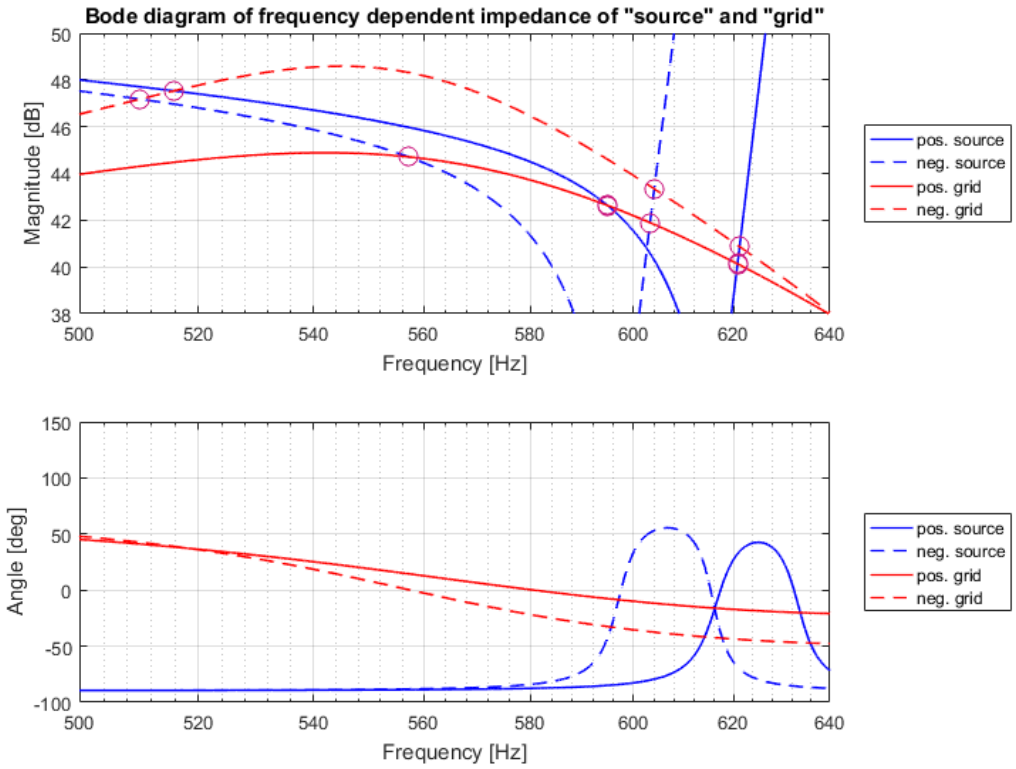

Figure 2.44: Caption bode zoom

For each intersection, the values of angle depending on the difference between appropriate curves is calculated in MATLAB. Table 2.25 presents the values of frequencies for which the crossings occur, also the values of angles indicating stability are included.

Table 2.25: Table fi

Frequency order [-]	$\Phi = 180° - \varphi\ [deg]$
Positive Grid – Positive Source	
11.90	102.61
12.42	130.28
23.81	0.64
Positive Grid – Negative Source	
11.14	77.25
12.07	117.44
23.81	0.64
Negative Grid –Positive Source	
10.32	51.66
12.43	101.61
23.81	0.18
Negative Grid – Negative Source	
10.20	48.01
12.08	89.40
23.81	0.18

2.3.2 Case 2 stability

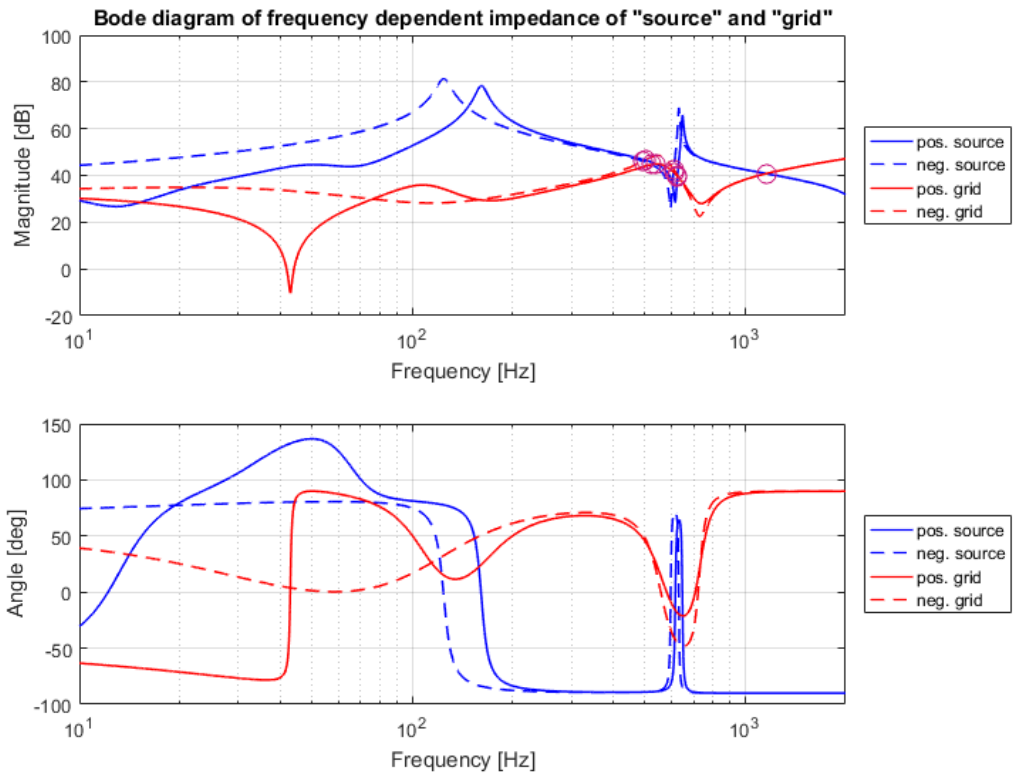

Figure 2.45: Caption bode

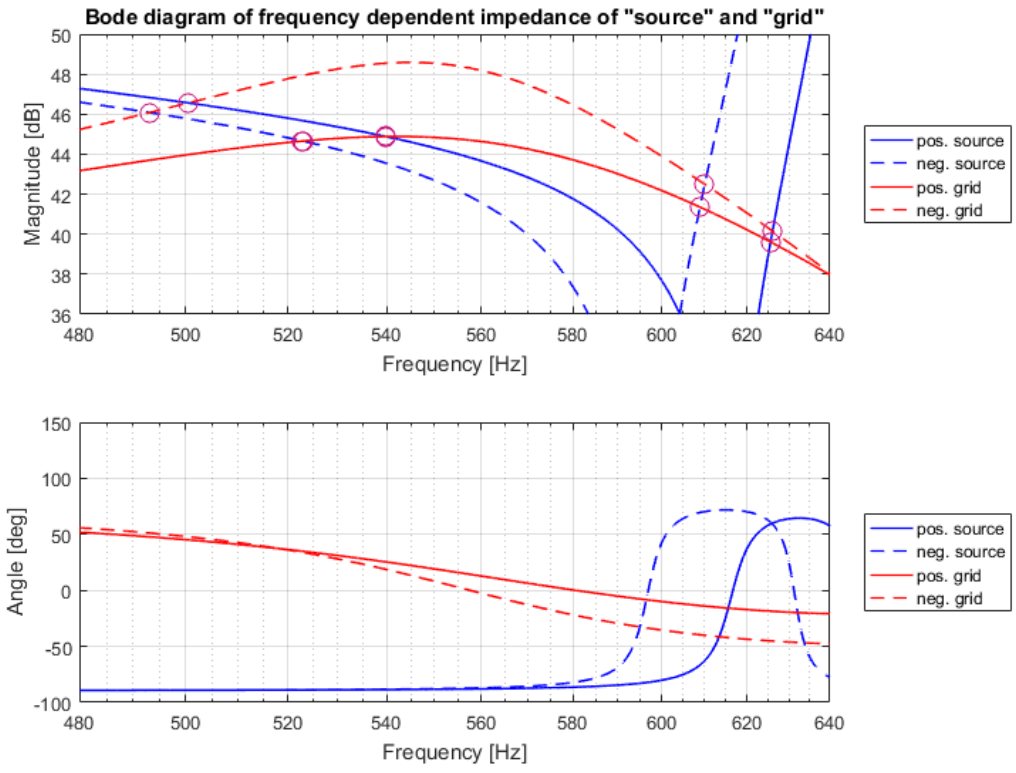

Figure 2.46: Caption bode zoom

Table 2.26: Table fi

Frequency order [-]	$\Phi = 180° - \varphi\ [deg]$
Positive Grid – Positive Source	
10.80	66.03
12.51	102.31
23.11	0.78
Positive Grid – Negative Source	
10.46	56.37
12.18	96.94
23.11	0.78
Negative Grid –Positive Source	
10.00	43.12
12.52	74.85
23.12	0.26
Negative Grid – Negative Source	
9.86	39.72
12.20	69.60
23.12	0.24

2.3.3 Case 3 stability

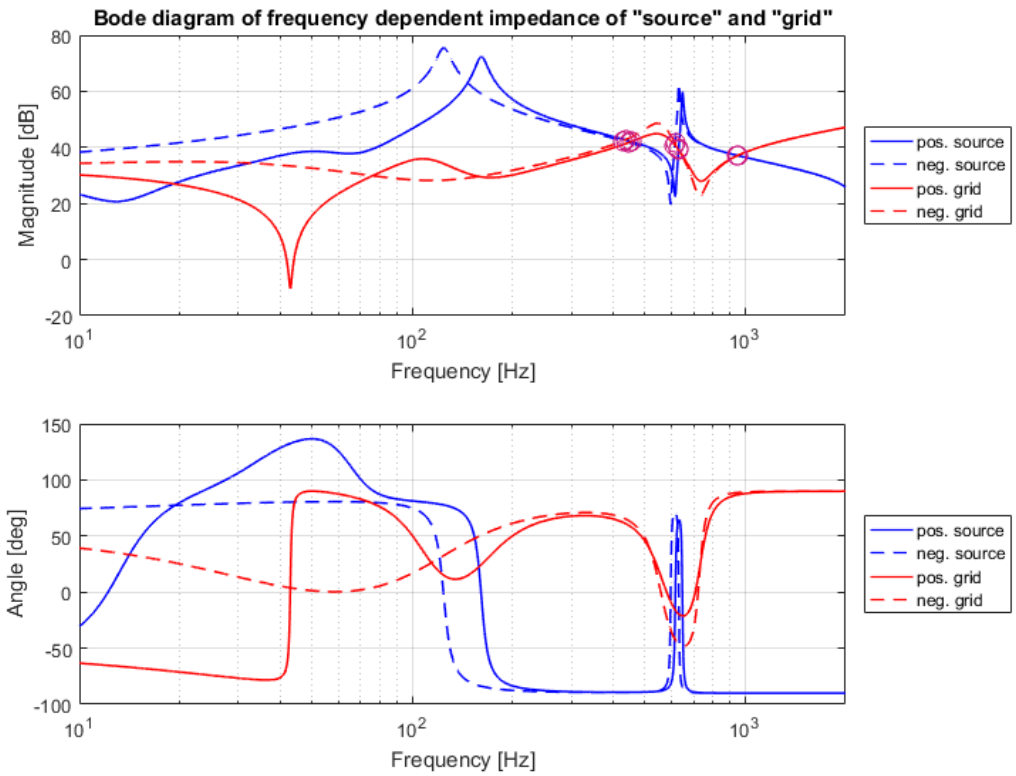

Figure 2.47: Caption bode

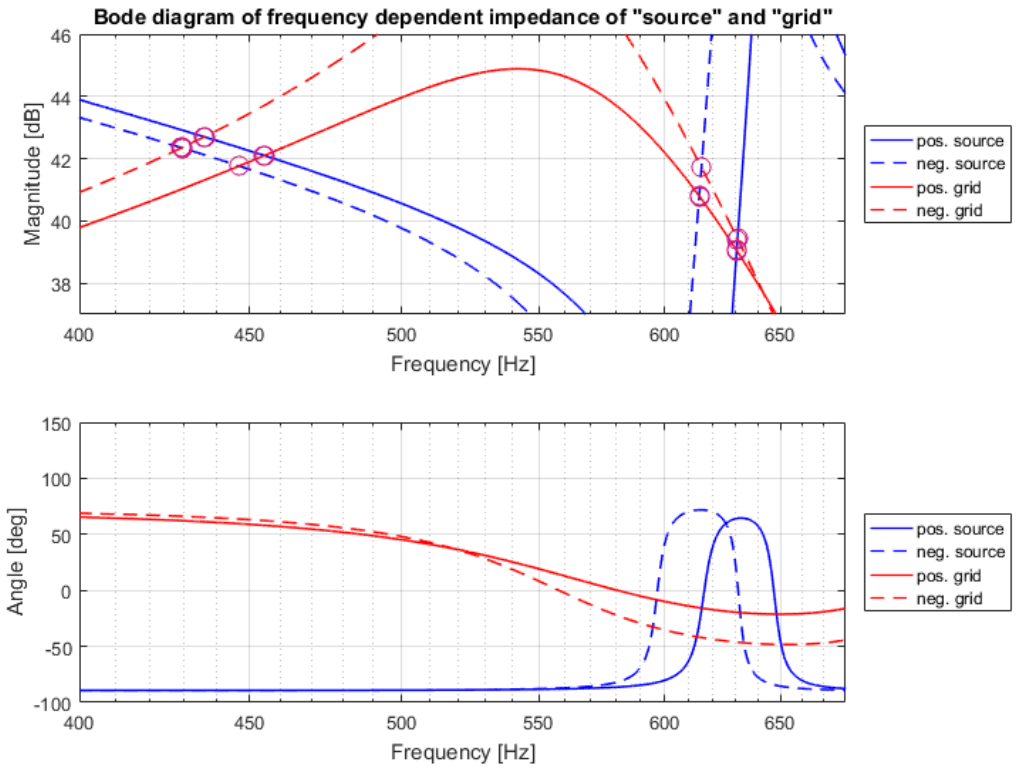

Figure 2.48: Caption bode zoom

Table 2.27: Table fi

Frequency order [-]	$\Phi = 180° - \varphi\ [deg]$
Positive Grid – Positive Source	
9.09	32.71
12.61	96.31
18.96	3.28
Positive Grid – Negative Source	
8.94	31.14
12.29	92.7
18.95	3.29
Negative Grid –Positive Source	
8.72	25.45
12.62	69.49
18.99	1.29
Negative Grid – Negative Source	
8.59	24.47
12.31	66.09
18.99	1.29

2.3.4 Comparison to FS and HRMA and conclusions

Table 2.28: Table stability comparison

Method / model	Frequency order [-]		
FS / Z(s)	**Case 1**	**Case 2**	**Case 3**
	12.42	12.33	12.33
	23.87	23.18	19.13

Table 2.29: Table stability comparison

Method / model	Frequency order [-]			Dominant bus
HRMA / Z(s)	**Case 1**	**Case 2**	**Case 3**	
		9.51	8.73	Middle LCL bus (7)
	12.42	12.34	12.34	
	23.81	23.11	18.98	Cable 33 kV terminal buses (4, 5)

Table 2.30: Table stability comparison

Method / model	Frequency order [-]		
	Case 1	**Case 2**	**Case 3**
Bode / Z(s)	11.90	10.80	9.09
	11.14	10.46	8.94
	10.32	10.00	8.72
	10.20	9.86	8.59
	12.42	12.51	12.61
	12.07	12.18	12.29
	12.43	12.52	12.62
	12.08	12.20	12.31
	23.81	23.11	18.96
	23.81	23.11	18.95
	23.81	23.12	18.99
	23.81	23.12	18.99

Table 2.31: Table stability comparison

Method / model	Frequency order [-]		
	Case 1	**Case 2**	**Case 3**
Bode / Z(s)	10.20 - 11.90	9.86 - 10.80	8.59 - 9.09
	12.07 - 12.42	12.18 - 12.52	12.29 - 12.62
	23.81	23.11 – 23.12	18.96 -18.99

Bibliography

[1] *Power System Harmonics and Passive Filter Designs.* , 2015.

[2] *Harmonics and Power Systems.* , 2006.

[3] *Power System Harmonics.* , 2003.

[4] IEEE, "The effects of power system harmonics on power system equipment and loads," *IEEE Transactions*, 1985.

[5] W. X. Z. H. Y. C. H. Wang, "Harmonic resonance mode analysis," *IEEE TRANSACTIONS ON POWER DELIVERY, VOL. 20, NO. 2,*, APRIL 2005.

[6] , "Selective modal analysis with applications to electric power systemsii. the dynamic stability problem," *IEEE Trans. Power App. Syst.*, 1982.

[7] M. B. B. B. E. C. D. M. J. S. T. S. T. S. M. S. R. W. I. P. W. P. C. S. D. W. Group, "Harmonics and resonance issues in wind power plants," , 2012.

[8] *Introduction to Matrix Analysis, 2nd ed.* New York: Mc-Graw-Hill, 1970.

[9] *Selective modal analysis with applications to electric power systemsI. Heuristic introduction.* IEEE Trans. Power App. Syst, 1982.

[10] L. Pham, "A review of full scale converter for wind turbines," *IEEE*, 2013.

[11] C. B. C. R. A. M. D. J. Jung, "Borwin1 first experiences with harmonic interactions in converter dominated grids," *International ETG Congress 2015*, 2015.

[12] H. L. J. Sun, "Voltage stability and control of offshore wind farms with ac collection and hvdc transmission," *IEEE JOURNAL OF EMERGING AND SELECTED TOPICS IN POWER ELECTRONICS*, 2014.

[13] J. Sun, "Impedance-based stability criterion for grid-connected inverters," *IEEE TRANSACTIONS ON POWER ELECTRONICS*, 2100.

[14] *Input filter considerations in design and application of switching regulators.* IEEE Ind. Appl. Soc. Annu. Meeting, 1976.

[15] H. Liu and J. Sun, "A study of offshore wind hvdc system stability and control," *Department of Electrical, Computer and Systems Engineering, Rensselaer Polytechnic Institute, Troy, NY, USA*, 2013.

[16] Z. B. K. J. Karimi; and J. Sun, "Input impedance modeling and analysis of line-commutated rectifiers," *IEEE Trans. Power Electron*, 2009.

[17] M. Cespedes and J. Sun, "Impedance modeling and analysis of gridconnected voltage-source converters," *IEEE Trans. Power Electron.*, 2014.

[18] E. L. G. Drobnjak; and H. Elahi, "Standardization of vsc-hvdc interface with offshore wind generation," *11th Int. Workshop Large-Scale Integr. Wind Power Power Syst.*, 2012.

[19] , "Iec series 61000 standards," tech. rep., , .

[20] , "Voltage characteristics of electricity supplied by public distribution systems," tech. rep., Brussels, 1994.

[21] , "Ieee recommended practice and requirements for harmonic control in electrical systems," tech. rep., , 1992.